UNIVERSITY OF READING

Department of Meteorology

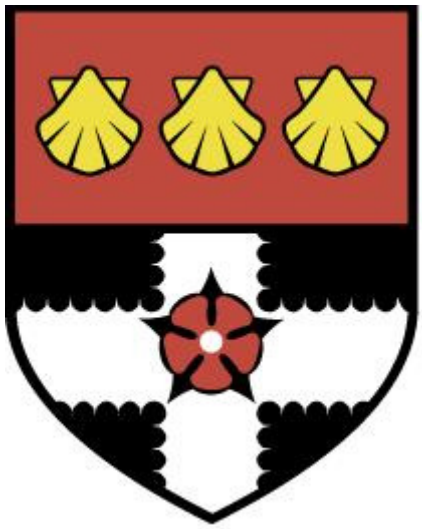

Sea Ice - Ocean Feedbacks in the Southern Ocean

REBECCA CAITLIN FREW

A thesis submitted for the degree of Doctor of Philosophy

September 2019

DECLARATION

I confirm that this is my own work and the use of all material from other sources has been properly and fully acknowledged.

Rebecca. C. Frew

ABSTRACT

Observed changes in Antarctic sea ice are poorly understood, in part due to the complexity of its interactions with the atmosphere and ocean. Sea ice and ocean interactions and feedbacks around Antarctica are subtle, complex and difficult to elucidate either from observations or coupled climate models. There is a need for a conceptual model/understanding of the important feedbacks and processes in the Southern Ocean sea ice–atmosphere–ocean system, to better understand Antarctic sea ice variability in both warm and cold Antarctic shelf ocean regimes. In this thesis a modelling approach has been used to investigate the relationship between the sea ice and the ocean mixed layer in the Antarctic shelf seas.

A highly simplified, coupled sea ice–ocean mixed layer model has been developed to investigate the importance of sea ice–ocean feedbacks on the evolution of sea ice and the ocean mixed layer in two contrasting regions of the Antarctic continental shelf ocean: the Amundsen Sea, which has warm shelf waters; and the Weddell Sea, which has cold and saline shelf waters. The model was developed to include a variable snow layer and snow ice formation. Snow ice formation proved to be a significant process, particularly in the Amundsen Sea simulations where snowfall rates are relatively high. Sensitivity studies were carried out, investigating the response of the sea ice and mixed layer to the ocean conditions and atmospheric forcing fields. In the Weddell Sea the water column completely destratified during winter in response to all atmospheric perturbations, however the timing becomes earlier/later depending on whether the rate of sea ice growth is increased/decreased. Decreased winter sea ice growth and a shorter period of complete destratification could decrease the rate of formation of Antarctic Bottom Water. In the Amundsen Sea, changes to the surface energy balance that promote ice growth and ocean cooling also promote mixed layer deepening. Changes to entrainment of warm deep waters oppose the direct impact of the atmospheric perturbation on the ice cover through changes in the rate of basal ice melting. These competing processes are evident in the sensitivity responses. A shallower mixed layer could also result in more warm CDW on the continental shelf, resulting in increased melting of the ice shelves.

The response of five different feedbacks to surface air temperature perturbations are investigated: ocean feedback, sea ice feedback, the albedo feedback, the insulation feedback and the freezing temperature feedback. Modelling studies where we deny the feedback response to surface air temperature perturbations show the importance of feedbacks on the mixed layer and ice cover in the Weddell Sea to be smaller than the sensitivity to surface atmospheric conditions. In the Amundsen Sea the effect of surface air temperature perturbations on the sea ice are opposed by changes in the entrainment of warm deep waters into the mixed layer. The net impact depends on the relative balance between changes in sea ice growth driven by surface perturbations and

basal driven melting. The changes in the entrainment of warm water in the Amundsen Sea were found to have a much larger impact on the ice volume than perturbations in the surface energy budget. This creates a net negative ice albedo feedback in the Amundsen Sea, reversing the sign of this typically positive feedback mechanism.

Coupling the sea ice CICE model to a mixed layer model improved the representation of the sea ice physics and dynamics. The sensitivity of the sea ice cover in CICE to the coupling to the mixed layer model was investigated, indicating which regions of the Southern Ocean were most sensitive to the sea ice-mixed layer processes. The snow ice parameterisation in CICE was modified, to account for the weight of the sea water flooding the snow. The Amundsen-Bellingshausen Seas were shown to be particularly sensitive to this change, resulting in an increase in sea ice thickness. The ocean feedback on the sea ice was investigated for the Amundsen Sea region, as this was the strongest feedback from the idealised modelling work. Due to the unrealistic sea ice state when using climatological atmospheric forcing, the feedback was investigated using years of shallower/deeper mixed layer depth as opposed to perturbing climatological atmospheric conditions, but no clear relationship between the mixed layer depth and the response of the sea ice cover was found. This can be partly attributed to the difference in ocean profiles being used. Our studies provide insight into the nature and strength of sea ice–ocean feedback processes in these regions, and could be helpful in the analysis of fully coupled models.

ACKNOWLEDGEMENTS

I would like to thank the following people for their help and support:

- My husband Chris for being my non-scientist proof reader, and supporting me in every way throughout my PhD.
- To my supervisors Danny Feltham and Paul Holland, for guidance and support throughout the PhD. And the rest of the Reading sea ice group for their discussions and help.
- My monitoring committee, David Ferreira and Ed Hawkins for constructive questioning over the past four years.
- To the PhDs in Meteorology for being such a supportive and sociable community, I've really enjoyed being a part of it for the past four years. In particular thanks to my fellow tap dancer and tea break partner Hélène.
- My sisters, for providing emotional support from afar, mostly in the form of pictures of the cats and extended Skype calls in times of need.
- My fellow Dungeons & Dragons nerds who have provided me with some escapism, and plenty of entertainment.
- The Killers and The Stereophonics for providing me with the music I needed to write my thesis.
- This PhD was funded by the Natural Environment Research Council, with case sponsorship from the British Antarctic Survey.

Contents

List of Figures

List of Tables

List of Acronyms

Table 0.1: List of acronyms

Acronym	Definition
AABW	Antarctic Bottom Water
AASW	Antarctic Surface Water
ABW	Antarctic Bottom Water
ACC	Antarctic Circumpolar Current
APFZ	Antarctic Polar Frontal Zone
AS	Amundsen Sea
ASL	Amundsen Sea Low
CDW	Circumpolar Deep Water
CMIP5	Coupled Model Intercomparison Project 5
ENSO	El Niño Southern Oscillation
FD	Feedback Denied
GSLR	Global Sea Level Rise
HSSW	High Salinity Shelf Water
IDW	Indian Deep Water
IPCC	Intergovernmental Panel on Climate Change
ISW	Ice Shelf Water
LCDW	Lower Circumpolar Deep Water
MOC	Meridional Overturning Circulation
MWDW	Modified Warm Deep Water
NADW	North Atlantic Deep Water
PDW	Pacific Deep Water
PIB	Pine Island Bay
SAMW	Subantarctic Mode Water
SAT	Surface Air Temperature
SIE	Sea Ice Extent
SO	Southern Ocean
SST	Sea surface temperature
UCDW	Upper Circumpolar Deep Water
WAIS	West Antarctic Ice Sheet
MCDW	Modified Circumpolar Deep Water
WDW	Warm Deep Water
WS	Weddell Sea
WSBW	Weddell Sea Bottom Water

Acronym	Definition
WSDW	Weddell Sea Deep Water
WW	Winter Water

LIST OF MATHEMATICAL SYMBOLS

Table 0.2: List of variables

Variables	
A	ice concentration
d_{mix}	mixed layer depth
E	evaporation rate
F_c	conductive heat flux through the ice and snow
$F_{lw} \downarrow$	incoming longwave radiative heat flux
F_{mo}	heat flux from the mixed layer to the open water surface layer
F_{mi}	heat flux into the base of the sea ice at the mixed layer–sea ice boundary
F_{sb}	basal heat flux
$F_{si} \uparrow$	salt flux from snow ice formation
$F_{sm} \uparrow$	freshwater flux from snow melt
$F_{sw} \downarrow$	incoming shortwave radiative heat flux
$F_T \uparrow$	surface heat flux out of the mixed layer
$F_S \uparrow$	surface salt flux out of the mixed layer
H_{fr}	ocean surface heat potential
h_i	ice thickness
h_s	snow thickness
h_{si}	snow ice thickness
P	snowfall rate
P_b	rate of mechanical energy input to the mixed layer from the surface buoyancy fluxes
P_w	rate of thermal kinetic energy input from wind stirring
P_E	power required to entrain deep water
q_{sat}	saturation specific humidity
q_a	specific air humidity at 2 m
R_b	basal melt fraction, 0.75 ($R_b = 1$ when all melt is basal)
S_b	salinity below the mixed layer base
S_{mix}	mixed layer salinity
S_{trap}	effective salinity of the seawater inltrating the submerged snow
T_a	atmospheric temperature at 2 m
T_b	temperature below the mixed layer base
T_f	freezing temperature, calculated as: 273.14 - 0.054S_{mix}

Variables	
T_{mix}	mixed layer temperature
T_S^i	snow covered ice surface temperature
T_S^o	open water surface temperature
U_a	wind speed at 2 m
$u_\star$	effective friction velocity at the upper surface of the mixed layer
$u_\star^0$	fraction velocity between the open water surface layer and mixed layer
$u_\star^i$	friction velocity between the ice and mixed layer
$u_\star$	effective friction velocity at the upper surface of the mixed layer
w	entrainment rate of the mixed layer
Δb	difference in buoyancy of the waters across the mixed layer base
δh	thickness of snow removed during flooding (equal to the thickness of snow ice formed)

Table 0.3: List of constants

Constants	
α	thermal expansion coefficient, 5.82×10^{-5} K^{-1}
β	saline contraction coefficient, 8×10^{-4}
c_a	specific heat capacity of air, 1005 J kg^{-1} K^{-1}
c_w	specific heat capacity of water, 4190 J kg^{-1} K^{-1}
ϵ_s	longwave emissivity of snow, 1
ϵ_w	longwave emissivity of open water, 0.97
g	acceleration due to gravity, 9.81m s^{-1}
k_i	thermal conductivity of ice, 2.04 W m^{-1} K^{-1}
k_s	thermal conductivity of snow, 0.31 W m^{-1} K^{-1}
L_f	latent heat of fusion, 3.340×10^6 J kg^{-1}
L_s	latent heat of sublimation, 2.834×10^6 J kg^{-1}
L_v	latent heat of vaporisation, 2.501×10^6 J kg^{-1}
p_{atm}	atmospheric pressure, 100 kPa
ρ_a	density of air, 1.275 kg m^{-3}
ρ_i	density of ice, 930 kg m^{-3}

Constants	
ρ_s	density of snow, 400 kg m^{-3}
ρ_w	density of water, 1026 kg m^{-3}
σ	Stefan Boltzmann constant, 5.67×10^{-8} W m^{-2} K^{-4}

Table 0.4: List of fixed parameters

Fixed Parameters	
A_{max}	prescribed maximum ice concentration, 0.95
A_{ref}	reference ice concentration of sea ice being advected in to the domain, see Table 2.1
α_s	albedo of snow, 0.8
α_w	albedo of water, 0.06
c_1	maximum magnitude of wind stirring in the mixed layer, 0.8
C_D^i	turbulent transfer coefficient over ice fraction, 0.0013
C_D^o	turbulent transfer coefficient over lead fraction, 0.001
c_h	Stanton number for mixed layer to sea ice heat transfer, 0.006
c_m	unsteadiness coefficient, 0.03 ms^{-1}
d_w	scale depth of dissipation, 10 m
h_{min}	minimum sea ice thickness, 0.1 m
h_i^{ref}	reference ice thickness (total) of sea ice being advected in to the domain, see Table 2.1
h_s^{ref}	reference snow thickness of sea ice being advected in to the domain, see Table 2.1
h_{si}^{ref}	reference snow ice thickness of sea ice being advected in to the domain, see Table 2.1
$I_0(0)$	fraction of shortwave radiation that penetrates the open water surface layer, 0.45
κ_w	extinction coefficient of shortwave solar radiation in ocean waters, 0.1 m^{-1}
S_c	average bulk salinity of congelation sea ice, 5
S_{si}	average bulk salinity of snow ice, 10
R_T	oceanic relaxation time scale, 0.25
$\tau^\star$	relaxation time scale for advection, see Table 2.1

Chapter 1:

INTRODUCTION

The main objective of this thesis is to explore the role of sea ice–ocean feedbacks in the continental shelf seas of Antarctica using models. Of particular interest is whether the feedbacks amplify or dampen the response to atmospheric perturbations, and the relative magnitude of the feedbacks. In this thesis the importance of sea ice–ocean feedbacks on the evolution of sea ice and the ocean mixed layer in two contrasting regions of the Antarctic continental shelf ocean is investigated: the Amundsen Sea, which has warm shelf waters; and the Weddell Sea, which has cold and saline shelf waters. An overview of the Southern Ocean and the Weddell and Amundsen shelf seas is presented in Section 1.1, Antarctic sea ice processes, feedbacks and variability is discussed in Section 1.2, and the aims and outline for this thesis are given in Section 1.3.

1.1 The Southern Ocean

The Southern Ocean (SO) is the largest ocean on Earth, completely encircling Antarctica, and connecting the three main ocean basins, the Atlantic, Pacific and the Indian. The Antarctic Circumpolar Current (ACC) is a strong zonal, geostrophic circulation that flows eastward in the latitude band of Drake Passage, driven by strong westerly winds. The ACC mixes water masses from the Earth's ocean basins, allowing climate signals to be passed on from each of the basins, and zonally homogenising the water mass properties (Rintoul and Naveira Garabato, 2013). Estimates of the ACC transport range between 130 Sv (1 Sv = 10^6 m^3 s^{-1}) (Whitworth et al., 1982) up to 170 Sv, with more recent estimates falling in the upper part of the range (Cunningham et al., 2003; Donohue et al., 2016). The westerly winds also drive a northwards surface Ekman current, causing a region of convergences where the ACC is strongest, this is known as the Antarctic Polar Frontal Zone (APFZ). There are several strong jets/currents within this zone (Colling, 1994).

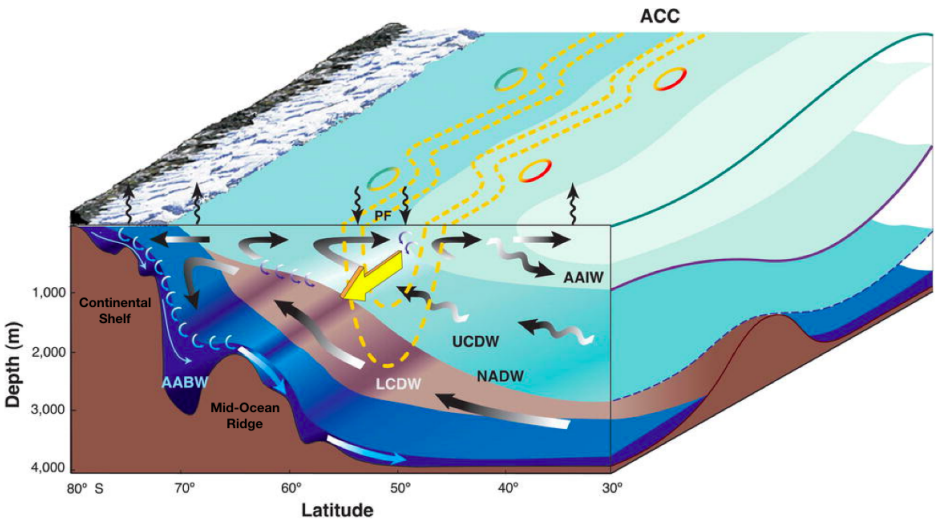

Figure 1.1: *Edited schematic of the ACC system in the SO from Olbers and Visbck (2005), based on the schematic of (Speer et al., 2000). The Eastward flow the ACC are indicated by the yellow arrow and dashed yellow lines. There are two cells, the upper cell is composed of a northward Ekman transport due to the strong, westerlies, and a southward transport of UCDW. The lower cell is driven by the formation of AABW over the continental shelves, and the inflow of LCDW/UCDW/NADW. Dark arrows represent the overturning circulation, with wavy arrows representing the eddy transports. Coloured surfaces indicate isopycnals. The thin, wavy, black arrows indicate air–sea buoyancy exchange (upwards represent buoyancy loss form the ocean, and vice versa). Small, wavy, blue arrows represent diapycnal mixing.*

The isopycnals in the SO slope away from the Antarctic continent, due to the northward surface Ekman flow (driven by the westerlies), and the meridional buoyancy gradient. The slope of the isopycnals is set by the balance of these steepening forces, balanced by mesoscale eddies which act to flatten the isopycnals (Karsten and Marshall, 2002). The sloping of the isopycnals allows deep waters to outcrop in the SO, exchanging heat and CO_2 with the atmosphere. A schematic of the zonal and meridional structure of the ACC is given in Figure 1.1.

The most voluminous water mass of the SO is Circumpolar Deep Water (CDW), which is a mixture of the water masses from the three main ocean basins (Talley, 2013). CDW can be split into two sub categories: Upper Circumpolar Deep Water (UCDW) and Lower Circumpolar Deep Water (LCDW). UCDW is formed from adiabatic upwelling of Pacific Deep Water (PDW) and Indian Deep Water (IDW). Some UCDW goes on to form Antarctic Bottom Water (AABW), and some goes on to form Sub Antarctic Mode Water (SAMW). The PDW and IDW source can be identified by the relatively old (compared to Atlantic deep waters) ventilation age, and the distinctive low oxygen and high nutrient content of the PDW and IDW. LCDW is North Atlantic Deep Water (NADW) which has been upwelled adiabatically, this is then recycled to form AABW (Warren, 1990). LCDW is denser than UCDW due to the high salinity of the NADW, and outcrops further south than UCDW (Talley, 2013), as shown in Figure 1.1. A schematic of the water mass interactions described, and the global overturning circulation from a Southern Ocean perspective

is shown in Figure 1.2.

There are two cells/limbs of the overturning circulation in the Southern Ocean, see Figure 1.1. The upper limb is composed of the upwelling of UCDW, and subsequent equatorward transport and conversion into intermediate waters. This ventilation of deep waters exchanges large amounts of heat and CO_2 with the atmosphere. It is estimated that 40% of global anthropogenic CO_2 enters the ocean poleward of 40°S (Khatiwala et al., 2009, 2013), into the freshly upwelled waters traveling northward through regions of large wind stress and large air–sea fluxes (Gruber et al., 2019).

The westerlies over the SO are one of the energy sources for the Meridional Overturning Circulation (MOC) (Kuhlbrodt et al., 2007). It is believed that stronger westerlies drive stronger Northward Ekman transports, and enhanced upwelling to the south of the ACC (Hall and Visbeck, 2002). Changes in the wind driven upwelling of deep waters in the SO is believed to have caused changes in the global climate and carbon cycle in the past (Toggweiler et al., 2006). Increased ventilation of Antarctic deep waters has been linked to the deglacial rise in atmospheric CO_2 (Anderson et al., 2009; Skinner et al., 2010). Skinner et al. (2010) suggests that during glacial times less water was upwelled, resulting in older ventilation ages. Then during deglacial times the old, CO_2 rich water was brought into contact with the atmosphere, releasing large amounts

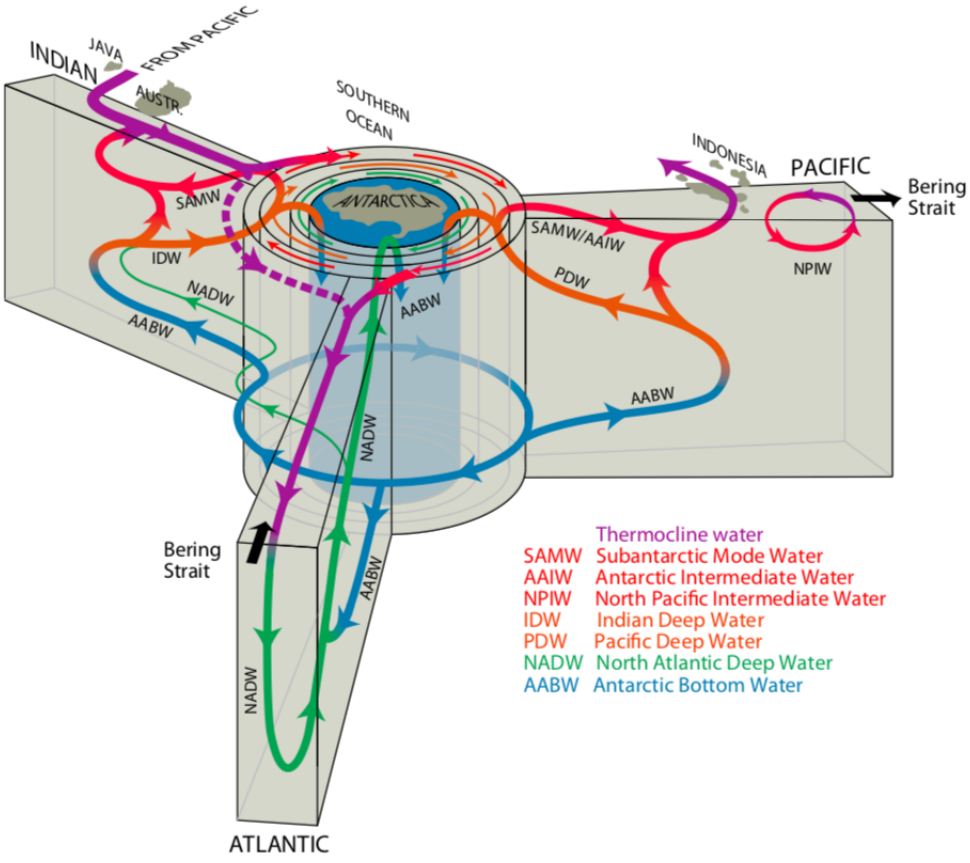

Figure 1.2: *Schematic of a Southern Ocean perspective of the global overturning circulation, taken from Talley (2013).*

of CO_2. The exact relationship of the MOC to the SO westerlies is uncertain. Results from eddy permitting models suggest that approximately 50% of the change in the wind driven Ekman flow is compensated by mesoscale eddies (Meredith et al., 2012; Morrison and Hogg, 2013; Gent, 2016).

Studies have suggested that the water mass conversion of the upwelled waters to mode and intermediate waters in the upper limb is aided by sea ice. The transport by the winds and gyres of sea ice away from formation sites and subsequent melting further north, acts to transport freshwater to lower latitudes (Abernathey et al., 2016; Haumann et al., 2016; Pellichero et al., 2017, 2018). This surface freshwater flux acts to help convert upwelled deep water to lighter intermediate and mode waters in the upper limb of the MOC. It is believed that this may be a dominant buoyancy contribution to the upper limb of the MOC (Pellichero et al., 2017, 2018), and therefore formation and subsequent transport of Antarctic sea ice may have consequences for the strength of the MOC, transporting a signal of Antarctic sea ice changes to the rest of the global climate system.

The lower cell is composed of the upwelling further south of the ACC of LCDW/NADW, which is subsequently converted into AABW through cooling and salinification from sea ice growth, sinking to fill the abyssal ocean. Relatively little carbon exchange occurs during the formation of AABW due to sea ice acting as a barrier to ocean–atmosphere exchange (Gruber et al., 2019). The formation of AABW is discussed further in Section 1.1.1.

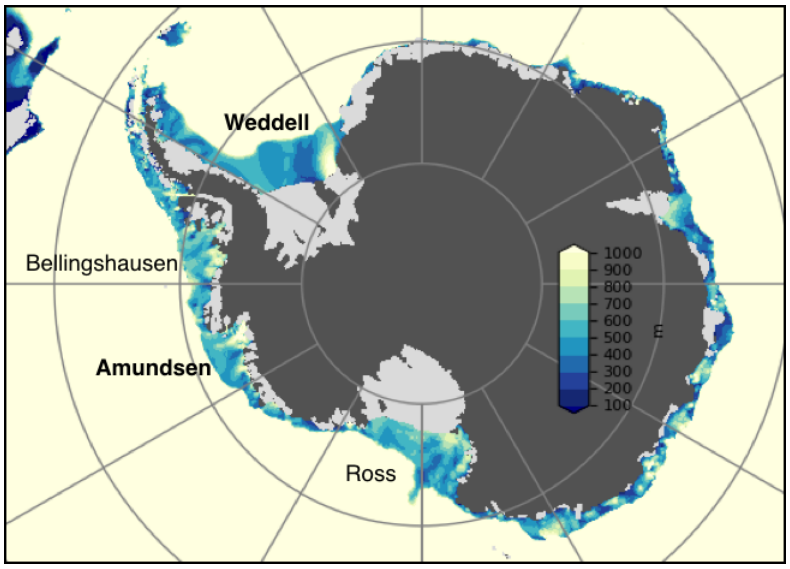

Figure 1.3: *Bathymetry of the Southern Ocean. The bathymetry and landmask are taken from the RTOPO dataset (Timmermann et al., 2010).*

At the Southern limit of the SO are the Antarctic continental shelf seas. This is where the continental shelf extends away from the coastline, up until a continental slope, where the depth rapidly increases to the deep ocean floor. Some examples of the larger Antarctic shelf seas

are found in the Weddell, Ross, Amundsen and Bellingshausen Seas, extending several hundred kilometres from the Antarctic coastline, see Figure 1.3. Definition of the Northward extent is usually taken to be given by the sudden change in depth/the bathymetry, which is taken to be the slope break.

The Antarctic shelf seas play an important role in the Antarctic, and global climate systems. The Weddell and Ross seas cool and ventilate the deep ocean through formation of AABW, feeding the lower limb of the Meridional Overturning Circulation (MOC). Meanwhile the Amundsen and Bellingshausen seas have a much closer proximity to the ACC, exposing their shelves to CDW. The presence of warm CDW on the continental shelf in the Amundsen Sea has been implicated in causing increased basal melting of the West Antarctic Ice Sheet (WAIS) (Shepherd et al., 2004). In this thesis the Weddell and the Amundsen Seas have been used as case studies to study the sea ice–ocean interactions in each of these Antarctic continental shelf sea regimes.

1.1.1 Weddell Sea

In the southwestern Weddell Sea (WS) the deep ocean is ventilated, and AABW, the densest water mass, is formed. AABW fills the abyssal ocean and is a collective term for non–circumpolar bottom waters that formed around Antarctica. It is found south of the CDW in the ACC (Orsi et al., 1999). It is estimated that over half of all AABW is formed in the Weddell Sea (Orsi et al., 1999) from High Salinity Shelf Water (HSSW).

To the North of the continental shelf is Warm Deep Water (WDW). WDW is formed from CDW, which enters the northeastern part of the Weddell gyre and is mixed with cold surface waters (Fahrbach et al., 1994). Below WDW is Weddell Sea Deep Water (WSDW), a component of AABW which is underlain by an even denser component of AABW called Weddell Sea Bottom Water (WSBW). HSSW is believed to be formed from Modified Warm Deep Water (MWDW), which is an intermediate water mass formed from the mixing of Warm Deep Water (WDW) and cold mixed layer waters (known as Winter Water, WW). MWDW is thought to be the dominant water mass on the Weddell continental shelf, and therefore the source water for HSSW formation (Nicholls et al., 2009). See Figure 1.4 for a schematic showing how these water masses interact with each other.

The cold and dry katabatic winds coming off the Antarctic continent drive a large surface buoyancy loss in the southwestern WS. This helps to drive deep mixing in the WS, extending down to the sea bed. At the southern boundary of the WS, where there is a large coastal polynya due to the winds coming off the ice shelf, and the tidal divergence of surface waters. Although the surface heat loss due to the polynya is large, it is not sufficient to form HSSW alone (Nicholls et al., 2009). The gradual brine flux from the rest of the sea ice pack in the Weddell Sea over the

continental shelf is also needed (Renfrew et al., 2002). This salinification from the sea ice growth is believed to be the dominant process for HSSW formation (Nicholls et al., 2009).

There are three main pathways for HSSW to form AABW: (i) Some HSSW mixes with WDW, forming WSBW, a type of AABW. WSBW remains in the Weddell basin until it mixes with the WSDW above it in order to overcome the dynamic barrier of the shelf break front as it is too dense to escape the basin and flow northward otherwise (Foster and Carmack, 1976); (ii) Some HSSW is made denser from sea ice formation to form WSDW, and flows down the continental slope; (iii) And finally some HSSW is converted to Ice Shelf Water (ISW). When HSSW meets the base of the Filchner–Ronne ice shelf (FRIS), ISW is produced due to basal melting of the ice shelf (Foldvik and Gammelsrød, 1988). Most ISW formed is believed to leave via the Filchner depression (Foldvik et al., 2004; Wilchinsky and Feltham, 2009), and therefore not impact the water properties in the southweastern shelf sea (Nicholls et al., 2003). The ISW goes on to form a fresher variety of WSDW (Gordon et al., 1993).

The abyssal waters in the SO have been warming since the 1990s, particularly near AABW formation sites (Purkey et al., 2019). WSBW and WSDW have been warming since the 1980s (Robertson et al., 2002; Fahrbach et al., 2011; Purkey and Johnson, 2010), as have the deep waters in the Scotia Sea (Meredith et al., 2008) and Argentine Basin (Johnson and Doney, 2006) which are fed by WSBW. This warming of the abyssal waters contributes to sea level rise through thermal expansion, and has consequences for the global heat budget (Purkey and Johnson, 2013).

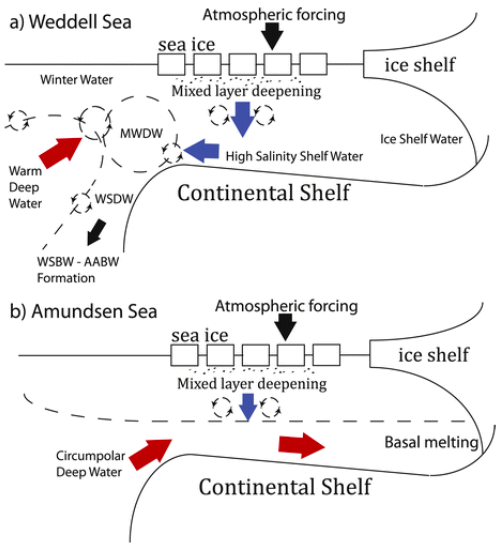

Figure 1.4: *Schematic showing processes in the (a) Weddell and (b) Amundsen Seas, edited from the schematic in Petty et al. (2013). CDW: Circumpolar Deep Water, HSSW: high salinity shelf water, MWDW: modified warm deep water, WW: Winter Water, WSDW: Weddell Sea Deep Water, WDW: warm deep water, WSBW: Weddell Sea Bottom Water, AABW: Antarctic Bottom Water, AASW: Antarctic Surface Water.*

1.1.2 Amundsen Sea

Due to the proximity of the Amundsen Sea (AS) to the ACC, the continental shelf is flooded with LCDW, overlain by WW and Antarctic Surface Water (AASW) (Jacobs et al., 2012). See Figure 1.4 for a schematic of the Amundsen continental shelf. The mixed layer depths in the Amundsen Sea are insufficient to mix into the CDW and convert it into colder shelf water, meaning that CDW persists at depth in the AS. The depth of the thermocline determines whether there is inflow of warm CDW onto the continental shelf. Increased oceanic basal melting of the ice shelves in Pine Island Bay (PIB), caused by intrusion of CDW onto the AS continental shelf has been blamed for the observed increase in the thinning of West Antarctic Ice Sheet (WAIS), particularly in PIB (Shepherd et al., 2004, 2012; Rignot et al., 2019) and therefore contributing to global sea level rise (GSLR). Complete melting of WAIS would equate to between 3 (Bamber et al., 2009) to 5 m of GSLR (Mercer, 1978), fuelling the current interest in the region.

It is believed that CDW periodically pulses onto the shelf, along glacially carved troughs and depressions in the bathymetry along the shelf break (Walker et al., 2008; Thoma et al., 2008; Wählin et al., 2010). This predominantly occurs through a particularly deep, eastern trough that extends form the ice shelf edge to the grounding line (Schodlok et al., 2012).Variations in the pycnocline/thermocline can be caused by changes in regional atmospheric conditions on both seasonal and interannual timescales (Dutrieux et al., 2014). The position of the Amundsen Sea Low (ASL), strongly influences the wind fields over the Amundsen Sea. Seasonally, the ASL moves to the West and South in winter and spring. This causes the easterlies to become westerlies over the Amundsen Sea. The eastward winds cause northward Ekman transport, tilting the sea surface up towards the north, hence driving an eastward barotropic flow that enhances the flow of warm water onto the shelf in pulses (Thoma et al., 2008). Warmer tropical Pacific sea surface temperatures have also been linked with a westward shift in the ASL, increased westerlies over the AS, and therefore increased CDW intrusion and thinning rates of glaciers in PIB (Ding et al., 2011; Steig et al., 2012; Thoma et al., 2008). As a result, trends and events in the central tropical Pacific may dictate the rate of thinning of WAIS (Steig et al., 2012). Changes in atmospheric conditions and wind fields in the region may also be triggered by ozone depletion (Turner et al., 2009), this is covered in more detail in section 1.2.2.2.

1.2 Antarctic Sea Ice

1.2.1 Seasonal sea ice processes

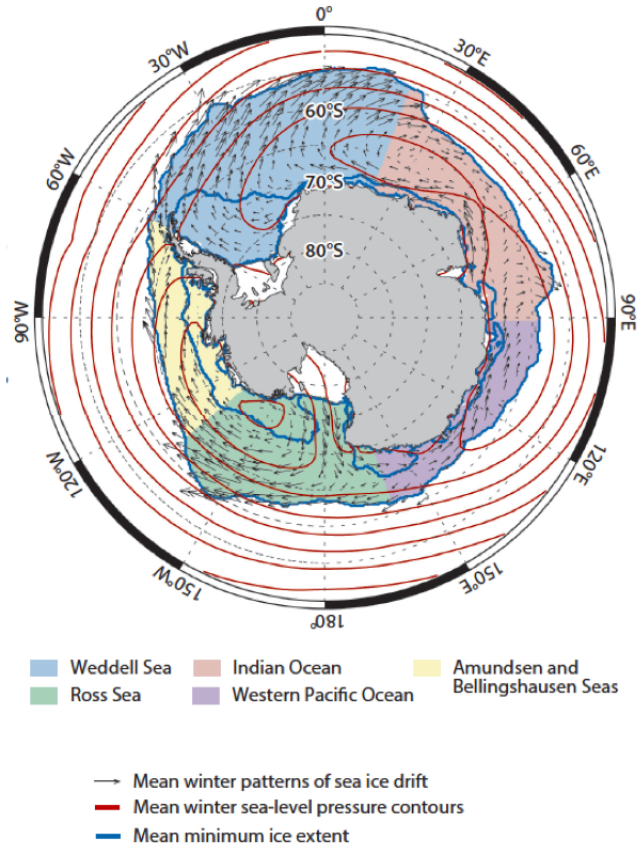

Figure 1.5: *An overview of the typical sea ice and atmospheric conditions in the Southern Ocean, taken from Maksym (2019). Coloured ocean area indicates the average (1979–2016) annual maximum (September) sea ice extent. The blue lines indicate the mean minimum (February) and maximum (September) Antarctic sea ice extent. The black arrows indicate the mean winter sea ice drift, largely driven by the winds. The red lines show the mean winter (July–September) sea level pressure contours (2-ha intervals). The sectors typically used to split up the Southern Ocean are given in different colours.*

The Antarctic sea ice cover is highly seasonal and, unlike the Arctic, there is very little multiyear sea ice (Maksym et al., 2012). This large seasonal change in sea ice extent is illustrated in Figure 1.5, which shows the average positions of the annual minimum and maximum Antarctic sea ice extent. Also see Figure 1.6 for the observed Antarctic sea ice extent time series, showing how the sea ice extent changes by a factor of 6 over the seasonal cycle each year. Sea ice forms from frazil crystals which float to the ocean surface and accumulate. In calm water the crystals eventually form a sheet of ice which thickens and expands over the winter. In turbulent ocean conditions the frazil crystals are jostled about forming disks called pancake ice. These are then consolidated together by the wave action to form a larger sheet.

Thermodynamic sea ice thickening occurs at the base of the sea ice during winter due to a vertical conductive heat flux up through the sea ice, forming congelation (columnar) ice. Thicker sea ice grows more slowly due to a reduced conductive heat flux, which acts as a negative feedback on ice thickness during the growth period. Sea ice growth results in a flux of brine into the ocean as the salt is rejected from the ice crystals, creating a negative buoyancy flux which promotes enhanced vertical mixing in the ocean. Summer sea ice melt results in a flux of freshwater to the ocean aiding restratification of the water column. During spring and summer the higher albedo of sea ice relative to open ocean means that a reduction in sea ice concentration (SIC) results in more solar shortwave radiation being absorbed by the ocean, causing the SIC to reduce further. This means that an earlier melt season delays the subsequent autumn freeze up due to this positive feedback (Perovich et al., 2011; Stammerjohn et al., 2012). The albedo feedback has been shown to be a significant contributor to Arctic amplification of global warming (Pithan and Mauritsen, 2014).

Unlike in the Arctic, in the Southern Ocean there is very little surface melting of the sea ice as it is covered by a thicker layer of snow and surface air temperatures are much colder. The snow acts to insulate the sea ice, slowing the rate of sea ice thickening and reflecting most of the incoming shortwave radiation. The thick snow layer also means that surface melt ponds are uncommon on Antarctic sea ice (Scott and Feltham, 2010), whereas in the Arctic they are prevalent and contribute to the albedo feedback. The relatively thin ice and high snowfall rates in the Southern Ocean mean that snow ice formation is widespread (Fichefet and Morales Maqueda, 1999; Massom et al., 2001). Snow ice forms if the weight of snow is great enough to force the snow-sea ice interface below the surface of the seawater, flooding the submerged snow with seawater which then freezes. The net Southern Ocean sea ice response to a snowfall increase is likely to be more sea ice (Powell et al., 2005), however the response is thought to be regionally variable, as shown in a modelling study by Wu et al. (1999), depending on whether there is sufficient snow for snow flooding to occur. It is currently unclear what role snow related processes may have played in the observed Antarctic sea ice changes, as there are large disagreements in the snowfall trends between different reanalysis products (Bromwich et al., 2011).

Sea ice is continuously moved around, primarily by the winds and also by the ocean currents. This can cause the sea ice to pile up and thicken in particular regions, e.g. to the east of the Antarctic peninsula. Trends in the wind fields are able to explain some of the observed trends in sea ice concentration (Holland and Kwok, 2012).

1.2.2 Antarctic sea ice variability

1.2.2.1 Antarctic sea ice in observations and model simulations

Satellite observations have shown Antarctic sea ice to be expanding over the past four decades (Parkinson and Cavalieri, 2012; Parkinson, 2019). Although this increasing trend is modest, it is in stark contrast to the well documented rapid Arctic sea ice decline e.g. (Parkinson and Cavalieri, 2008; Parkinson and Comiso, 2013). The small net increase is the result of stronger, opposing regional and seasonal trends (Holland, 2014). The Weddell Sea has an increasing trend in sea ice concentration which is roughly compensated by a decreasing trend in the Amundsen and Bellingshausen Seas. These observed trends grow in spring and decay in autumn, showing maximum trends in summer and no trend in the winter (Holland, 2014). After successive sea ice extent maximas in Antarctic sea ice extent in 2012 to 2014 (Reid and Massom, 2015), a rapid decline in Antarctic sea ice extent occurred 2016/2017 that has continued to the present (Stuecker et al., 2017; Turner et al., 2017; Parkinson, 2019), as shown in Figure 1.6.

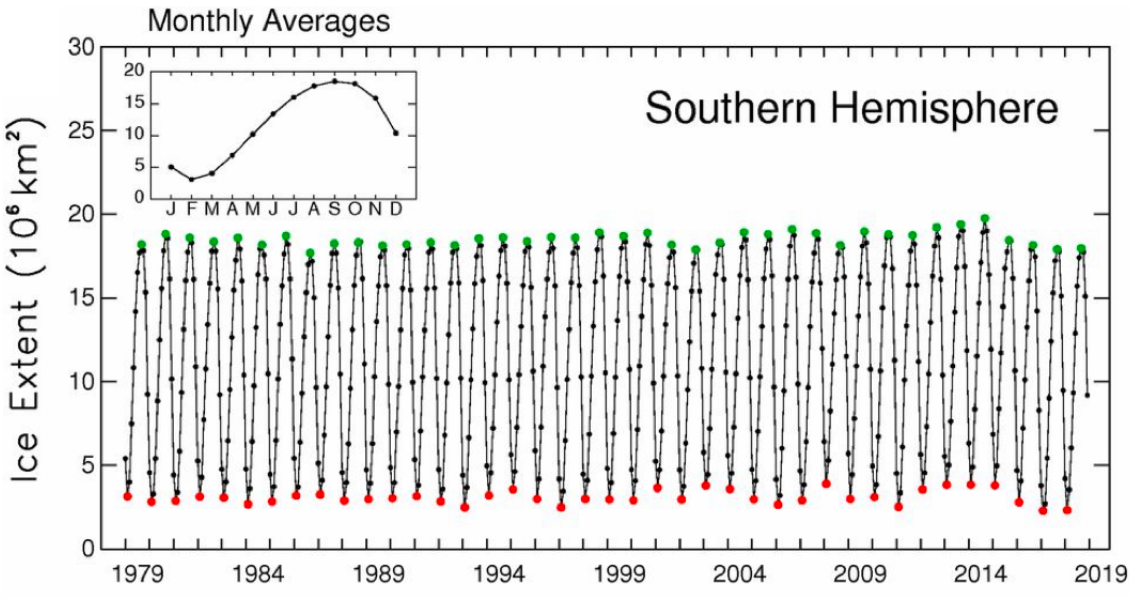

Figure 1.6: *Monthly average sea ice extent values for the Southern Hemisphere. Red dots indicate February extent values, green dots indicate September extent values, and all other months are in black. The inset graph shows the average annual cycle over the 40 years. Sea ice extents are derived from passive-microwave data from the NASA Nimbus 7 and Department of Defense DMSP satellites. Figure is taken from Parkinson (2019), see Parkinson (2019) for more details of the data set.*

Changes in the duration of the sea ice covered season can be defined as the difference between the autumn date at which the sea ice expands (date of advance) beyond a set location, until the summer date it melts (date of retreat) (Stammerjohn et al., 2008, 2012). One of the most striking changes between comparing 1979/1980 to 2010/2011 is in the Amundsen and Bellingshausen Sea the sea ice free season lengthened by 3 months, due to 1 month earlier retreat

and a 2 month later advance (Stammerjohn et al., 2012). Due to the positive ice albedo feedback, a longer summer season will mean a longer period where solar radiation can warm the ocean, acting to slow the future sea ice advance (Meredith and King, 2005). This positive feedback creates a stronger correspondence between sea ice retreat and subsequent advance than the sea ice advance and the subsequent retreat (Stammerjohn et al., 2012). Wind driven circulation changes can influence the timing and location of this feedback through ice advection, for example this leads to decreased summer open water in the Ross Sea, creating a tendency to earlier sea ice advance (Holland et al., 2017). This may explain some of the seasonality seen in the sea ice trends (Holland, 2014), where the trends grow throughout the spring and summer, possibly due to this positive ocean warming feedback.

We do not currently have an observational record of Antarctic sea ice thickness trends. In situ observations have large spatial and temporal gaps (Worby et al., 2008), and getting reliable estimates of sea ice thickness from satellites is tricky due to the thick snow covering the sea ice. Variability in the penetration of snow using radar altimetry in the Southern Ocean creates a large uncertainty in the ice freeboard, and therefore the ice thickness values (Giles et al., 2008). The freeboard can be identified by laser altimeters, then assuming that the sea ice freeboard is at sea level and using estimates for the snow thickness, snow density and ice density an estimate of ice thickness can be obtained (Kurtz and Markus, 2012; Ozsoy-cicek et al., 2013). Kurtz and Markus (2012) provides a Southern Ocean wide estimate of ice thickness using ICESat data. There is currently no observational record of the variability in Antarctic sea ice thickness and therefore of Antarctic sea ice volume variability and trends, however ICESat-2 which launched in September 2018, aims to be able to provide this. There have been a number of efforts using models to investigate Antarctic sea ice thickness trends (Holland et al., 2014; Zhang, 2014; Massonnet et al., 2013; Zhang, 2007). Largely the results of these efforts are consistent with each other and show an overall increase in Antarctic sea ice volume that is the sum of differing regional trends, and significantly smaller in magnitude than the Arctic decline in sea ice volume. Around the sea ice edge, changes in ice thickness mirror the changes in ice concentration (i.e. sea ice thickening where there is expansion). Dynamic thickening, due to advection of ice towards the coast, is seen in the inner Weddell, Amundsen and Bellingshausen Seas (Holland, 2014).

The models in the Coupled Model Intercomparison Project (CMIP5) (Taylor et al., 2012) produce a large range of projections for Antarctic sea ice extent. Few are able to produce simulations with results close to the observed satellite observations of Antarctic sea ice concentration (Turner et al., 2013; Zunz et al., 2013). Most produce a net decreasing trend over the past few decades in response to global warming, and spatial patterns of SIC trends that are inconsistent with satellite observations (Turner et al., 2013). However, the CMIP5 models also simulate a frequency distribution of ice concentration (Roach et al., 2018) and seasonal cycle in sea ice extent (Turner et al., 2013) that differs from satellite observations. Even models that

appear to simulate a realistic seasonal cycle for the Antarctic sea ice cover mostly do so due to compensating errors (Holmes et al., 2019). Due to these issues, the IPCC states that the current confidence in the ability for CMIP5 models to produce meaningful future projections of the Antarctic sea ice cover is low due to "the wide intermodel spread and the inability of almost all of the available models to reproduce the mean annual cycle, and overall increase of the Antarctic sea ice coverage observed during the satellite era" (Collins et al., 2013).

1.2.2.2 Atmospheric drivers of Antarctic sea ice variability

Local wind forcing can explain some of the trends seen in Antarctic sea ice (Holland and Kwok, 2012). The forcing can be dynamic and/or thermodynamic. Relatively cool offshore (southerly) winds can cause sea ice expansion dynamically by advecting the sea ice further Northward away from the coast, or through cooling and promoting sea ice growth. Conversely, relatively warm onshore (northerly) winds can cause contraction of the ice cover by pushing the ice back towards the coast, or through warming. Trends in the winds can explain a large proportion, but not all of the trends in Antarctic sea ice extent observed (Holland and Kwok, 2012; Holland, 2014). Dynamic wind forcing appears to dominate sea ice extent trends in the Amundsen and Ross Seas, whereas thermodynamic wind forcing dominates in the Bellingshausen Sea (Holland and Kwok, 2012; Holland, 2014; Matear et al., 2015).

Variations and trends in the winds are associated with variability in the Amundsen Sea Low (ASL), the Southern Annular Mode (SAM) and El Niño Southern Oscillation (ENSO). The Amundsen Sea Low (ASL) is a deviation from the zonal low pressure field that extends from the coast of Antarctica to just north of the sea ice cover. It is a low pressure centre centred between 110 to 150°W and 60 to 70°S (Raphael et al., 2016; Maksym, 2019), see Figure 1.5 for the average winter sea level pressure contour map. Variability in the location (Hosking et al., 2013), intensity (Holland and Kwok, 2012) and spatial extent (Clem and Fogt, 2013) of the ASL has been linked to sea ice variability in the Ross Sea, and the Amundsen and Bellingshausen Seas. A deepening of the ASL results in warm northerly winds over the Amundsen and Bellingshausen Sea (promoting sea ice loss) and cold southerly winds over the Ross Sea (promoting sea ice expansion) (Holland and Kwok, 2012). Both the SAM and ENSO influence the ASL.

The leading mode of natural variability in the Southern hemisphere, the SAM has been shown to have strong links with Antarctic sea ice extent in observations (Stammerjohn et al., 2008) and models (Hall and Visbeck, 2002; Sen Gupta and England, 2006). A positive SAM indicates a stronger sea level pressure difference between the pole and the midlatitudes in the southern hemisphere, driving a poleward shift and a strengthening of the surface westerlies. This is associated with cooler sea surface temperatures (SSTs) and northward expansion of the sea ice cover (due to increased Equator-ward surface ocean Ekman currents) on seasonal/inter-annual

timescales. The SAM has been in a mostly positive phase since the mid 1990s, and has been on an increasing trend since the mid 1960s (Marshall, 2003). This positive trend in the SAM, which is greatest in the summer/autumn (Thompson and Solomon, 2002), has been suggested as a cause of the Antarctic sea ice expansion (Thompson et al., 2000; Thompson and Solomon, 2002). The low sea ice extent from austral spring (November) 2016 through to austral spring 2017 has been associated with an early maximum winter sea ice extent, and a negative SAM index, and increased Northerly flow of warmer air masses towards the pole (Doddridge and Marshall, 2017; Stuecker et al., 2017; Turner et al., 2017).

Ozone depletion has been suggested as a possible cause of the positive summer trend in the SAM (Thompson and Solomon, 2002; Gillett and Thompson, 2003; Polvani et al., 2011; Thompson et al., 2011) from the 1970s onwards. However, a number of modelling studies (Sigmond and Fyfe, 2010; Bitz and Polvani, 2012; Sigmond and Fyfe, 2014) have shown a decrease in sea ice area in response to ozone depletion, simulating a decrease in Antarctic sea ice despite the linkage between ozone depletion and a positive SAM, and between a positive SAM and sea ice expansion. A modelling study by Ferreira and Marshall (2015) reconciled these opposing results, showing that the initial response to the ozone hole may be an increase in sea ice area, however over longer timescales (years to decades depending on the model) the change in winds may result in increased upwelling of warm waters from below the cold, fresh surface layer in the seasonal sea ice region, leading to less sea ice and warmer sea surface temperatures. This behaviour has since been displayed in other modelling studies, however the timescale for the transition in response, and the magnitude of the response remains poorly constrained (Holland et al., 2016; Seviour et al., 2016, 2017, 2019).

Extra-polar climate variability may also influence Antarctic sea ice. In particular variability in the ENSO in the tropical Pacific may play a key role in variability in sea ice in the Western section of the Southern Ocean, including the Ross, Bellingshausen and Weddell Seas (Yuan, 2004). An El Niño state triggers warming and decreased sea ice in the Bellingshausen Sea region (S. Pacific), and cooling of sea surface temperatures (SSTs) and sea ice expansion in the Weddell Sea (S. Atlantic). The opposite changes in SSTs and sea ice extent are triggered by a La Nina situation (Yuan, 2004). Kwok et al. (2016) found that around two thirds of the observed trend in the winter sea ice edge in the Pacific sector (Amundsen, Bellingshausen and Ross Seas) was due to ENSO driven trends in the winds (Kwok et al., 2016). One of the possible contributing factors for the sea ice extent decline in 2016/2017 is the extreme El Niño that peaked in December 2015 to February 2016. It resulted in anomalously warm sea surface temperatures in the Amundsen, Bellingshausen and eastern Ross Seas until the Spring of 2016, contributing to the anomalously low sea ice extent in those regions (Stuecker et al., 2017).

1.2.2.3 The role of the ocean in Antarctic sea ice variability

The surface waters in the SO have been observed to cool (Fan et al., 2014) and freshen (Durack and Wijffels, 2010), whilst the sub surface waters have been warming relatively rapidly since the 1950s (Gille, 2002, 2008). This observed increase in ocean stratification has been suggested to play a role in the observed long-term increasing Antarctic sea ice trend (Parkinson and Cavalieri, 2012) through a reduction in basal melting of the sea ice (Zhang, 2007), with a number of possible contributing factors for the observed increase in stratification.

Increased snowfall over the SO caused by an accelerated hydrological cycle due to global warming (Liu and Curry, 2010) may lead to a freshening of the surface ocean, increasing stratification. The cooler, fresher surface ocean then promotes increased sea ice growth, due to the reduced ocean-ice heat fluxes and increased freezing point. Increased snowfall may also lead to an increase in snow ice formation in some regions of the SO (Powell et al., 2005). Another increasing freshwater flux into the SO is from the increased melting of the Antarctic ice sheet (Bintanja et al., 2013; Haid et al., 2017). The lack of representation of ice sheet dynamics has been suggested as a possible reason for CMIP5 models failing to reproduce historical SO sea ice trends (Bintanja et al., 2013). The increase in ocean stratification causes warming at depth, possibly causing a positive feedback loop and increasing the basal ice sheet melting (Bronselaer et al., 2018). Although the sea ice sensitivity to freshwater injection experiments is inconsistent between models (Swart and Fyfe, 2013; Pauling et al., 2016).

A sea ice–ocean feedback in response to atmospheric perturbations, such as surface atmospheric warming, may act to increase ocean stratification. On seasonal timescales the change in stratification may be created or amplified by changes to the sea ice-ocean freshwater fluxes in response to increased atmospheric temperatures (Bitz et al., 2006; Zhang, 2007; Kirkman and Bitz, 2010). An increase in Antarctic sea ice can occur in response to atmospheric warming due to the negative feedback loop between the ice growth rate, and entrainment of warm deep waters (Martinson, 1990; Zhang, 2007). The atmospheric warming reduces the rate of sea ice growth due to a reduced winter conductive heat flux up through the ice, and therefore reduces the rate of brine rejection from sea ice growth, resulting in less entrainment of deep warm waters, and a reduction in basal melting of the sea ice. For this scenario to occur, the reduction in basal ocean melting of sea ice is larger than the decrease in ice growth due to atmospheric warming (Zhang, 2007). This feedback acts over the winter, limiting the winter ice growth and winter mixed layer depth (Martinson, 1990). However, on interannual and longer timescales the feedback loop associated with changes in ice growth is positive (Goosse and Zunz, 2014). Increased sea ice in a region increases the stratification (reducing entrainment of warm deep waters) due to the inflow of freshwater to the region (sea ice melt) and transport of brine (sea ice growth) to deeper in the water column (Goosse and Zunz, 2014; Lecomte et al., 2017).

Ocean cooling through the ice-albedo feedback could play a role in Antarctic sea ice expansion, as was mentioned earlier in Section 1.2.1. In regions where the sea ice free season has been shortening, the ocean surface may be cooled due to a reduction in solar radiation being absorbed by the surface ocean because of the increased spring/summer ice cover. This can then result in earlier sea ice growth the following autumn, acting as a positive feedback on the sea ice cover expansion. Note that all of these ocean drivers described require an initial atmospheric perturbation or driver such as surface warming or a change in the wind field in order to trigger one of the feedbacks discussed. A summary of how the feedbacks discussed could lead to an increase in Antarctic sea ice extent are illustrated in Figure 1.7.

A large proportion of the recent observed decrease in sea ice area loss was in the Weddell sea, partially due to a large open ocean polynya opening up over a shallow region called Maud Rise (Jena et al., 2019). The weak stratification in combination with a strong, relatively shallow thermocline in the region makes it susceptible for ventilation of warm sub thermocline waters, melting the sea ice (Muench et al., 2001; Lindsay et al., 2008). The last time the Weddell Polynya was observed was in the winters 1974–1976, however these were much larger than the more recently observed polynyas, and resulted in ocean mixing to depths of 4000 m or more (Gordon, 1978). The Weddell polynya is believed to be caused by warm eddies spinning off Maud Rise, carrying warm water from lower in the water column to the surface and melting the sea ice (Holland, 2001a,b). Strong storms may also trigger mixing into the warm sub thermocline waters (Francis et al., 2019; Wilson et al., 2019). Cooling of the Weddell Sea deep waters was observed during the Weddell Polynya of the late 1970s (Gordon, 1982), followed by warming (Robertson et al., 2002).

The surface ocean freshening trend in the Southern Ocean (SO) has been associated with a build up of heat at depth beneath the sea ice zone (Goosse and Zunz, 2014; Lecomte et al., 2017), and a reduction in the rate of production of AABW. Due the predicted continuation of surface freshening in the SO, the appearance of open ocean polynyas is predicted to decrease (Gordon, 2007; de Lavergne et al., 2014). However, changes in the frequency or strength of storms may counter this trend (Wilson et al., 2019).

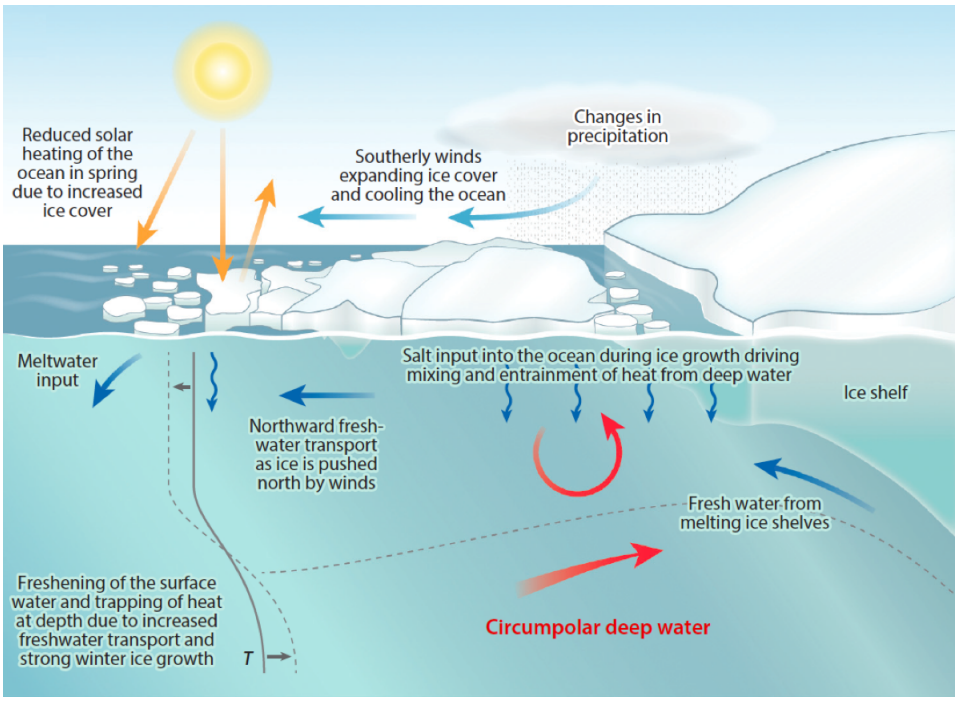

Figure 1.7: *Schematic from Maksym (2019) illustrating some of the processes that may contribute to an increase in Antarctic sea ice. These processes include: (i) stronger southerly winds cooling the ocean, and causing increased northward advection of sea ice, which acts to expand the sea ice cover to export freshwater northward; (ii) reduced ice–albedo feedback due to the a reduced open water season; (iii) freshening surface waters due to increased precipitation/melting ice shelves, and warming at depth due to strong winter ice growth deepening the winter mixed layer and trapping heat at depth, with the resulting increased stratification reducing the vertical ocean heat flux; (iv) strong winter ice growth and surface freshening acting to trap heat at depth; (v) negative feedback between ice growth and upward entrainment of heat, this may even act to increase sea ice in response to surface warming if the reduction in the basal heat flux is greater than the reduction to the sea ice growth rate. Orange and red arrows illustrate the flow of heat and warmer water, blue arrows illustrate the flow of freshwater, water (dark blue), and air (light blue).*

1.3 Thesis Aims and Outline

There is a need for a better understanding of the important feedbacks and processes in the Southern Ocean sea ice–atmosphere–ocean system, to better understand Antarctic sea ice variability in both warm and cold Antarctic shelf ocean regimes. The main objective of this thesis is to explore the role of sea ice–ocean feedbacks in the continental shelf seas. To compare the role of feedbacks in a warm, and a cold ocean regime that have contrasting atmospheric conditions, and to quantify the feedback responses to atmospheric perturbations in model simulations. Of particular interest is whether the feedbacks act to amplify or dampen the sea ice or mixed layer response to perturbations, and what the relative magnitude of the impact of each feedback is in the two continental shelf regimes. Feedbacks are tricky to observe or quantify from observations. An idealised sea ice–ocean mixed layer model was used to quantify sea ice–ocean feedbacks. Using a model allows both control of the atmospheric and oceanic conditions, and cleaner isolation

of different processes, allowing quantification and comparison of the magnitude of different feedbacks.

Global climate models are notoriously poor at simulating Antarctic sea ice, typically simulating a Southern Ocean that is too warm (Schneider and Reusch, 2016) and with too little sea ice (Turner et al., 2013). Therefore, isolating the feedbacks using an idealised model removes some of these complications, as well as allowing easier interpretation of the simulation experiments. The feedback studies should bring some insight as to the important processes in the two regions, possibly giving insight into the observed differing observed trends in the two regions. Each of the regions play a significant role in the global climate system: Antarctic Bottom Water is formed in the Weddell Sea, and the rate of its formation has been observed to decrease over recent decades (Purkey et al., 2019); whilst the intrusion of warm CDW onto the continental shelf in the Amundsen Sea has been implicated in the increasing basal melting of the glaciers in Pine Island Bay, e.g. (Shepherd et al., 2004). A fuller understanding of sea ice–ocean interactions in these two regions could help to shed further light on how these regions may change and impact global climate in the future.

Before carrying out any feedback studies, the sensitivity of the sea ice cover and mixed layer evolution to the atmospheric conditions will be investigated, in order to better understand the impact of each atmospheric forcing variable on the sea ice cover. Doing this will also help to put the magnitude of the feedback responses in context, and give an appreciation for how the feedbacks typically combine. For example, whether they help to amplify each other, or whether one feedback dominates the response and inhibits the activity other feedbacks.

The feedback studies aim to clarify which processes amplify, and which dampen the impact of perturbations to the surface atmospheric conditions on the sea ice cover and mixed layer evolution, and by what magnitude. The feedbacks of interest are: (i) *The entrainment-ice growth feedback*, a negative feedback between increases/decreases in the rate of growth of the sea ice, and increased/decreased entrainment of warm deep waters in the the mixed layer. We will look at this from two perspectives, the impact of the changes in mixed layer depth on the sea ice cover (referred to as *ocean feedback*), and the impact of the sea ice cover in determining changes in the mixed layer evolution (referred to as *sea ice feedback*). (ii) *The albedo feedback*, a positive feedback of the sea ice area, whereby an increased sea ice cover in spring reduces the amount of solar radiation absorbed by the ocean, helping to increase the sea ice cover. (iii) *The ice thickness–ice growth feedback*, a negative feedback on the rate of sea ice thickening, whereby thicker sea ice results in a reduced conductive heat flux up through the ice, and a slower rate of ice thickening; (iv) *The freezing temperature feedback*, this is a negative feedback on the ice growth rate. Increased melting of sea ice freshens the surface waters, increasing the freezing temperature of seawater, making it easier to form sea ice. The novelty of this study over previous studies is the systematic study of multiple feedbacks under the same conditions, and under two

different regimes, allowing a direct comparison of the importance of different processes.

The final aim of this thesis is to explore the impact of the ocean on the sea ice cover in the coupled CICE–mixed layer model in the Amundsen Sea, and to compare findings as much as possible to the idealised modelling work. This will allow us to examine the impact of more sophisticated sea ice physics on the response, as well as the impact of simulating response in the Amundsen Sea in the context of the whole of the Southern Ocean and not just as an isolated system, as in the case in the idealised model.

The model equations, and the underlying physical processes in the idealised model are presented in Chapter 2, alongside the atmospheric and oceanic conditions used for the Weddell and Amundsen Seas. Model development that took place is presented, in particular the inclusion of snow ice formation. The sensitivity of the sea ice cover and mixed layer to perturbations in atmospheric and oceanic conditions is investigated in Chapter 3. This enables a comparison of the magnitude of the feedback responses in the subsequent chapter to the magnitude of response to perturbations in the surface energy balance. The feedback denial results are presented in Chapter 4. The feedbacks studied in the idealised model were chosen through systematic study of the underlying model equations. The feedbacks were studied in response to perturbations in the surface air temperature (SAT), using feedback denial simulations where the feedback response to the SAT perturbation is disabled. The five feedbacks studied include: the ocean feedback, the sea ice feedback, the albedo feedback, the insulation feedback and the freezing temperature feedback. The majority of the work presented in Chapters 3 and 4 comes from the publication:

Frew, R. C., D. L Feltham., P. Holland. and A. Petty. *in press*: Sea Ice - Ocean Feedbacks in the Antarctic Shelf Seas, *Journal of Physical Oceanography*, DOI: 10.1175/JPO-D-18-0229.1

The ocean feedback on the sea ice is then investigated in the Amundsen Sea in the CICE–mixed layer model in Chapter 5. This allows the impact of more sophisticated sea ice physics on the feedback behaviour to be explored. Finally, the findings of the thesis are discussed and summarised in a conclusion in Chapter 6.

Chapter 2:

THE IDEALISED SEA ICE–OCEAN MIXED LAYER MODEL

2.1 Overview

This chapter presents the idealised sea ice–mixed layer model used in Chapters 3 and 4 for sensitivity and feedback studies. The main processes in the model and the boundary conditions are outlined in Section 2.2.5. The main developments to the model are the inclusions of snow ice formation and a prognostic snow layer, the details for this are in Section 2.2.3. The resulting simulations using the idealised model for the Weddell and Amundsen Seas using climatological atmospheric forcing, and using a time series of ERA-Interim atmospheric forcing 1980–2016 to compare interannual variability are presented in Sections 2.3.3 and 2.3.4, followed by a summary in Section 2.4.

2.2 The Sea Ice–Mixed Layer Model

The idealised sea ice–mixed layer model is based on the coupled sea ice–mixed layer model used in Petty et al. (2013). This section summarises the details of the model in Petty et al. (2013), with the details of any changes to the model. A schematic in Figure 2.1 illustrates the heat and salt fluxes in the model. The coupled mixed layer-sea ice model (see the schematic in Figure 2.1) uses the balance of heat fluxes at the sea ice–air and ocean–air interfaces to calculate the surface temperatures. Energy balance equations are used to calculate basal and lateral freezing/melting of sea ice. The entrainment rate is calculated from a balance of buoyancy fluxes and turbulent mixing (from wind shearing) and the mixed layer temperature and salinity are calculated from balance equations. The ambient water properties (temperature and salinity) below the mixed layer are given by vertical profiles that relax back to the imposed, initial profile after shoaling of

the mixed layer. The heat and salt fluxes along with the sea ice thickness, concentration, snow and snow ice thickness and ocean mixed layer are illustrated in Figure 2.1. The following subsections give a description of each of the model components. For values of variables, constants and fixed parameters used, see Tables 0.2, 0.3, and 0.4.

2.2.1 Surface heat balance

The snow covered surface ice temperature T_S^i is calculated following Maykut and Untersteiner (1971), by balancing the atmospheric surface heat fluxes (sensible, latent, blackbody, incoming longwave, and incoming shortwave heat fluxes) and the conductive heat flux upwards through the sea ice as

$$\rho_a c_a C_D^i U_a (T_S^i - T_a) + \rho_a L_s C_D^i U_a (q_{sat}(T_S^i) - q_a) + \epsilon_s \sigma (T_S^i)^4 - \epsilon_s F_{lw}\downarrow - (1-\alpha_s) F_{sw}\downarrow = F_c(T_S^i)\uparrow, \tag{2.1}$$

and the open water surface temperature T_S^o is calculated by balancing the atmospheric surface heat fluxes with the heat flux from the mixed layer to the open water surface ocean

$$\begin{aligned} \rho_a c_a C_D^o U_a (T_S^o - T_a) + \rho_a L_s C_D^o U_a (q_{sat}(T_S^o) - q_a) + \epsilon_w \sigma (T_S^o)^4 - \epsilon_w F_{lw}\downarrow \\ -(1-\alpha_w)[1 - I_o(0)] F_{sw}\downarrow = F_{mo}(T_S^o)\uparrow, \end{aligned} \tag{2.2}$$

where U_a is the wind speed at 10 m, q_{sat} is the saturation specific humidity, q_a is the specific

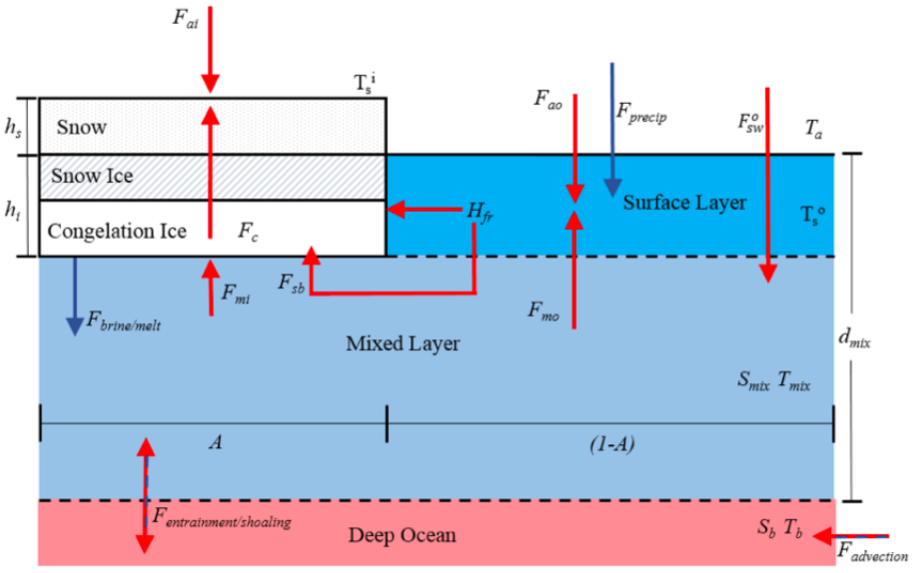

Figure 2.1: *Schematic of the sea ice–mixed layer model. Heat fluxes are in red, freshwater/salt fluxes are in navy blue. Adapted from Petty et al. (2013).*

air humidity at 2 m, $F_{lw}\downarrow$ is the incoming longwave radiation heat flux, $F_{sw}\downarrow$ is the incoming shortwave radiation heat flux. All other variables and constants are defined in Tables 0.2 and 0.3.

2.2.2 Sea ice thermodynamics

The zero–layer sea ice model has been used (Semtner, 1976), this assumes that there is a linear temperature gradient through the snow and sea ice, with the conductive heat flux F_c given by

$$F_c = \frac{k_i k_s (T_f - T_S^i)}{(k_i h_s + k_s h_i)}, \tag{2.3}$$

where h_i is the ice thickness, h_s is the snow thickness, and T_f is the freezing temperature of seawater (the mixed layer), given as $T_f = 273.15 - 0.054 S_{mix}$, where S_{mix} is the mixed layer salinity.

The heat flux to the base of the sea ice from the ocean mixed layer F_{mi} is

$$F_{mi} = \rho_w c_w c_h u_\star^i (T_{mix} - T_f), \tag{2.4}$$

where $u_\star^i$ is the friction velocity between the ice and the mixed layer, and T_{mix} is the temperature of the mixed layer. The heat flux from the mixed layer to the open water surface layer F_{mo} is

$$F_{mo} = \rho_w c_w u_\star^o (T_{mix} - T_S^o), \tag{2.5}$$

where $u_\star^o$ is the friction velocity between the open water surface layer and the mixed layer.

The rate of change of ice concentration $\frac{dA}{dt}$ is calculated by balancing the ocean surface heat potential, with the latent heat released/absorbed by the ice growth/melt as

$$\frac{dA}{dt} = \begin{cases} \frac{H_{fr}(1-A)}{L_f \rho_i h_i} & \text{for } A < A_{max} \text{ and } T_S^o < T_f \text{ (freezing)} \\ \frac{H_{fr}(1-R_b)(1-A)}{L_f \rho_i h_i} & \text{for } A > 0 \text{ and } T_S^o > T_f \text{ (melting)} \\ 0 & \text{otherwise,} \end{cases} \tag{2.6}$$

where A is the ice concentration and the maximum ice concentration value, A_{max} is 0.95. Setting $A_{max} < 1$ represents the net effect of processes that are unresolved in the model, for example advection of ice by winds opening up leads. The ocean surface heat potential H_{fr} is given as

$$H_{fr} = F_{mo}(T_S^o) - F_{mo}(T_f) = \rho_w c_w u_\star^o (T_f - T_S^o), \tag{2.7}$$

and $F_{mo}(T_f)$ is used later in the calculation of the resultant temperature change of the mixed

layer, except for when $A = 0$ and $T_S^o > T_f$. Once the ice concentration has expanded to the maximum value so that $A = A_{max}$, the ocean surface heat potential is used to grow ice vertically. This vertical growth $\frac{dh_i^R}{dt}$ is considered to be due to redistribution of the sea ice grown in the permanent lead fraction $(1 - A_{max})$ through pressure ridging.

A significant percentage of the ocean surface heat potential is believed to contribute to basal melting instead of lateral melting (Maykut and Perovich, 1987). The parameter R_b is used to partition the melt. $R_b = 0$ when all melt is lateral, and $R_b = 1$ when all melt is basal, giving a basal heat flux F_{sb} of

$$F_{sb} = \begin{cases} -H_{fr} R_b (1 - A) & \text{for } A > 0 \text{ and } T_S^o > T_f \\ 0 & \text{otherwise.} \end{cases} \tag{2.8}$$

The rate of basal melting or freezing $\frac{dh_i}{dt}$ depends on the sum of the heat fluxes at the mixed layer–ice interface, which gives

$$\frac{dh_i}{dt} = (F_c - F_{mi} - F_{sb})/(\rho_i L_f), \tag{2.9}$$

where a positive (negative) value of $\frac{dh_i}{dt}$ indicates basal ice growth (melting).

2.2.3 Snow and snow ice

This subsection details the addition of snow ice formation to the model. In the original (Petty et al., 2013) model, the snow layer had a fixed depth. This has been adapted so that the thickness of snow h_s is governed by

$$\frac{dh_s}{dt} = P - S - F, \tag{2.10}$$

where P is the rate of precipitation (assumed to be all snowfall), S is the rate of sublimation and F is the rate of snow ice formation. There is assumed to be no surface melting of the snow.

If the ice expands laterally, the existing snow layer is redistributed to conserve the mass of snow. This decreases the average snow thickness, reflecting the increase in newly formed sea ice which is not yet snow covered. If the ice concentration decreases, then the snow covering that area of ice also melts and acts to freshen the mixed layer, in this instance the snow thickness remains the same, but the volume has decreased. Under all scenarios the albedo of the (snow covered) ice fraction remains constant.

Whenever the weight of snow is great enough it pushes the snow-ice interface below the surface of the ocean so that the snow that is below the ocean surface floods with seawater and

freezes to form snow ice. Sampled snow ice is found to be saltier than congelation sea ice, which we have assumed to be 5 psu. The salinity of the snow ice formed is set to 10 psu in the model, which falls within the observed range of values (Jutras et al., 2016). This means that the volume of brine release per unit volume of snow ice formed is lower than that of congelation ice formation. In the situation that all the congelation sea ice below has melted, and the snow ice is melting, less freshwater per unit volume will be released into the mixed layer.
Assuming that the snow and sea ice are in hydrostatic balance, with the ice/snow interface at sea level,

$$\rho_i h_i + \rho_s h_s = \rho_{sw} h_i, \tag{2.11}$$

where ρ_i is the density of sea ice (both congelation and snow ice), ρ_{sw} is the density of sea water, ρ_s is the density of snow, h_s is the thickness of snow, and h_i is the total sea ice thickness (congelation + snow ice). The relatively small variations in density between congelation and snow ice is assumed to be small enough to be neglected in this simple model.

On a given timestep of equation 2.11 the snow ice interface lies below sea level whenever

$$h^* = h_s - \frac{(\rho_{sw} - \rho_i)h_i}{\rho s} > 0. \tag{2.12}$$

In this case snow ice is instantly formed so that $h_i \to h_i + \delta h$ and $h_s \to h_s - \delta h$, where δh is the thickness of submerged snow. Due to the influx of seawater flooding the submerged snow the mass of snow ice formed is not equal to the mass of snow lost; the thickness of snow ice formed is equal to the thickness of snow lost.

Choosing δh such that (2.11) is satisfied yields

$$\delta h = \frac{\rho_s}{\rho_s + \rho_{sw} - \rho_i} h^*. \tag{2.13}$$

The effective salinity (after partial brine escape) of the water that is trapped in the submerged snow, S_{trap}, is given by

$$S_{trap} = \frac{S_{si}}{1 - \frac{\rho_s}{\rho_i}}, \tag{2.14}$$

where $1 - \frac{\rho_s}{\rho_i}$ is the snow pore fraction. The salt flux into the mixed layer due to snow ice formation, F_{si} for a given sea ice concentration A is then given by

$$F_{si} = \begin{cases} (S_{mix} - S_{trap})(1 - \frac{\rho_s}{\rho_i})\frac{dh}{dt}A, & \text{for } \delta h > 0 \\ 0 & \text{otherwise,} \end{cases} \tag{2.15}$$

where S_{mix} is the mixed layer salinity, S_{si} is the salinity of the snow ice formed and $\frac{dh}{dt}$ is the rate of snow ice thickening. The associated heat release from snow ice formation is assumed to be predominantly lost to the atmosphere and is neglected in the model.

2.2.4 Ice dynamics

Ice dynamics are predominantly neglected within the model. In Petty et al. (2013) there is a sink of ice concentration due to ice divergence. This has been modified to reflect the influence of ice advection across ice thickness gradients on the vertical structure of the ice. Ice advection is parameterised in the model as a relaxation over time scale τ^*, towards a reference ice concentration A^{ref} and vertical ice structure (total ice thickness h_i^{ref}, snow ice thickness h_{si}^{ref} and snow thickness h_s^{ref}) values. These reference values represent typical ice concentration and ice thickness values being advected into the simulated region, and are given in Table 2.1. Physically this is representing sea ice being flushed through the region, altering the ice concentration, ice thickness and snow ice thickness.

2.2.5 Mixed layer model

The mixed layer model component is based on the bulk mixed layer model of Kraus and Turner (1967) and Niiler and Kraus (1977), and is largely similar to the model used in (Petty et al., 2013). It is assumed that temperature and salinity are uniform throughout the mixed layer, and that there is a complete balance of turbulent kinetic energy (TKE) sources and sinks.There are more sophisticated one dimensional mixed layer models (Large et al., 1994; Price et al., 1986; Mellow and Yamada, 1982), however a number of these, as well as the Kraus and Turner (1967) model have been shown to overestimate entrainment in the Weddell Sea region (Timmermann and Beckmann, 2004; Timmermann and Losch, 2005). However, despite the overestimation of entrainment, the simplicity of the Kraus and Turner (1967) model is ideal for the feedback studies we utilise it for, as it means that we can more easily interpret the results. The computational efficiency has also allowed us to carry out a large number of sensitivity simulations.

	Amundsen	Weddell
τ^* (yr^{-1})	0.6	1.0
A^{ref}	0.2	0.2
h_i^{ref} (m)	0.5	1.0
h_{si}^{ref} (m)	0.1	0.2
h_s^{ref} (m)	0.2	0.3

Table 2.1: Reference ice and snow values used in the advection parameterisation for the Amundsen and Weddell model set ups.

2.2.5.1 Surface Buoyancy Fluxes

The rate of mechanical energy input from surface buoyancy forces to the mixed layer (power input per unit mass per unit area) is computed as

$$P_B = c_2 d_{mix}(\frac{g\alpha}{\rho_w c_w})F_T \uparrow - g\beta F_S \uparrow, \tag{2.16}$$

where d_{mix} is the mixed layer depth and c_2 is a coefficient characterising the power dissipation as a result of convective mixing and has a value of 1 (0.8) when the mixed layer is losing (gaining) energy (Tang, 1991). The heat F_T and salt F_S fluxes out of the mixed layer are given as

$$F_T \uparrow = (1 - A)(F_{mo} - F^o_{sw} \downarrow) + AF_{mi}, \tag{2.17}$$

$$F_S \uparrow = \frac{\rho_i}{\rho_\omega}(S_i - S_{mix})[\frac{dh_i}{dt}A + \frac{dA}{dt}h_i] + (P - E)S_{mix}(1 - A) + F_{sm} \uparrow - F_{si} \uparrow, \tag{2.18}$$

where the sea ice salinity S_i is equal to S_c, the salinity of congelation ice whenever congelation ice is forming/melting, and is equal to S_{si}, the salinity of snow ice whenever snow ice is being melted. $F_{sm} \uparrow$ is the freshwater flux into the mixed layer from snow whenever the ice concentration decreases, and snow melt is released into the mixed layer, calculated as

$$F_{sm} \uparrow = \begin{cases} \frac{dA}{dt} h_s S_{mix} \frac{\rho_s}{\rho_w}, & \text{for } \frac{dA}{dt} < 0 \\ 0, & \text{otherwise,} \end{cases} \tag{2.19}$$

and $F_{si} \uparrow$ is the salt release into the mixed layer due to snow ice formation, calculated as

$$F_{si} \uparrow = \begin{cases} (S_{mix} - S_{trap})(1 - \frac{\rho_s}{\rho_i})\delta h_{si} A, & \text{for } \frac{dh_{si}}{dt} > 0 \\ 0, & \text{otherwise,} \end{cases} \tag{2.20}$$

where S_{mix} is the mixed layer salinity (the practical salinity scale is used), P is the precipitation rate, E is the evaporation rate, calculated from the latent heat flux over the open water surface. Note that equation 2.18 differs from equation 13 in Petty et al. (2013). The term representing brine rejection into the mixed layer from ridging has been removed. The thickening here is dynamic, not thermodynamic growth, and therefore should not result in brine rejection. The shortwave radiation that enters the open water fraction is absorbed in the mixed layer (the surface layer is assumed to completely absorb incoming longwave radiation (Maykut and Untersteiner, 1971)), and is calculated as

$$F^o_{sw} \downarrow = F_{sw} \downarrow (1 - e^{\kappa_w d_{mix}})(1 - \alpha_w) I_0(0). \tag{2.21}$$

Over the ice fraction, the snow layer absorbs all non–reflected solar radiation.

2.2.5.2 Wind Mixing

The rate of turbulent kinetic energy (TKE) input from wind stirring into the mixed layer is given by

$$P_w = c_1 e^{-d_{mix}/d_w} u_\star^3, \tag{2.22}$$

where the effective friction velocity at the upper surface of the mixed layer $u_\star$ is calculated, assuming free drift, as

$$u_\star = U_a \sqrt{(\rho_a/\rho_w)[AC_D^i + (1-A)C_D^o]}. \tag{2.23}$$

2.2.5.3 Mixed Layer Entrainment

The power needed to entrain deep water into the mixed layer at rate w is calculated as

$$P_E = w(d_{mix}\Delta b + c_m^2), \tag{2.24}$$

where c_m is a bulk turbulent velocity scale describing the turbulent fluctuations of the mixed layer that lead to a frictional sink of TKE, and Δb is the buoyancy difference across the mixed layer base

$$\Delta b = g\alpha(T_{mix} - T_b) - g\beta(S_{mix} - S_b), \tag{2.25}$$

where T_b and S_b are the temperature and salinity directly beneath the base of the mixed layer.

Constructing an energy balance for the mixed layer from (2.16), (2.22) and (2.24) gives an entrainment rate

$$w = \frac{dd_{mix}}{dt} = \frac{1}{d_{mix}\Delta b + c_m^2}(P_w + P_B). \tag{2.26}$$

This equation is used to deepen and shoal the depth of the mixed layer.

The temperature and salinity evolution of the mixed layer are given by the conservation equations for heat and salt

$$\frac{dT_{mix}}{dt} = \begin{cases} \frac{-F_T\uparrow}{\rho_w c_w d_{mix}} + \frac{w}{d_{mix}}(T_b - T_{mix}) & \text{for } w > 0 \\ \frac{-F_T\uparrow}{\rho_w c_w d_{mix}}, & \text{for } w \leq 0, \end{cases} \tag{2.27}$$

$$\frac{dS_{mix}}{dt} = \begin{cases} \frac{-F_S\uparrow}{d_{mix}} + \frac{w}{d_{mix}}(S_b - S_{mix}) & \text{for } w > 0 \\ \frac{-F_S\uparrow}{d_{mix}}, & \text{for } w \leq 0, \end{cases} \tag{2.28}$$

which show that whenever the mixed layer shoals, T_{mix} and S_{mix} can only change through the surface fluxes and not from advection of the ambient properties. This is also true whenever the water column is completely destratified, representing when the mixed layer has reached the shelf seabed.

2.3 Application of the Model to the Weddell and Amundsen Seas

The model needs to be driven by boundary conditions and set up with initial conditions suitable for the regions being simulated. The boundary conditions and initial conditions for the atmospheric and oceanic conditions used for the Weddell and Amundsen Seas are described in this section.

2.3.1 Atmospheric conditions

ERA Interim reanalysis data (Dee et al., 2011) was used to create climatological forcings. The forcing data has been spatially averaged over the boxed regions in Figure 2.2 and temporally averaged over 38 years (1979-2016) from 12 hr data. The fields are shown in Figure 2.3 and 2.4; the black lines show the smoothed (15 day) climatological forcing fields. The smoothed upper and lower standard deviations (+/- σ) are plotted in red and blue (for precipitation the 84th and 16th percentiles are used, due to the skewed distribution), and are calculated using a 2.5 day averaging window. The 2.5 day time scale is the auto–decorrelation time-scale, taken to be the time for weather systems to pass over the modelled regions. The autocorrelations for all of the variables after the mean has been removed are shown in Figure 2.5 and Figure 2.6. The 2.5 day averaging window was used to reduce the impact of short period, high amplitude variability present in the forcing fields caused by storms, on the standard deviations. The wind speed is cubed in equation 2.22, which calculates the momentum transfer to the mixed layer, therefore the wind speed was cubed before any spatial and temporal averaging.

The 2 m surface air temperatures (SATs) show a clear seasonal cycle in both regions. SATs in the Amundsen Sea reach a minimum of -15 °C whilst the Weddell Sea reach a lower winter minimum of -25 °C. The standard deviation is largest in the winter with the Amundsen Sea region displaying greater variability. Both regions display low variability in the summer where SATs are consistent around 0 °C. The 2 m specific humidity is also greater in the Amundsen than in the Weddell Sea, as would be expected due to the cold, dry katabatic winds coming off from the continent in the Weddell Sea region. In the Amundsen Sea the standard deviation seen is larger

in the winter than in the summer, but in the Weddell Sea the standard deviation is more uniform throughout the year, and is just slightly larger in the winter. The incoming longwave radiation also shows slightly greater variability in the winter, with the Amundsen Sea displaying greater variability than the Weddell Sea region. The incoming shortwave radiation shows a clear seasonal cycle which is similar in both regions, going from 0 Wm^{-2} in the winter to a maximum of 300 Wm^{-2} in the summer, when the maximum standard deviation is shown. The wind speed is greater in the Amundsen Sea by around 1 ms^{-1}. Both regions display a similar standard deviation all year round, and a seasonal cycle that has an amplitude of 2 ms^{-1}. The snowfall rate and interannual variability is greater for the Amundsen Sea. Typical snowfall values in the Amundsen Sea are 1.5×10^{-4} $\mathrm{kgm}^{-2}\mathrm{s}^{-1}$ and in the Weddell Sea are 1×10^{-5} $\mathrm{kgm}^{-2}\mathrm{s}^{-1}$.

2.3.2 Ocean profiles

Our model is initialised with representative summer–time profiles of temperature and salinity for the Amundsen and Weddell Seas that are the same as those used in Petty et al. (2013). The profiles are shown in Figure 2.7. Observations of the Amundsen Sea suggest a surface layer of near freezing water, typically extending to a depth of 200 m (Walker et al., 2008; Jacobs et al., 2011), although observations of the depth of this layer do range from 100 m to 300 m (Jacobs et al 1996, Dutrieux et al 2014). Below the mixed layer, observations indicate that the temperature rises up to values of +1°C at about 600 m. The Amundsen shelf sea is filled with warm (+1°C) Circumpolar Deep Water (CDW) (Jacobs et al., 1996, 2011; Walker et al., 2008). CDW intrudes beneath the ice shelves in the Amundsen Sea, where, as a result of basal melting, it is implicated in ice loss from West Antarctica (Shepherd et al., 2004). The salinity increases approximately linearly from 33.8 to 34 at the surface to 34.5 at 600 m (Walker et al., 2008; Dutrieux et al., 2014). Our temperature and salinity profiles used for the Amundsen Sea simulations are in good agreement with these observations.

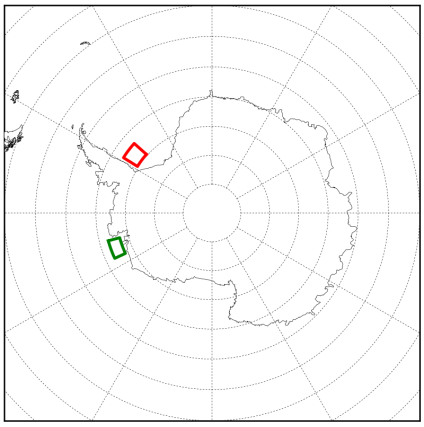

Figure 2.2: *Latitude-longitude boxes used for spatial averaging of atmospheric forcings, the Weddell Sea is marked in red and the Amundsen Sea is marked in green.*

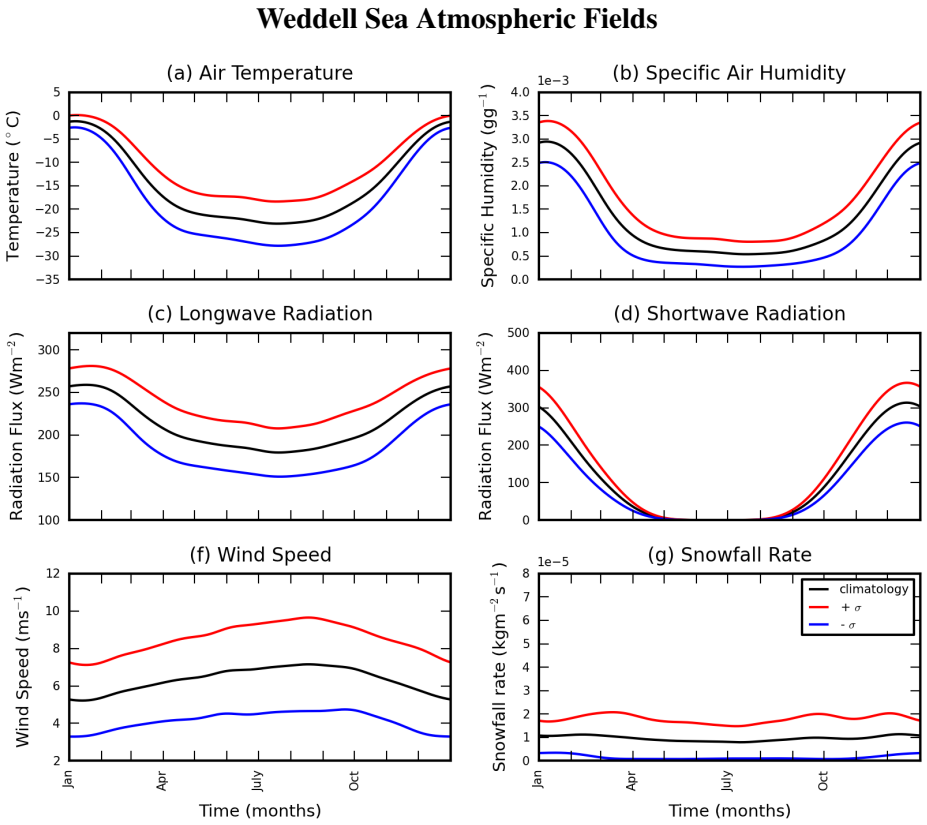

Figure 2.3: *Climatology for the Weddell Sea, calculated from ERA-I reanalysis, 1979–2016, over the latitude longitude region; 58°W to 48.5°W, 72°S to 74.8°S.*

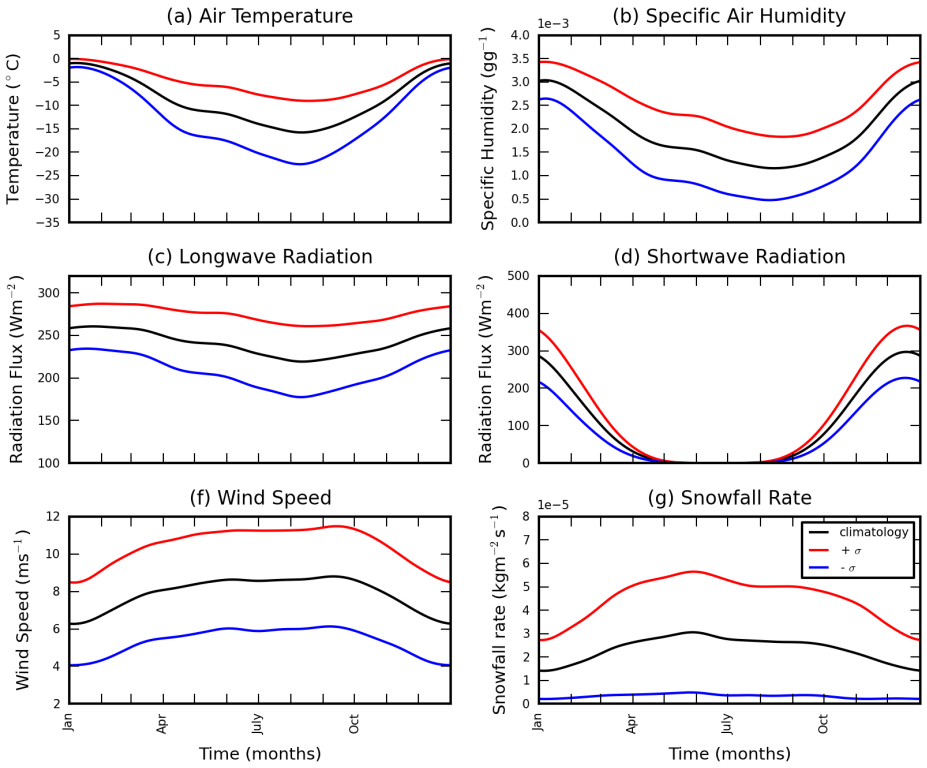

Figure 2.4: *Climatology for the Amundsen Sea, calculated from ERA-I reanalysis, 1979–2016, over the latitude longitude region; 115°W to 105°W, 71.5°S to 73.5°S.*

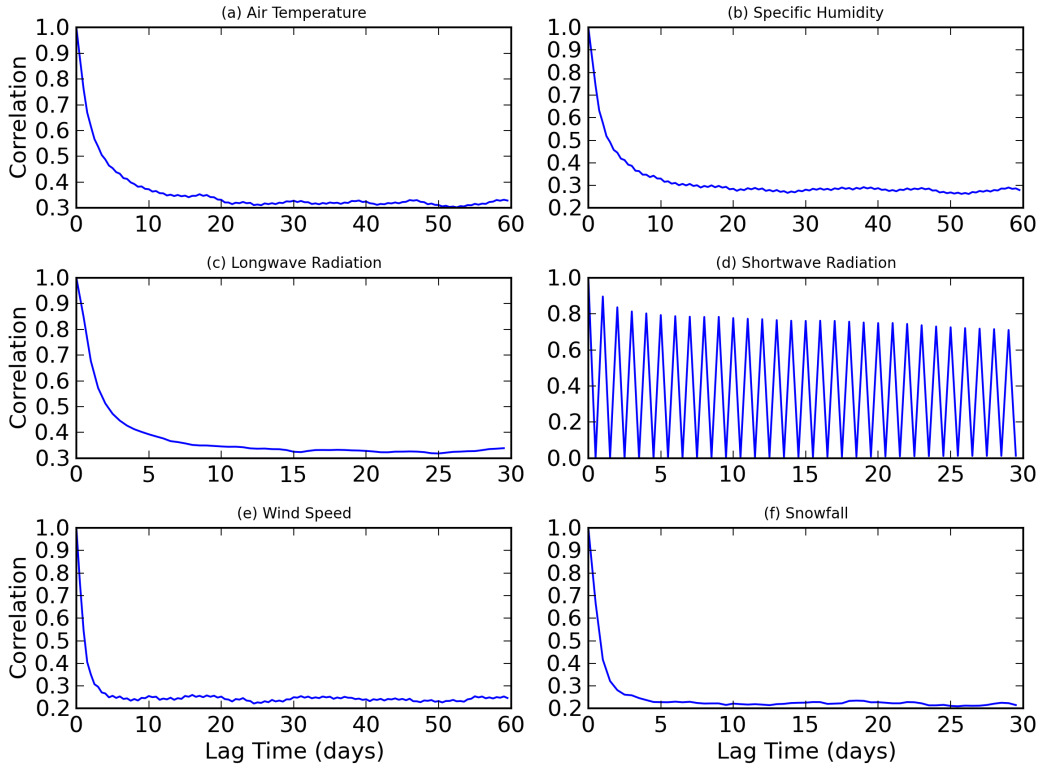

Figure 2.5: *Autocorrelations for the atmospheric forcing variables, calculated after the mean has been removed. All variables were averaged over the Weddell Sea (58°W to 48.5°W, 72°S to 74.8°S).*

The Weddell Sea has a much less stratified profile, with higher salinity values than in the Amundsen Sea, ranging from values of 34.4 at the surface to approximately 34.6 at 600m (Nicholls et al., 2003, 2008). High Salinity Shelf Water (HSSW) is formed in the Weddell Sea, which is a precursor to Antarctic Bottom Water. HSSW is predominantly formed in this region from relatively warm Modified Weddell Deep Water (MWDW) that is salinified and cooled due to sea ice growth over the continental shelf (Renfrew et al., 2002; Nicholls et al., 2009). The temperature of the waters from mid depth to the continental shelf is observed to be -1.5°C (Nicholls et al., 2003, 2008). Winter observations of the region are limited due to the treacherous conditions. The only winter observations available of the region indicate that winter mixing in the southwestern part of the Weddell Sea continental shelf is deep, spanning the depth of the observed profiles (up to 400m) (Nicholls et al., 2008). The Weddell temperature and salinity profiles are designed to reflect the MWDW source waters on to continental shelf, based on observations taken from the southwestern (Nicholls et al., 2003, 2008) and northwestern Weddell Sea (Gordon, 1998; Nicholls et al., 2004). Note that denser, more saline HSSW has been found in the south western boundary of the Weddell Sea (Nicholls et al., 2003), with salinities up to 34.8, however this is believed to be formed by the coastal polynya in this region and therefore is not what we seek to represent. After mixed layer shoaling, temperature and salinity are restored to these profiles

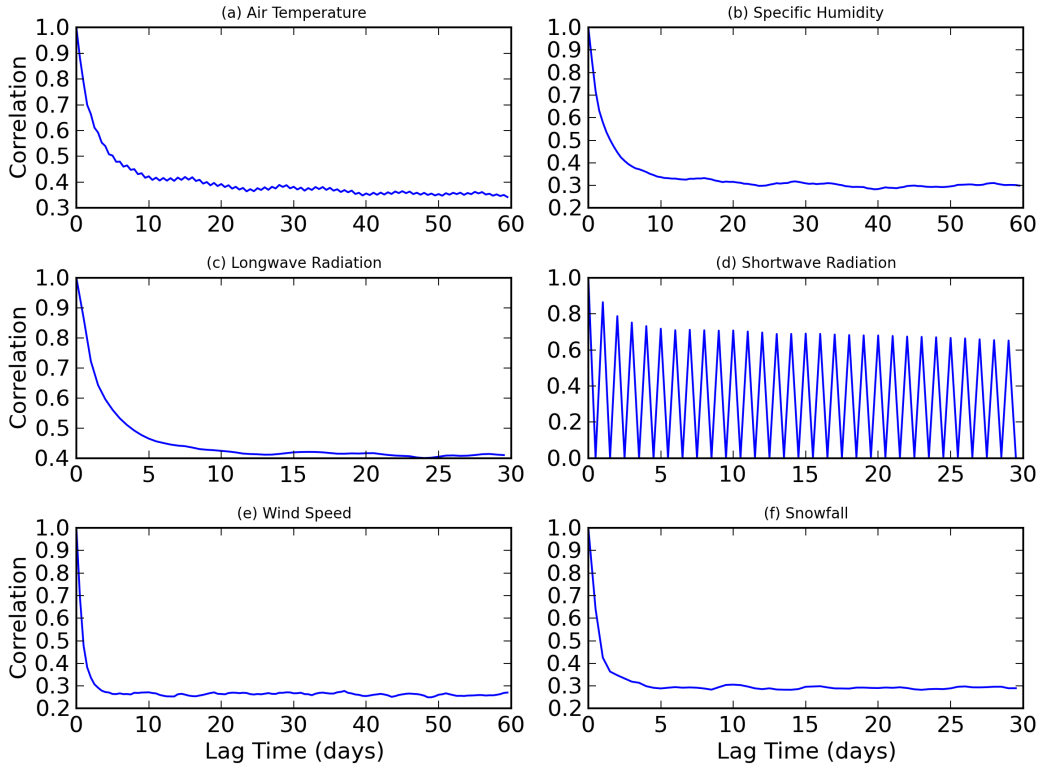

Figure 2.6: *Autocorrelations for the atmospheric forcing variables, calculated after the mean has been removed. All variables were averaged over the Amundsen Sea (115°W to 105°W, 71.5°S to 73.5°S).*

during the simulations over a time scale of three months, mimicking ocean advection.

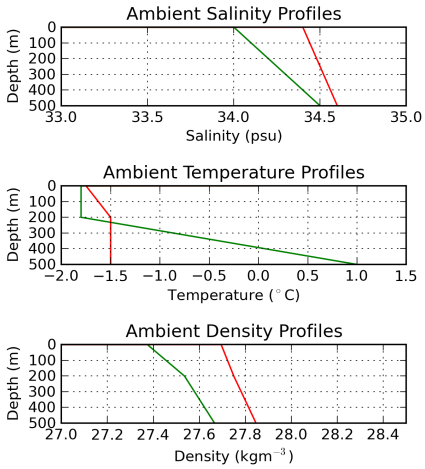

Figure 2.7: *Ambient ocean profile for the Weddell Sea in red, and the Amundsen Sea in green.*

2.3.3 Weddell and Amundsen Sea simulations with climatological atmospheric forcing

Simulations were carried out with the model set up described in Section 2.2.5 and the climatological atmospheric forcing in order to establish a reference state for each region, presented in Figures 2.8 and 2.9.

In the Weddell Sea (Figure 2.8) the mixed layer reaches the continental shelf every winter, the ice concentration varies between 0.6 and 0.95 every year, and the ice thickness varies between about 1 to 1.75 m. Snow ice forms between 25–60% of the sea ice. The secondary, smaller decrease in ice concentration after the main summer minimum is due to the warming of the ocean as the mixed layer deepens into the warm deep waters. The ice concentration then increases again once the mixed layer reaches the maximum mixed layer depth. At this point no more heat is added from the ocean and the ocean cools dramatically. This causes a rapid increase in ice concentration to the maximum ice concentration value. The jagged pattern in the snow thickness reflects these changes in ice concentration, as whenever the ice concentration increases the existing snow layer is redistributed to give a new average snow thickness to prevent artificial creation of snow. Snow thickness is also removed by formation of snow ice. In the Weddell simulation the snow ice is formed as the sea ice thickness starts to decrease, which increases the ratio of snow to ice. Snow ice formation halts once the sea ice thickness increases again, at this point the snow ice thickness decreases slightly due to relaxation of ice thickness and snow ice thickness values, representing the advection of ice (of differing composition) through the region, see Section 2.2.4 for details.

In the Amundsen Sea (Figure 2.9) the ice concentration varies between 0.5 and 0.95 each year, and the ice thickness between 1.2 and 1.8 m. Due to the high snowfall rate, snow ice forms 90–100 % of the sea ice. At the summer ice minimum all of the sea ice is snow ice, as all of the congelation ice at the base melts, and then the snow ice begins to melt. The mixed layer depth reaches 310 m each winter. As the mixed layer penetrates the 200 m thermocline during winter, the ice concentration starts to decrease due to increased ocean heating from below the ice.

Observations of snow ice are sparse; the limited observations indicate that between 8-38 % of Antarctic sea ice is composed of snow ice (Jeffries et al., 1997; Massom et al., 2001). However, a large range of values have been reported, including much higher values where snow ice makes up nearly all of the sea ice sampled (Massom et al., 2001). In general observations for the Weddell Sea fall at the at lower end of estimates (Lange et al., 1990), and those in the Amundsen Sea fall in the upper end of the estimates (Jeffries et al., 1997, 2001). Possible causes of the very high fraction of snow ice in the Amundsen Sea simulations could be a higher snowfall rate in the ERA-I dataset, or a higher basal melt rate than occurs in reality.

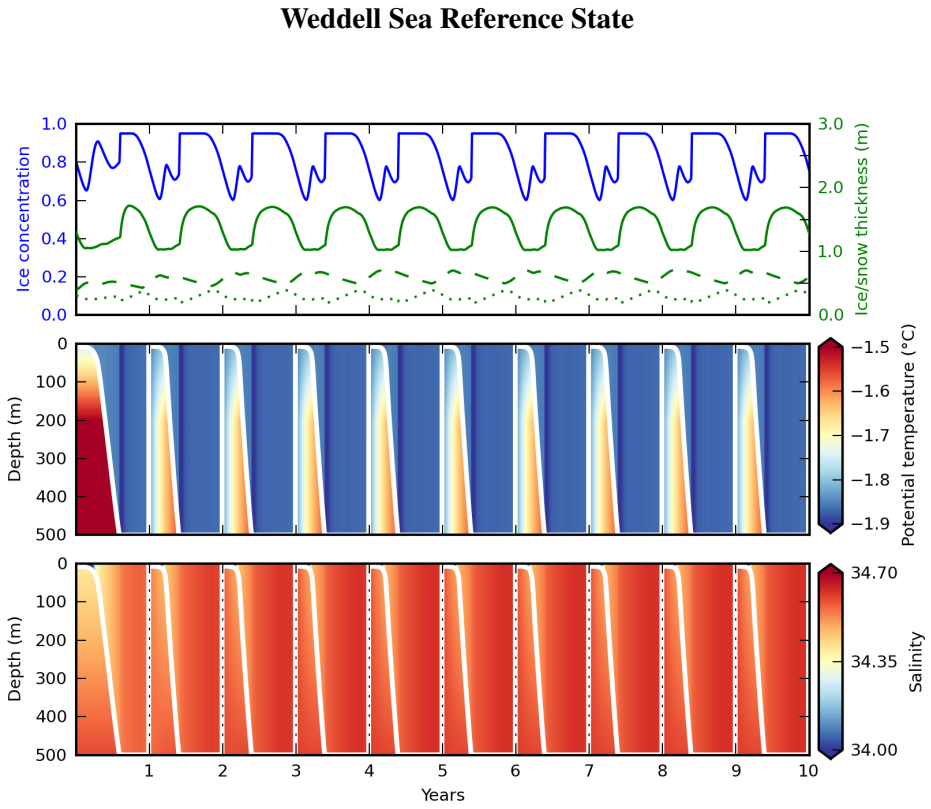

Figure 2.8: *Results for the Weddell Sea when forcing the model with the climatology. Ice concentration (blue), total (congelation+snow ice) ice thickness (green), snow ice thickness (dashed green) and snow thickness (dotted green) in the top panel, mixed layer depth (white) plotted over the potential temperature in the middle panel and salinity in the bottom panel.*

2.3.4 Weddell and Amundsen Sea simulations 1980-2016

The model was run with the 1979–2016 ERA-I atmospheric fields with 5 years of spin up, the atmospheric forcings are plotted in Figures 2.10 and 2.11, and the results for the Amundsen and the Weddell Seas are plotted in Figures 2.12 and 2.13.

The Weddell Sea displays much less interannual variability than the Amundsen Sea, consistent with the lower variability seen in the atmospheric variables over the times series. Two anomalously low sea ice years stand out in the Weddell Sea time series. 1989/1990 which was caused by a warm winter followed by a summer with anomalously high shortwave radiation. And also 2010/2011, which can be explained by anomalously high shortwave radiation that summer.

The Amundsen Sea time series shows much greater variability than the Weddell Sea in both ice properties (concentration and thickness), as well as mixed layer depth. The dramatic low sea ice minimum in 1980 is likely a combination of effects of switching from the climatology to the time series, which results in a dramatic change in seasonal cycle in some variables, so it may be associated with spin up and adjustments to this change. However, the forcing suggests it would be expected to be a low sea ice summer, as the summer air temperature, specific humidity, longwave radiation and wind speed are all relatively high, so may add together. The following

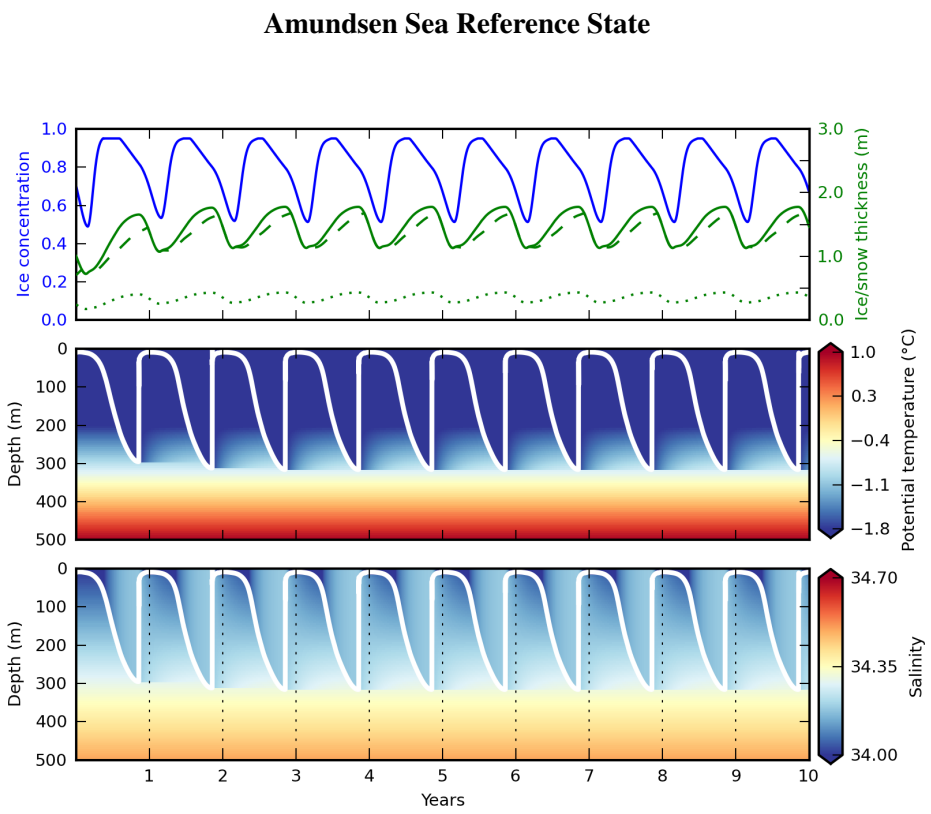

Figure 2.9: *Results for the Amundsen Sea when forcing the model with the climatology. Ice concentration (blue), total (congelation+snow ice) ice thickness (green), snow ice thickness (dashed green) and snow thickness (dotted green) in the top panel, mixed layer depth (white) plotted over the potential temperature in the middle panel and salinity in the bottom panel.*

winter temperature is anomalously high, which in combination with the increased sea ice melt resulting in the anomalously shallow mixed layer.

In general there is a pattern throughout the Amundsen Sea time series that winters in which the mixed layer is deeper than the normal values are followed by summers with lower sea ice minimums due to the extra ocean heat that has been mixed upwards. This pattern can be seen in winter/summers 1982/82, 1994/95, 1996/97, 2004/05 and 2009/10. In general the deeper mixed layer winters correspond to winters in which the air temperature is lower, and often with the winter longwave and specific humidity acting to amplify the mixed layer deepening.

There are no clear trends in either region, despite observations indicating an increase in sea ice extent in the Weddell and a decrease in the Amundsen Sea over this period (Parkinson and Cavalieri, 2012). However, as the model is not simulating extent, but ice concentration over specific regions in the Amundsen and Weddell Seas making it is hard to make a direct comparison. Also there is no variability in ocean advection, or rate of ice advection within this model, both of which could provide an extra source of interannual variability. Simulations using the unsmoothed atmospheric fields resulted in very little change to the sea ice and ocean mixed layer evolution and values in both regions.

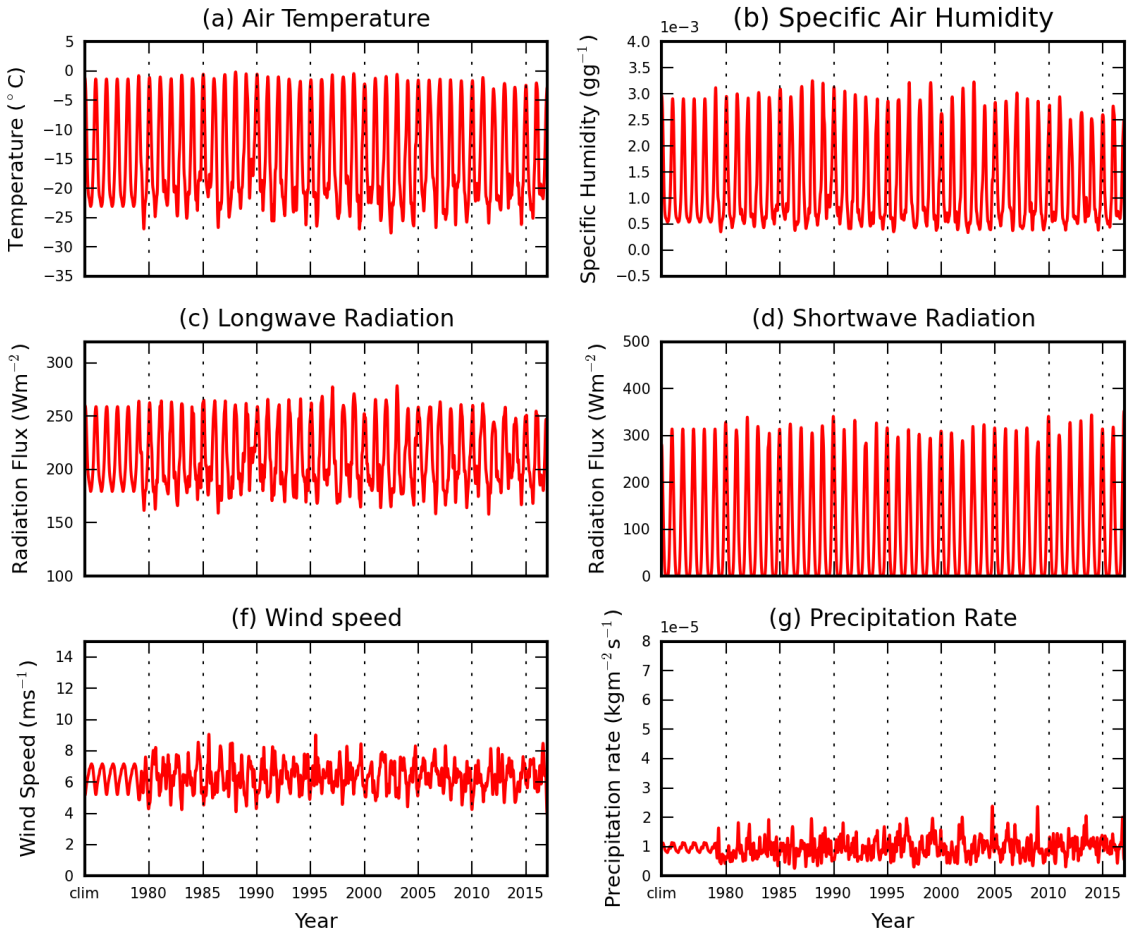

Figure 2.10: *Atmospheric forcing fields for the Weddell Sea, from 1979 to 2016 with 5 years of the climatology for spin up.*

2.4 Summary

A simple sea ice–mixed layer model has been adapted from Petty et al. (2013). The main changes are the inclusion of snow ice and a variable thickness snow layer. This was found to be a particularly significant process in the Amundsen Sea which has a relatively high snowfall rate, and formed sea ice that was nearly completely snow ice in the simulations. The snow thickness in the Amundsen Sea simulations was predominantly controlled by the rate of snow ice formation and therefore the thickness of sea ice and rate of snowfall. The parameterisation of ice advection was also changed to account for the thickness gradients of sea ice in the two regions, reflecting the advection of ice that is thinner into the region than is being exported.

The reference state results for the two regions are presented, where the model is forced with the climatological atmospheric conditions. The model is able to simulate realistic annual sea ice and mixed layer evolution, similar to results in Petty et al. (2013), with the Amundsen Sea partially destratifying (mixed layer depth of 310 m), and the Weddell Sea completely destratifying to the continental shelf (500 m). The ice concentration and thickness are within the range of realistic

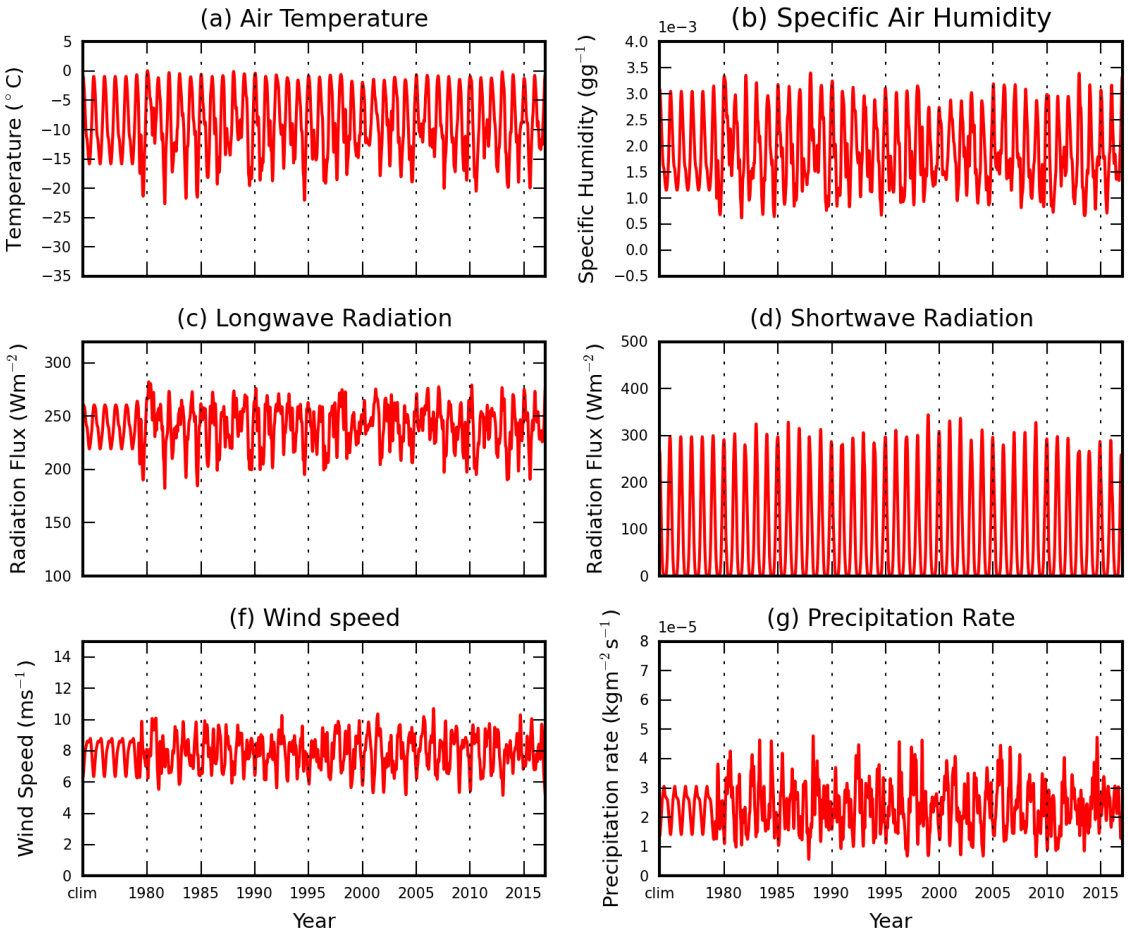

Figure 2.11: *Atmospheric forcing fields for the Amundsen Sea, from 1979 to 2016 with 5 years of the climatology for spin up.*

values from observations. In both regions the ice thickness varies between 1–1.8 m in each year, and between roughly 50% to 95 % ice concentration (the maximum ice concentration) in the Amundsen Sea, and 60% to 95% in the Weddell Sea. No clear trends in the sea ice cover were seen in either region over the time period 1979–2016.

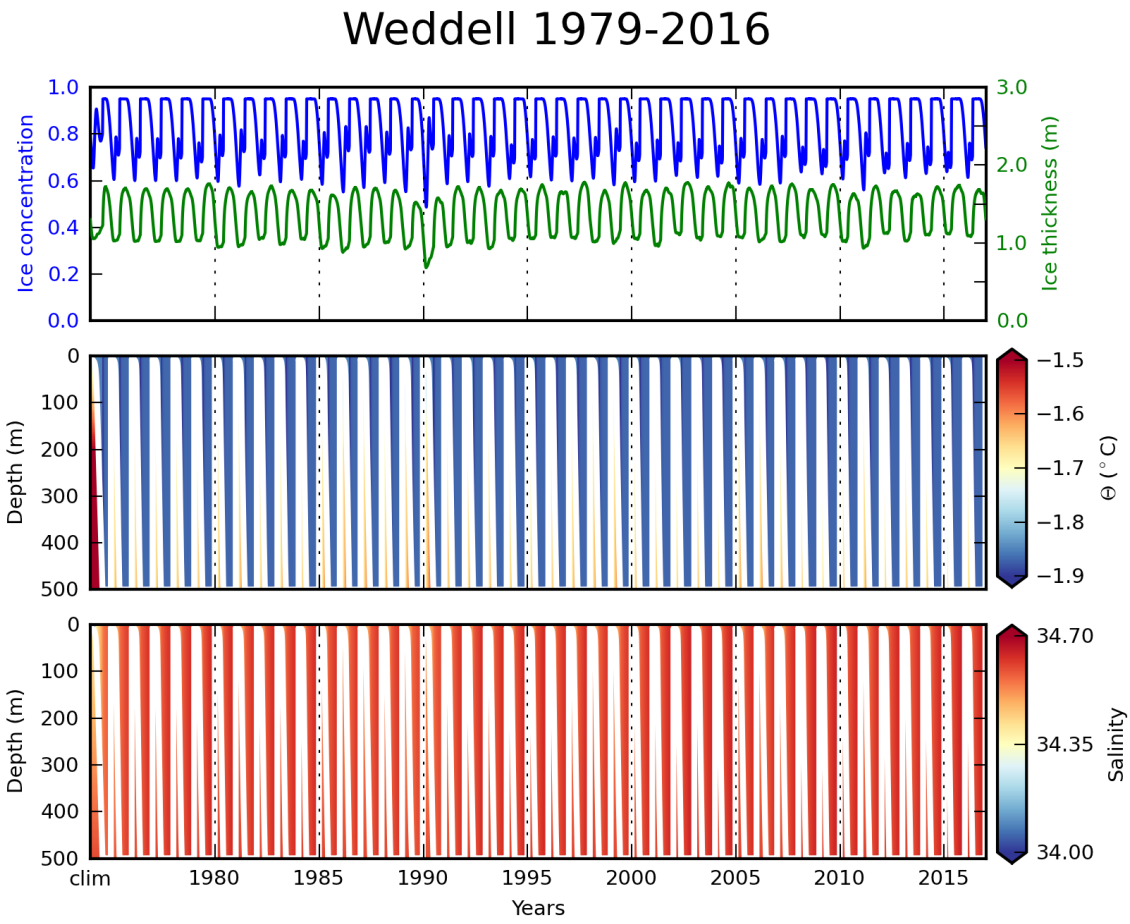

Figure 2.12: *Simulation results for the Weddell Sea, from 1979 to 2016 with 5 years of spin up with the climatological forcing.*

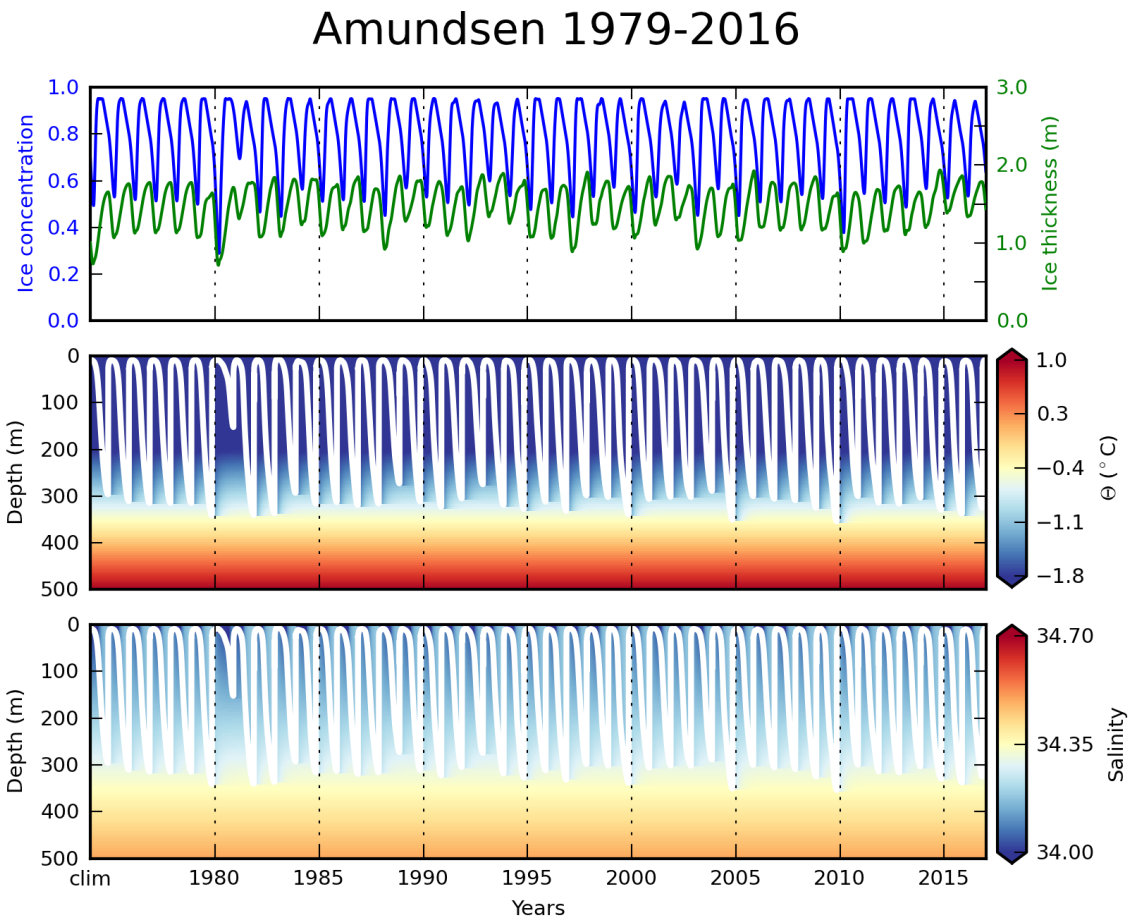

Figure 2.13: *Simulation results for the Amundsen Sea, from 1979 to 2016 with 5 years of spin up with the climatological forcing.*

Chapter 3:

IMPACT OF ATMOSPHERIC AND OCEANIC FORCING IN THE ANTARCTIC SHELF SEAS

3.1 Overview

In this chapter the sensitivity in the Weddell and Amundsen Sea simulations to the atmospheric conditions is investigated. This was done in order to explore the behaviour of the sea ice cover and mixed layer evolution in the two regions, to provide a scale for which the magnitude of the feedback responses in Chapter 4 can be compared and to establish which atmospheric forcing variables have the largest impact on the sea ice and mixed layer evolution. The sensitivity to the atmospheric forcing variables is presented in Section 3.2, the sensitivity to uncertainty in the oceanic conditions in Section 3.3 and a summary of the chapter is given in Section 3.4.

3.2 Sensitivity to Atmospheric Conditions

A set of simulations was performed in which each atmospheric forcing parameter was altered in turn to its +/– σ values with all other forcings given by the climatology. There is large uncertainty in future projections for Southern Ocean climate, however studies suggest that conditions are likely to get warmer and wetter (Christensen et al., 2013), therefore non-linearity of the response to increasing both surface air temperature and snowfall fields by σ was explored in an additional warmer and wetter (WW) simulation. Note that in this approach unphysical atmospheric conditions are applied due to decoupling atmospheric fields that are not independent.

In Sections 3.2.1 the changes to the seasonal cycle will be shown, then a summary of the results for the Weddell and Amundsen Seas is presented in Sections 3.2.2.1 and 3.2.2.2.

3.2.1 Sea ice and mixed layer response

Here the responses of the seasonal cycle of the sea ice and mixed layer depth to the perturbations in the atmospheric forcing variables for both the Weddell and the Amundsen Seas are presented and briefly described. The surface air temperature results are given in greater detail, due to surface air temperature perturbations being used for the feedback studies in Chapter 4. A summary of the results for each region follows in Sections 3.2.2.1 and 3.2.2.2.

Surface air temperature Plots of the response of the sea ice and mixed layer variables to perturbations in SAT are shown in Figure 3.1 (Weddell Sea) and Figure 3.2 (Amundsen Sea). The temperature change is largest in the winter +/- 6.2°C in the Amundsen Sea and +/- 4.7°C in the Weddell Sea. For both regions the + σ SATs resulted in thinner sea ice (max and min). In the Weddell Sea the water column destratified later, as shown in Figure 3.1, whilst in the Amundsen Sea the mixed layer was shallower and fresher (deeper and saltier), as shown in Figure 3.2. This is predominantly due to a decreased winter conductive heat flux up through the ice, resulting in decreased sea ice growth and therefore decreased brine rejection, which strongly controls the rate of mixed layer deepening, and maximum mixed layer reached. The opposite statements are true for the – σ SAT results.

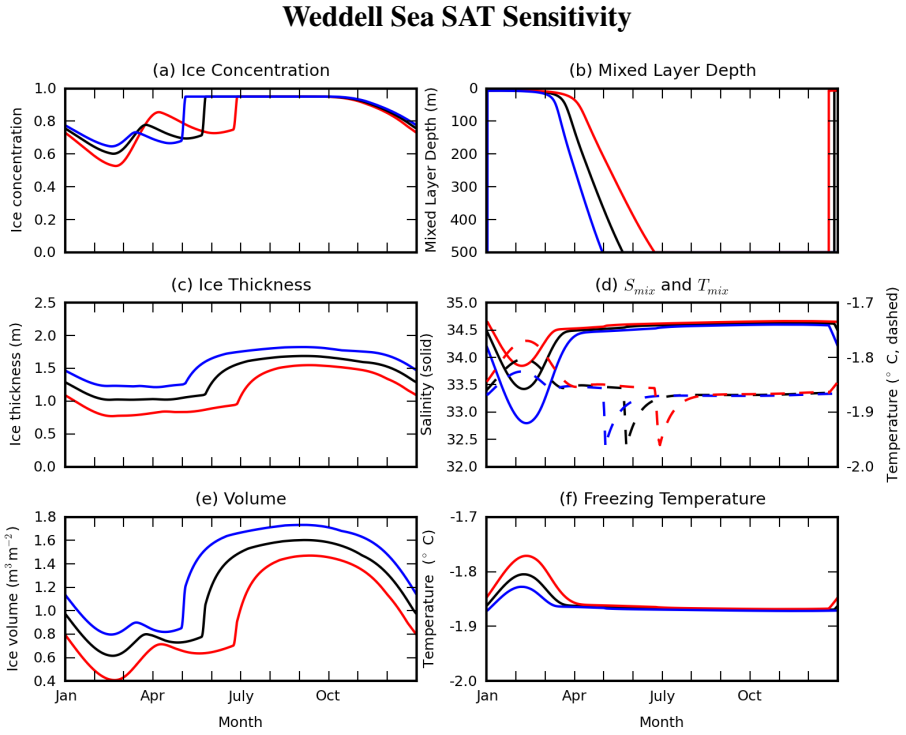

Figure 3.1: *Steady state ice concentration, mixed layer depth, ice thickness, mixed layer salinity, ice volume, mixed layer temperature (dashed) and freezing temperature (dotted) for the reference (black), + (red) and – (blue) σ SAT runs. For the snowfall rate the 16th and 84th percentile are used instead of +/-σ.*

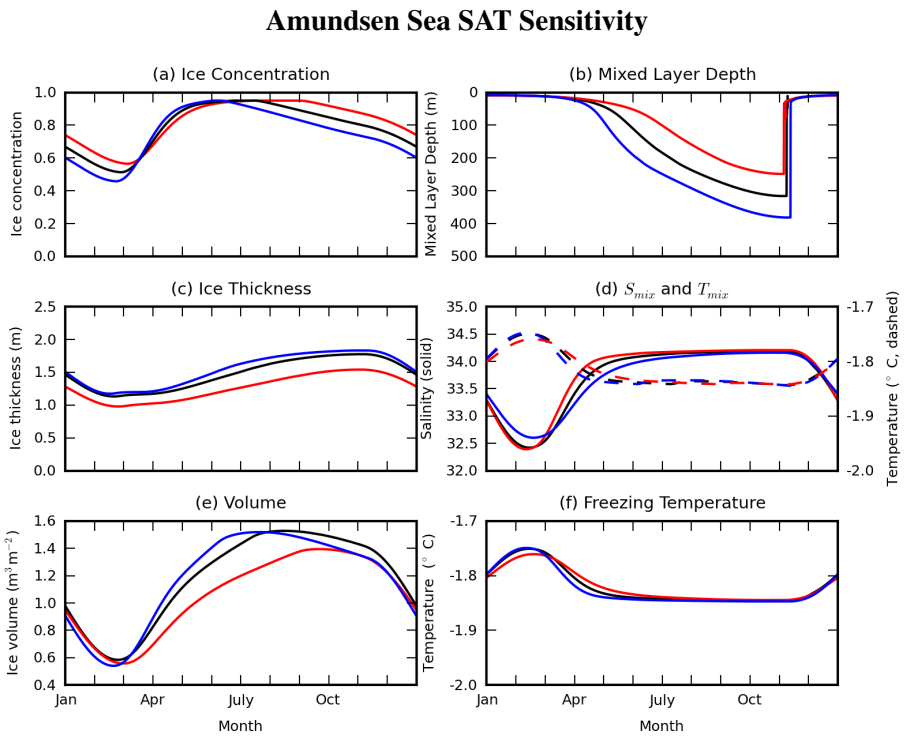

Figure 3.2: *See Figure 3.1 caption.*

In the Weddell Sea, Figure 3.1, the + σ SATs resulted in later destratification of the water column, and earlier restratification. The timing of mixed layer destratification determines the timing of ice thickening and expansion as the mixed layer cools dramatically once it reaches the ocean floor as warm deep ocean water is no longer being mixed upwards. The whole water column is being cooled, resulting in an increase in ice volume. The rate of winter ice thickening, and the seasonal change in ice thickness is similar in the perturbed and reference runs, the difference being the duration spent near the maximum ice thickness (the winter ice season), which is longer in the cooler case due to the longer duration of the completely destratified water column. For the Weddell sea the + σ SAT run has a larger total change in ice volume, with a later winter increase in ice volume leading to a short winter ice season. The opposite statements are true for the – σ SAT run.

In the Amundsen Sea, (Figure 3.2) the minimum ice concentration increased slightly in response to + σ SATs. Although it appears counter intuitive that warming should increase summer ice concentration and cooling should decrease it, this result is explained by changes in the amount of basal ocean heating, with a decrease in heating associated with a shallower mixed layer. In the – σ SAT run the mixed layer is deeper, mixing up more ocean heat, resulting in an earlier spring ice cover reduction (decrease in ice concentration). The opposite scenario is true for the + σ SAT run where the mixed layer shoals to above the thermocline. The – σ SAT run has the largest seasonal change in volume. Growth is faster than the reference run during the main growth phase and melting starts earlier due to the earlier deepening of the mixed layer below 200 m. In the + σ

SAT run the seasonal change in ice volume is slightly reduced (the max decreases more than the min), growth is slower, but melting starts later in the year.

In both regions the mixed layer temperature is close to the freezing temperature. In the Amundsen Sea, the mixed layer temperature starts to become very slightly greater than the freezing temperature as the mixed layer deepens into the warmer waters below the thermocline. A similar process happens in the Weddell Sea, except that once the water column becomes completely destratified the mixed layer temperature becomes supercooled, promoting rapid ice growth. In reality this supercooling would result in frazil ice formation, which is not represented in our model.

In both regions there is a reduction in S_{mix} and an increase in T_{mix} during the summer. The salinity decrease is caused by sea ice melting, releasing freshwater into the mixed layer, meanwhile the temperature of the mixed layer increases due to the shallow summer mixed layer and the warmer surface air temperatures. S_{mix} increases as sea ice grows during Autumn and rejects brine, and T_{mix} drops. The cooling and salinification of the mixed layer then promotes mixed layer deepening. There is a strong correlation between the dip/hump in the mixed layer salinity and temperature, as they are both dependent on the seasonal change in ice volume. In the Amundsen Sea reference and -σ SAT run we can see that the temperature of the mixed layer rises slightly as the mixed layer deepens below 200 m. In the Weddell Sea we see that T_{mix} decreases significantly as the mixed layer completely destratifies the water column. The magnitude of this cooling is not dramatically different, the main difference is the timing of the cooling, which is earlier for the – σ SAT run, and later in the + σ SAT run.

Specific humidity The mean increase/decrease in specific humidity was 6.4×10^{-4} gg^{-1} in the Amundsen Sea (AS) and 3.8×10^{-4} gg^{-1} in the Weddell Sea (WS). Increasing specific humidity reduces the rate of sublimation of snow from the surface, increasing the rate of snow ice formation. This slightly increases the summer ice thickness in the WS, and increasing the ice thickness all year round in the AS, as shown in Figure 3.3. These changes reflect how in the simulations, snow ice is formed in the summer only in the WS, whilst in the AS it is formed all year round in the simulations. The slower autumn increase in ice concentration in the AS is due to the thicker sea ice, meaning a larger volume change per unit of expansion, see Equation 2.6. The mixed layer changes in both regions reflect the change in timing of the autumn/winter ice growth in the WS, and the seasonal ice volume change in the AS.

Shortwave Radiation Flux The total increase/decrease in the shortwave radiation flux over the annual cycle was 3.6×10^{14} Wm^{-2} in the AS and 4.7×10^{14} Wm^{-2} in the WS. The increased shortwave radiation flux warms the mixed layer, resulting in slower destratification in the WS and shoaling the winter mixed layer in the AS and later restratification in both regions,

shown in Figure 3.4. The amplitude of the seasonal cycle in ice thickness is increased in both regions reflecting the increased shortwave radiation seasonal cycle, and the sea ice melt duration is shortened, resulting in a longer period where the sea ice volume is at its seasonal maximum in the WS. In the AS, the seasonal cycle in the ice concentration more strongly reflects the increase in mixed layer depth, and therefore the basal ocean heat flux. The opposite statements are true for a decrease in shortwave radiation flux.

Longwave Radiation Flux The total increase/decrease in the longwave radiation flux over the annual cycle was 5.6×10^{14} Wm^{-2} in the AS and 4.7×10^{14} Wm^{-2} in the WS. Similar to the shortwave radiation, an increase in longwave radiation results in slower destratification in the WS and shoaling the winter mixed layer in the AS and later destratification in both regions, shown in Figure 3.5. However, the amplitude of seasonal ice thickness change remains similar for the WS, the ice thickness increases all year round, and the winter ice season is lengthened due to earlier destratification. The ice concentration changes in the WS and AS are similar to the shortwave responses, strongly responding to changes in the mixed layer depth in both regions. The opposite statements are true for the decrease in longwave radiation in the WS. In the AS, the ice thickness decreases very slightly all year round. However, for the decrease in longwave, the ice thickness remains very similar to the reference case due to the increased winter basal heat flux, and only increases very slightly in the summer.

Wind Speed The mean increase/decrease in wind speed is 2.6 ms^{-1} in the AS and 2.2 ms^{-1} in the WS. The increased wind speed increases wind stirring. This plays a role in the initial mixed layer deepening, whilst the mixed layer is still shallow, which can be seen in the results of both regions in Figure 3.6 between late Feb–March/April. An increase in wind speed also slightly increases the turbulent heat fluxes, resulting in quicker destratification and a slightly increased winter ice thickness in the WS. In the AS the ice thickness slightly decreased as a result of the slightly deeper mixed layer, and increased basal heat flux. However, the increased turbulent heat flux results in a more rapid autumn increase in ice concentration in the AS.

A clear limitation of using the idealised model is that only the impact of wind strength on the turbulent heat fluxes and wind stirring could be investigated. In reality both wind speed and direction is important for the sea ice cover. Generally in the Southern Ocean, northerly winds tend promote compression of the ice, pushing the sea ice towards the coast, promoting thickening by rafting and ridging whilst slowing expansion. Northerly winds also tend to be warmer, acting to increase melting rates/slow ice growth. The opposite is true for southerly winds, which tend to promote expansion of the sea ice cover and enhanced growth/reduced melt due to the cooling effect. As discussed in Section 1.2.2.2, trends in the winds have been shown to explain a significant proportion of the sea ice variability in the Antarctic sea ice cover.

Snowfall Rate The increase in snowfall over the whole year was 3.6×10^8 kgm^{-2}yr^{-1} in the AS and 1.4×10^8 kgm^{-2}yr^{-1} in the WS. Whilst the decrease was 3.4×10^8 kgm^{-2}yr^{-1} in the AS and 1.4×10^8 kgm^{-2}yr^{-1} in the WS. Increasing the snowfall rate increases the rate of snow ice formation, and acts to freshen the ocean surface. In the WS (see Figure 3.7), increased snow ice formation increases the thickness of the sea ice, predominantly in the summer, which is when most of the snow ice formation occurs in the WS simulations, due to the thinner ice. Destratification also occurs slightly later, due to the increased surface freshwater flux. The opposite statements are true in the WS in response to a decrease in snowfall rate. In the AS, snow ice formation increases, dramatically increasing the ice thickness (note the different scale used for the AS in Figure 3.7). However, the brine flux from the snow ice formation outweighs the surface freshening, resulting in a slightly deeper winter mixed layer depth. In the lower snowfall rate case, where there is essentially no snowfall, the ice thickness dramatically decreases, and there is essentially no ice in the summer (minimum thickness and concentration values are reached).

Warmer and Wetter Scenario Studies suggest that the Southern Ocean is likely to get warmer and wetter. Therefore the + σ fields for surface air temperature and snowfall (along with the climatology for the other atmospheric fields) have been used as a future forcing scenario. The model results for ice concentration, thickness and mixed layer depth when forcing the Amundsen and Weddell with this future scenario are plotted in Figure 3.8, alongside the reference results for comparison.

In the WS the destratification is slower resulting in the winter sea ice thickness being reached later, and the summer ice concentration is reduced. The summer ice thickness slightly increases due to an increase in snow ice formation. In the AS there is a much more dramatic change, note the difference in scale in the ice thickness for the AS in Figure 3.8. The ice thickness dramatically increases due to the increase in snow ice formation.The winter mixed layer shoals due to the increased surface freshwater flux, and the surface warming. This decreases the basal heat flux, increasing the summer ice concentration. However the winter ice concentration decreases, due to slower expansion of the dramatically thicker sea ice (see Equation 2.6).

3.2.2 Summary of sensitivity to atmospheric forcing

In this section the sensitivity of the sea ice cover and the mixed layer depth in the two regions shown in the previous section is summarised and compared. The change to the sea ice and mixed layer seasonal cycle is shown in Figures 3.9 and 3.10. The sensitivity simulations are then summarised in Figures 3.9 and 3.10, where all metrics shown are calculated after 8 years of simulation, to make sure that the model has reached a steady state (this typically only takes 2–3 years).

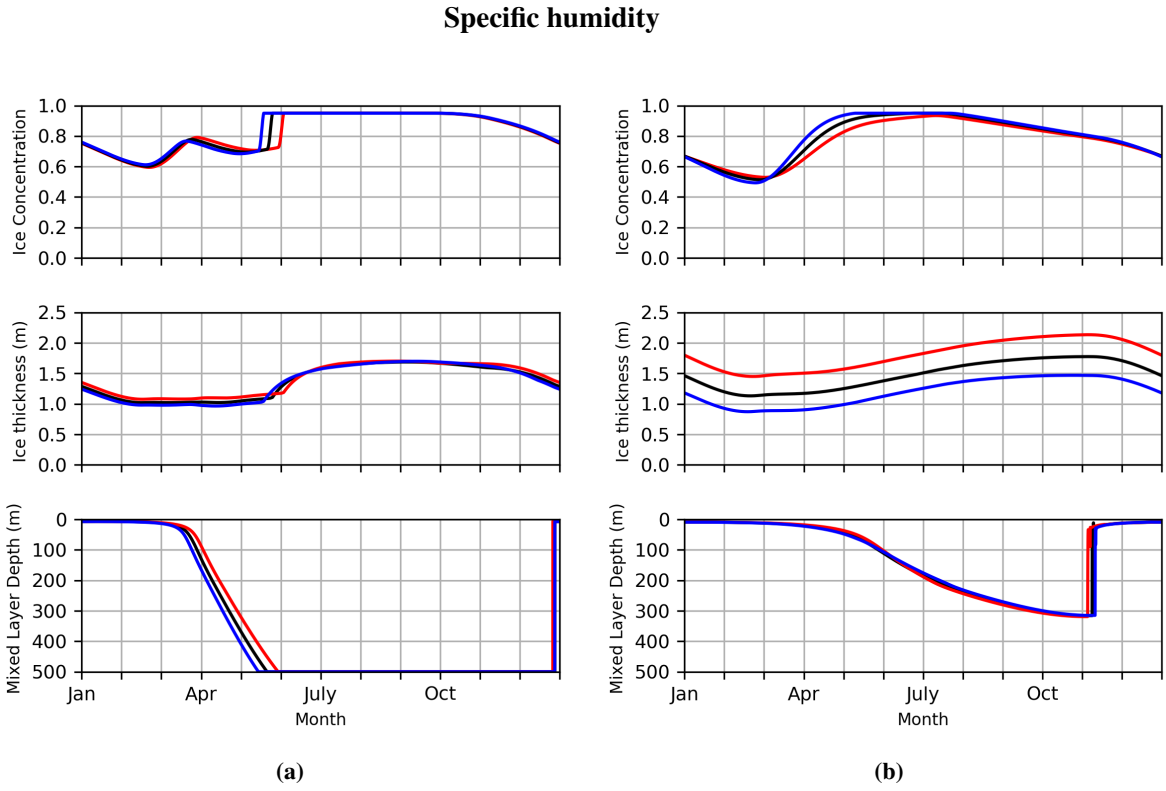

Figure 3.3: *Steady state ice concentration, ice thickness and mixed layer depth for the reference (black), + (red) and – (blue) σ specific humidity runs for the (a) Weddell Sea and (b) Amundsen Sea.*

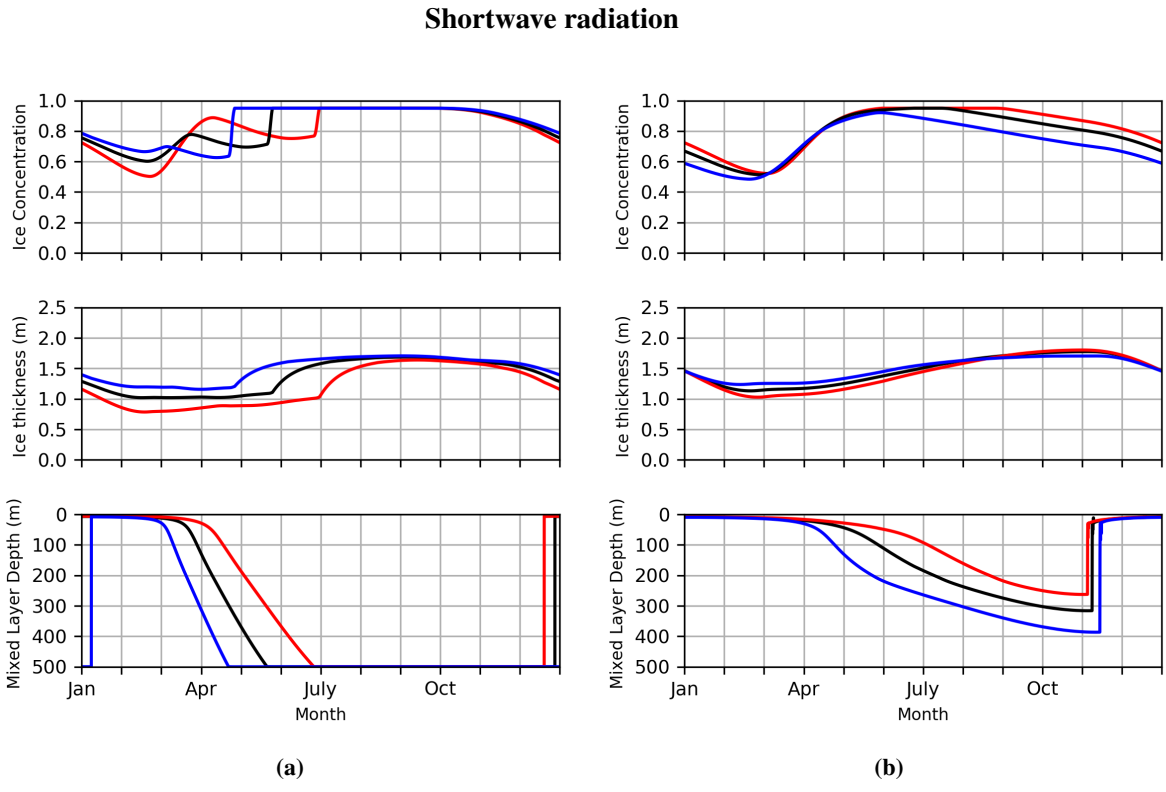

Figure 3.4: *Steady state ice concentration, ice thickness and mixed layer depth for the reference (black), + (red) and – (blue) σ shortwave radiation runs for the (a) Weddell Sea and (b) Amundsen Sea.*

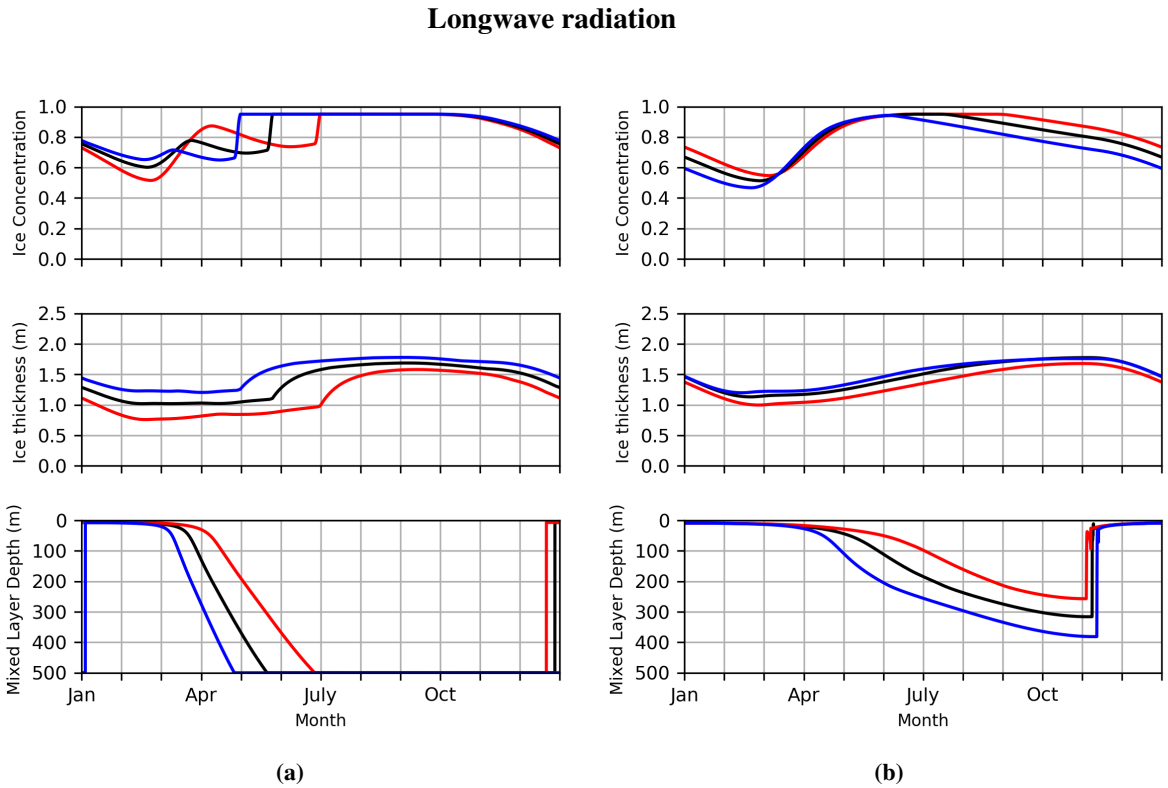

Figure 3.5: *Steady state ice concentration, ice thickness and mixed layer depth for the reference (black), + (red) and – (blue) σ longwave radiation runs for the (a) Weddell Sea and (b) Amundsen Sea.*

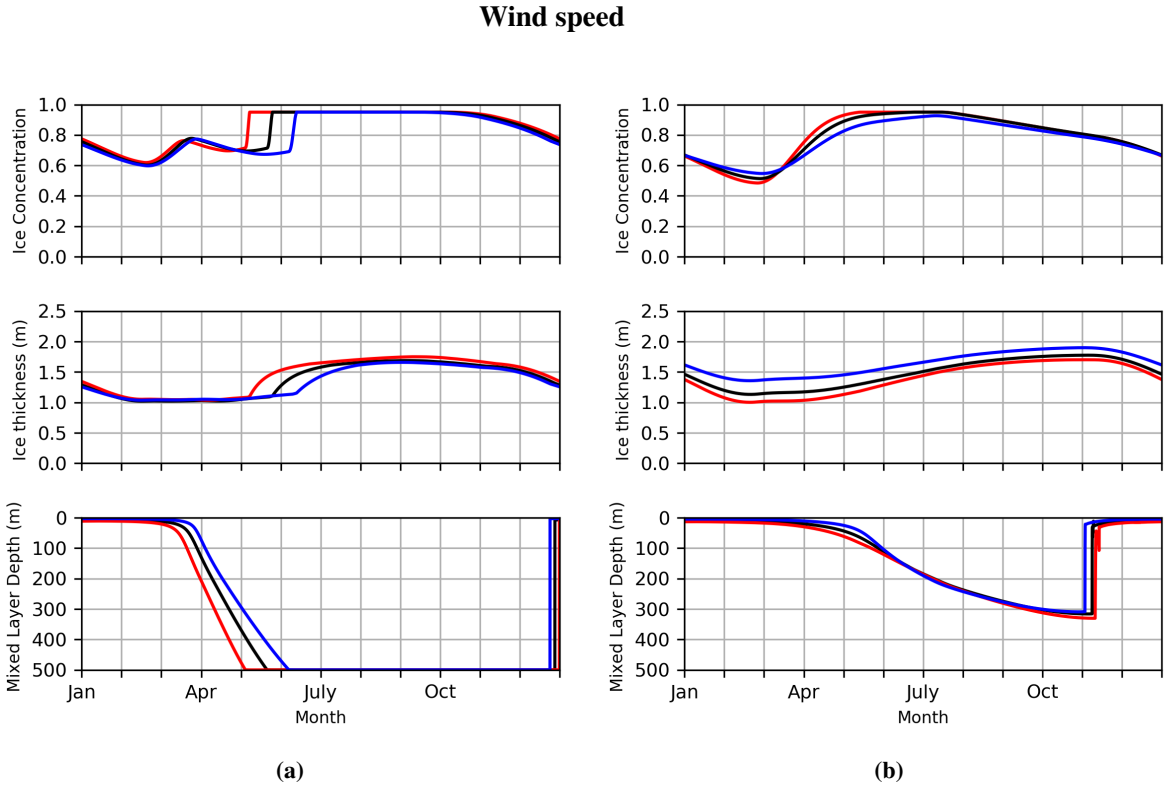

Figure 3.6: *Steady state ice concentration, ice thickness and mixed layer depth for the reference (black), + (red) and – (blue) σ wind speed runs for the (a) Weddell Sea and (b) Amundsen Sea.*

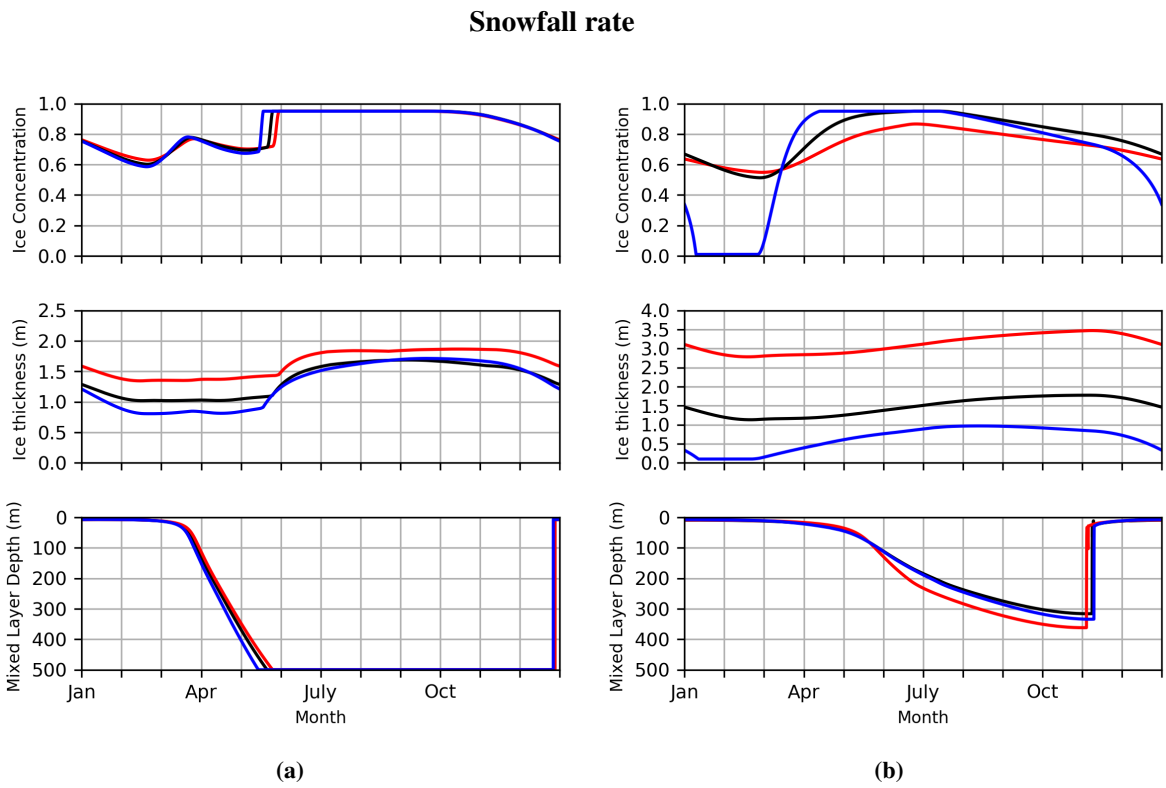

Figure 3.7: *Steady state ice concentration, ice thickness and mixed layer depth for the reference (black), 84th (red) and 16th percentiles (blue) for the snowfall rate runs for the (a) Weddell Sea and (b) Amundsen Sea.*

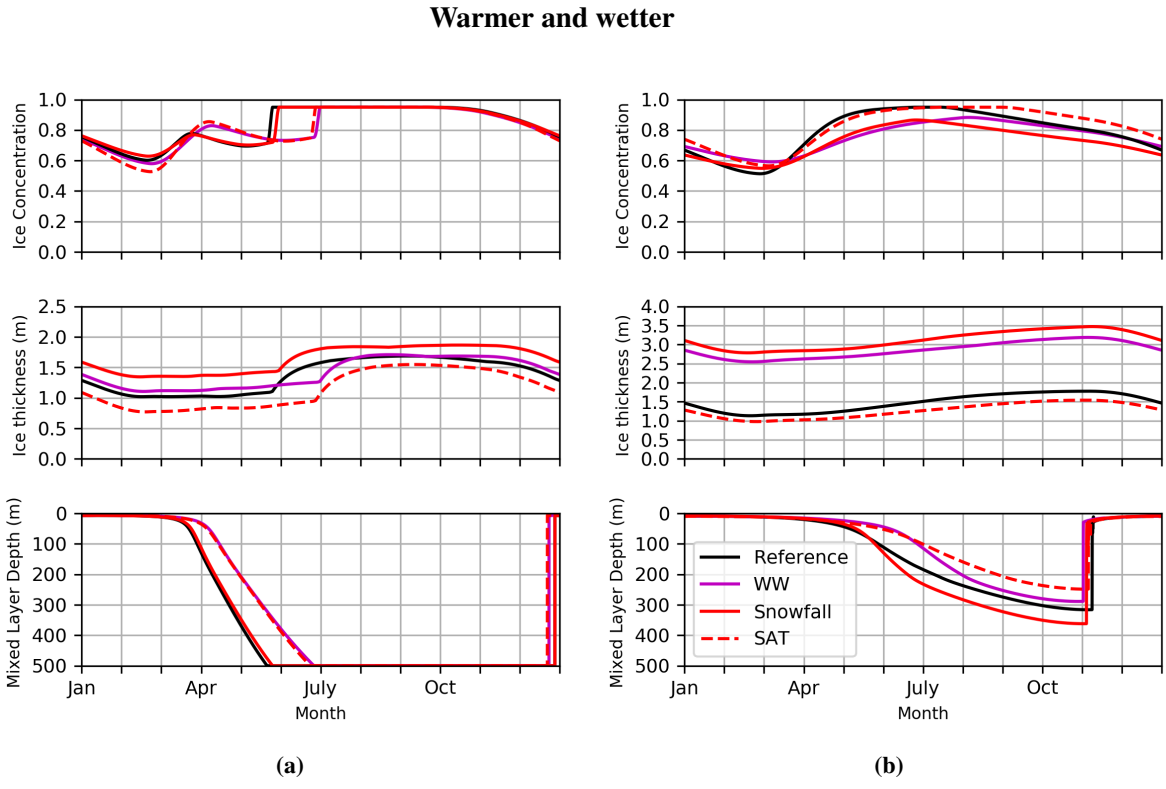

Figure 3.8: *Steady state simulation results for + σ SAT and the 84th percentile for the snowfall rate (purple), the reference run (black), + σ SAT (red) and the 84th percentile for the snowfall rate (red dashed) for (a) Weddell Sea and (b) Amundsen Sea.*

For the Weddell Sea, the timing of water column destratification and the mean ice volume were chosen as metrics to compare the mixed layer and sea ice sensitivity in Figure 3.9. In the Weddell Sea simulations the mixed layer always reaches the continental shelf during winter, meaning that a different metric to the maximum mixed layer depth used in the Amundsen Sea had to be used to summarise mixed layer changes. The timing of mixed layer destratification and the duration spent with the water column completely destratified was found to be important in determining the timing of the sea ice thickness and concentration increase, which coincide with dramatic cooling of the water column as the water column completely destratifies. The winter growth period generally coincides with the time where the mixed layer is completely destratified. An earlier destratification also means that there is thicker sea ice, as there is a longer period of sea ice growth. For the Amundsen Sea, the maximum mixed layer depth was used in Figure 3.10, this was found to be important as it determines how much warm deep water is entrained. Mean ice volume was used to compare sensitivity of the sea ice in both regions.

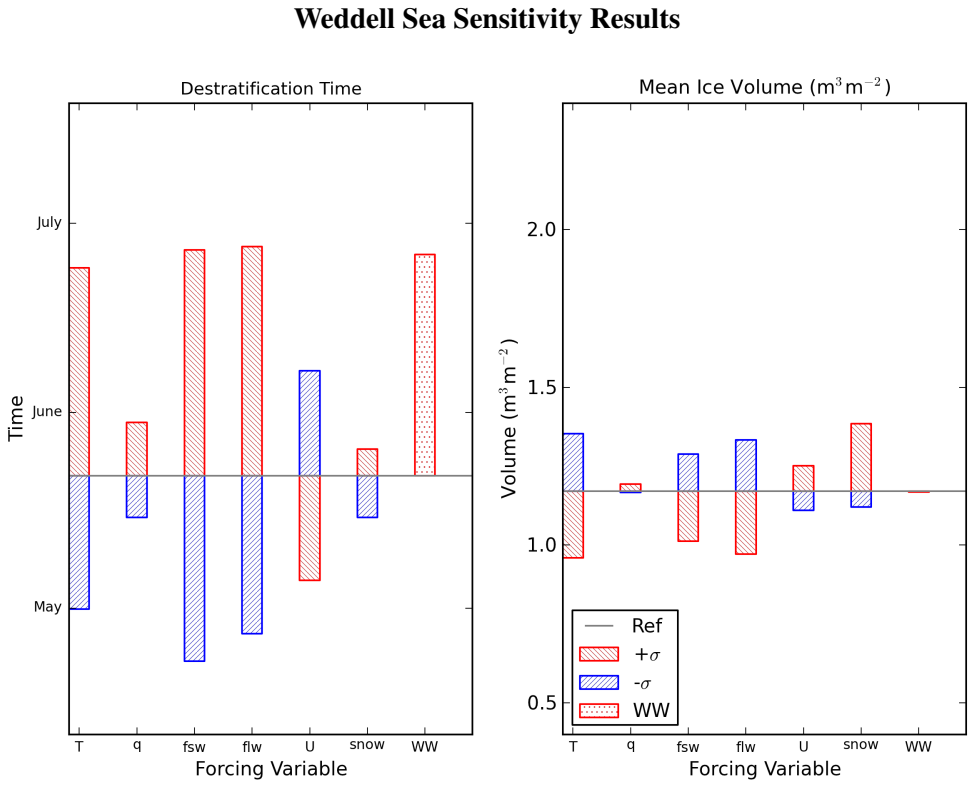

Figure 3.9: *Sensitivity study results for the Weddell Sea for +/– σ of each atmospheric parameter and + σ temperature and snowfall (warmer and wetter, WW). The top of each bar is the destratification time/mean ice volume for each perturbed run. The grey line indicates the reference value and the size and sign of each bar shows the difference between each perturbed run with the reference run value. All values are calculated from when the simulation has reached a steady state.*

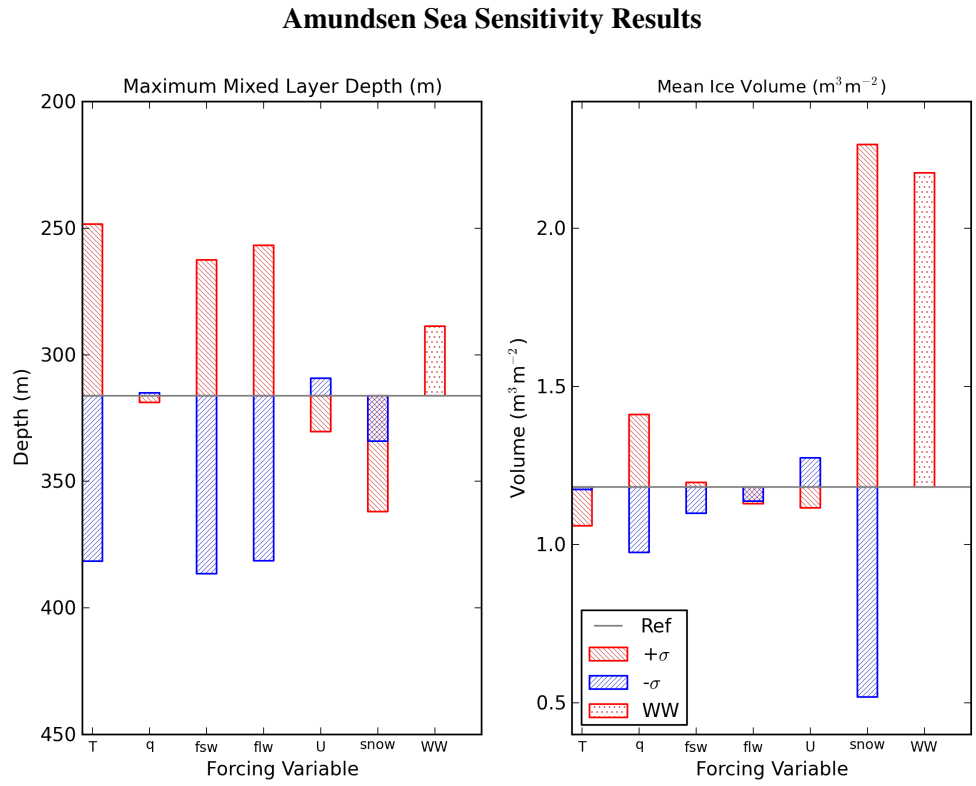

Figure 3.10: *Sensitivity study results for the Amundsen Sea for +/– σ of each atmospheric parameter and + σ temperature and snowfall (warmer and wetter, WW). The top of each bar is the maximum mixed layer depth/mean ice volume for each perturbed run. See Figure 3.9 for more details.*

3.2.2.1 Weddell Sea results

Figure 3.9 shows that greater sensitivity for both the mixed layer and sea ice response was found to shortwave, longwave radiation and surface air temperature (SAT) which all had similar responses of +/– one month in destratification time, and changes in ice volume of +/–0.2 m^3m^{-2}.

The mixed layer and ice volume response to increasing/decreasing each variable by σ is mostly fairly symmetric apart from snowfall. The sea ice and mixed layer responses are generally slightly larger for the + σ perturbation to each variable. Most responses are driven by changes in the surface energy balance promoting ice growth (decrease in SAT, shortwave radiation, longwave radiation, specific humidity or an increase in wind speed) and resulting in an earlier water column destratification or vice versa. Increasing wind speed also increases wind stirring, promoting mixed layer deepening. This is only important for shallower mixed layer depths, and the impact of wind speed on the turbulent heat fluxes and the surface energy balance dominates.

Increasing specific humidity reduces the rate of sublimation of snow from the surface, increasing the rate of snow ice formation, slightly increasing the mean ice volume and the rate of destratification. The Weddell Sea sea ice cover and mixed layer is less sensitive to the perturbations in the snowfall rate than the Amundsen, as the lower snowfall rate means that there

is less snow ice formation, and any snow ice that forms generally forms during the spring/summer months when the sea ice is thinner. An increase in snowfall rate increases the thickness of snow ice, this also increases the brine flux into the mixed layer, offsetting some of the impact of the increased surface freshwater flux on the rate of destratification. A decrease in snowfall rate results in less snow ice and faster destratification due to a reduced freshwater flux.

In the warmer and wetter run (+ σ SAT and + σ snowfall) the impact of increased temperature dominates over the impact of increased snowfall. The sea ice becomes marginally thinner, and the mixed layer destratification slows due to an increased surface freshwater flux from snow and surface warming. Overall the increase in snow ice and decrease in ice growth due to surface warming balance and result in little change in mean ice volume, although the snow ice fraction of the sea ice increased to become the main component.

3.2.2.2 Amundsen Sea results

Figure 3.10 shows that the mixed layer depth displayed the largest sensitivity to the (– σ) shortwave radiation flux, followed closely by SAT and longwave radiation flux, which all showed changes in the mixed layer depth +/– 70–80 m. The ice volume showed greatest sensitivity to the snowfall rate, showing a maximum change of just under 1.0 m^3m^{-2}, followed by specific humidity which resulted in changes in the order of 0.2 m^3m^{-2}. The Amundsen Sea sea ice cover showed much less sensitivity to SAT, shortwave and longwave radiation than seen in the Weddell sensitivity results.

Atmospheric perturbations that change the surface energy balance with a tendency for ice growth also promote mixed layer deepening. This increases the entrainment of warm deep waters (if the mixed layer is below the 200 m thermocline), acting to decrease the rate of ice growth and therefore ice volume, opposing the direct impact of the atmospheric perturbation on the ice cover. For example, in response to a decrease in SAT, shortwave radiation, longwave radiation or an increase in wind speed the ice volume decreases. Changes to the maximum mixed layer depth predominantly impact the summer minimum ice volume, as the maximum mixed layer is reached in early November, around the time that the ice volume is starting to decrease, meaning that an increase in the maximum mixed layer depth will cause the ice growth to plateau and then start to decrease earlier. This negative feedback explains some of the lack of symmetry in the ice volume responses to +/- σ perturbations in SAT, shortwave and longwave radiation.

Similar behaviour has been found in other studies (Martinson, 1990; Zhang, 2007). The relationship between mixed layer deepening and enhanced basal melt means that: (i) the ice volume changes in response to perturbations are highly nonlinear, for example an increase and a decrease in incoming longwave radiation both result in a decrease in the mean ice volume; and (ii) the sea ice volume changes in response to all atmospheric perturbations (except snowfall)

are damped, and are smaller than those in the Weddell Sea. Both the sea ice volume and mixed layer depth showed a high sensitivity to the snowfall rate, which determines the rate of snow ice formation.

As in the Weddell sensitivity results, decreasing the specific humidity increases the rate of sublimation of snow, decreasing the rate of snow ice formation and decreasing the ice volume. The small change in mixed layer depth reflects both the changes in salt flux from snow ice formation and changes to the surface energy balance (latent heat flux), which in this scenario oppose each other. An increase in the wind speed causes more wind stirring, promoting mixed layer deepening that brings heat into the mixed layer that acts to buffer changes in the ice cover due to changes in the surface energy balance. This causes the resulting changes in mean ice volume for the Amundsen Sea to be the opposite of those in the Weddell Sea in response to changes in wind speed.

The Amundsen Sea ice cover showed greatest sensitivity to the snowfall rate. The relatively thin sea ice and high snowfall rates in the Amundsen Sea region mean that snow ice formation is an important process, forming a majority of the sea ice in the Amundsen Sea simulations. Changes in snowfall also lead to changes in stratification and the amount of basal ocean heating. This means that both increased and decreased snowfall lead to a deeper mixed layer, due to increased snow ice formation (and associated brine flux) or reduced freshwater surface input. However, some caution must be taken in any extrapolation of the Amundsen sensitivity results, particularly to the snowfall rate, as the snow ice fraction in the Amundsen reference simulation exceeds the (limited) range of observations (see Section 2.3.3).

In the warmer and wetter run (+ σ SAT and + σ snowfall), and in contrast to the Weddell Sea, the impact of the increased precipitation dominates over the increased temperature impact. The sea ice thickens due to the increased rate of snow ice production in response to increased snowfall. The mixed layer shoals due to increased freshwater input from snowfall. The shallower mixed layer means that the minimum ice concentration increases due to reduced basal ocean heating.

Broadly speaking the variability seen in both regions seems to exceed the interannual variability displayed in Section 2.3.4, indicating that the variability in the forcing parameters tend to cancel each other out to some degree, dampening variability. The interannual variability displayed in Section 2.3.4 indicated that the Amundsen displayed greater interannual variability than the Weddell Sea, which is consistent with the smaller sensitivity shown here to the atmospheric forcing variables, and the lower variability displayed in the atmospheric forcings over the time series.

3.3 Sensitivity to Oceanic Conditions

The sensitivity to uncertainty in the oceanic forcing was investigated for the two regions by varying the ocean ambient profiles and the rate of advection. The same metrics as Section 3.2.2 have been used to create Figures 3.12 and 3.13.

3.3.1 Weddell Sea

In the Weddell (Figure 3.12), the gradient of the salinity profile was halved and doubled (see the dotted and dashed lines in Figure 3.11) to investigate the influence of changes in high salinity shelf water properties on the shelf. Halving the gradient so that there is a 0.1 change in salinity from surface to bottom of the water column (500 m) makes it easier for the water column to destratify, causing earlier destratification. The opposite is true when the gradient was doubled, so that there was a 0.4 salinity change over the water column.

Doubling (halving) the advection rate resulted later (earlier) destratification. This decreases (increases) the length of the winter growth season, resulting in an increase (decrease) in mean ice volume, despite minimal changes to the maximum and minimum sea ice volumes.

3.3.2 Amundsen Sea

In the Amundsen (Figure 3.13), the depth of the thermocline was changed from 200 m to 100 m and 300 m (see the dotted and dashed lines in Figure 3.11), based on observed interannual variability (Assmann et al., 2013). The temperature gradient below the thermocline has been kept

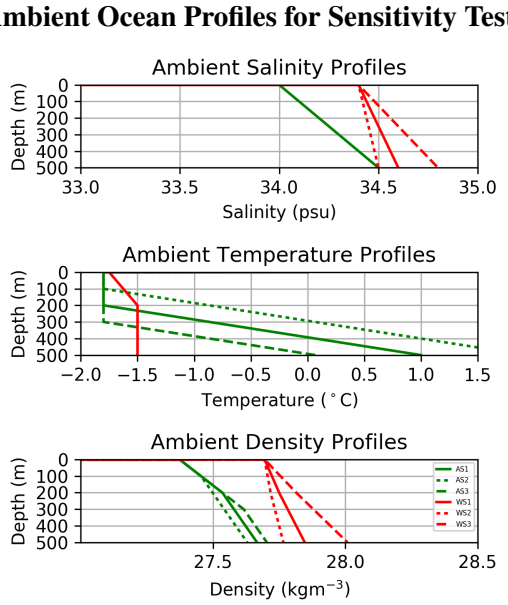

Figure 3.11: *Ambient ocean profiles used to test the sensitivity to the ocean conditions in the Weddell and Amundsen Seas.*

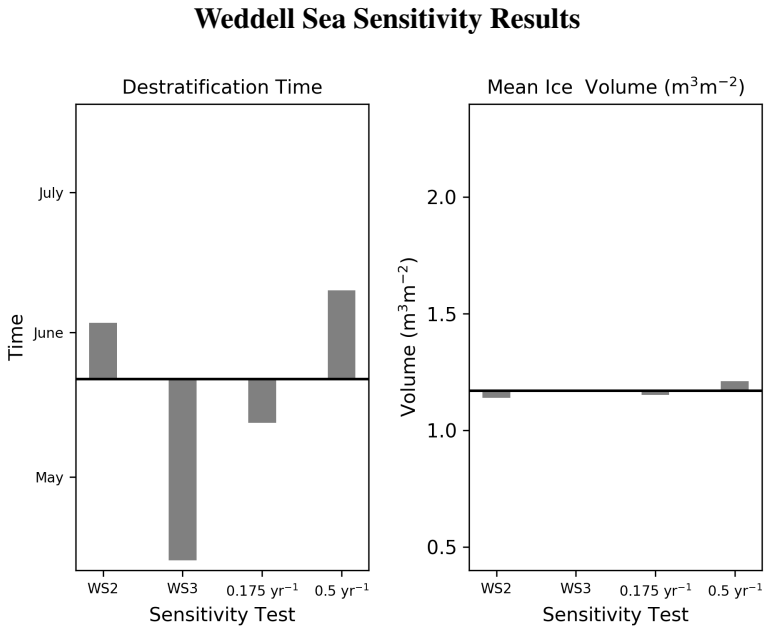

Figure 3.12: *Ocean sensitivity results for the Weddell Sea. The sensitivity tests include changing the ambient profiles used (WS2 and WS3), see Figure 3.11 for the profiles used for WS2 and WS3 tests. The advection timescale was also halved (0.175 yr^{-1}) and doubled (0.5 yr^{-1}).*

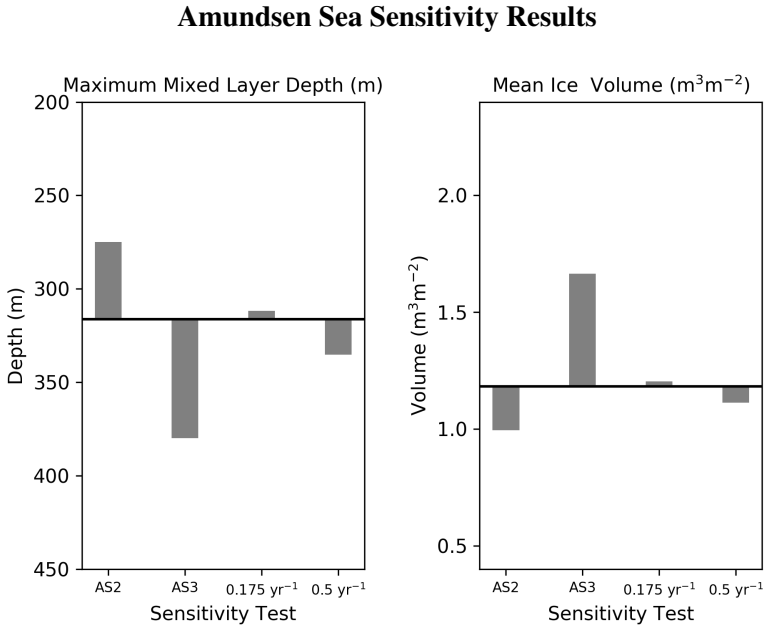

Figure 3.13: *Ocean sensitivity results for the Amundsen Sea. The sensitivity tests include changing the ambient profiles used (AS2 and AS3), see Figure 3.11 for the profiles used for AS2 and AS3 tests. The advection timescale was also halved (0.175 yr^{-1}) and doubled (0.5 yr^{-1}).*

constant in all cases. The density gradient is not identical due to the position of the thermocline relative to the salinity gradient which has been kept constant in this study. This means that the 300 m thermocline has the sharpest density contrast across the pycnocline, presenting a larger buoyancy barrier to overcome in order to mix below the pycnocline.

Shoaling the thermocline, results in a shallower winter mixed layer. However, the mixed layer entrains further into the warm water. This results in earlier and more rapid summer sea ice melt, decreasing the summer sea ice volume. Increasing the thermocline depth deepens the mixed layer, however less warm deep water is entrained, resulting in an increase in sea ice.

The timescale for advection was also halved and doubled from 3 months to 6 months and 1.5 months. Doubling the rate (1.5 month timescale), resulting in a shallower mixed layer, as the increased advection acts to increase the buoyancy barrier for mixed layer entrainment. The opposite is true for halving the rate.

3.4 Summary

In this Chapter the sensitivity of the simulated sea ice cover and mixed layer evolution in the Weddell Sea (WS) and the Amundsen Sea (AS) to the atmospheric and oceanic conditions was investigated. The sensitivity to each of the six atmospheric forcing variables: surface air temperature (SAT), specific humidity, shortwave radiation, longwave radiation, wind speed and snowfall rate. Each variable was varied individually by +/– σ, apart from snowfall rate where the 16th and 84th percentiles were used. The response was quantified by the change in the destratification time of the water column and mean ice volume in the Weddell Sea, and the maximum mixed layer depth and mean ice volume in the Amundsen Sea.

Very different sensitivity to surface atmospheric conditions was displayed in the two regions. In the Weddell Sea the water column completely destratified during winter in all sensitivity scenarios, however the timing becomes earlier/later depending on whether the rate of sea ice growth is increased/decreased. Decreased winter sea ice growth and a shorter period of complete destratification could decrease the rate of formation of Antarctic Bottom Water, as is currently being observed (Purkey et al., 2019).

In the Amundsen Sea, changes to the surface energy balance that promote ice growth and ocean cooling also promote mixed layer deepening. Changes to entrainment of warm deep waters oppose the direct impact of the atmospheric perturbation on the ice cover through changes in the rate of basal ice melting. These competing processes are evident in the sensitivity responses, and have been found in other modelling studies (Martinson, 1990; Zhang, 2007). A shallower mixed layer could also result in more warm CDW on the continental shelf, resulting in increased melting of the ice shelves.

The conditions in the Southern Ocean are predicted to get warmer and wetter (Christensen et al., 2013). The magnitude and regional variation in this is uncertain. The sensitivity results here suggest that reliable precipitation datasets are crucial. An increase in snowfall could promote an increase in the sea ice volume due to two processes: (i) an increase in snow ice formation; and (ii) freshening the surface ocean and decreasing the entrainment of warm deep waters. The formation of snow ice releases less brine into the ocean than the same volume of congelation ice from basal freezing, this effectively contributes to surface freshening. Our studies show that the sensitivity to continued warming and increased snowfall in the Weddell Sea response was dominated by sensitivity to air temperature, resulting in a decrease in sea ice, and slower destratification, whereas the Amundsen Sea response was dominated by sensitivity to increasing snowfall, resulting in more sea ice due to snow ice formation and a shallower mixed layer due to surface ocean warming and freshening.

Both regions were relatively insensitive to the rate of advection. The sensitivity to changes in the properties of high salinity shelf water (HSSW) on the WS shelf was investigated, showing that a more stratified profile (saltier shelf water), results in slower destratification, and eventually if the shelf water is saline enough, a shallower mixed layer. In the AS the depth of the thermocline was shown to have a large impact on the maximum mixed layer depth reached, a shallower thermocline resulting in a shallower maximum mixed layer and vice versa.

The displayed interannual variability is less than the magnitude of the response to the atmospheric perturbations in the sensitivity studies, suggesting that the variability in the atmospheric forcing parameters tend to cancel each other out to some degree, dampening the observed variability.

Chapter 4:

THE ROLE OF SEA ICE–OCEAN FEEDBACKS IN THE ANTARCTIC SHELF SEAS

4.1 Overview

In this chapter the strength and sign of selected feedbacks in the sea ice–ocean system in response to surface air temperature perturbations is investigated. In particular we study the impact of feedbacks in the ocean upon the sea ice (ocean feedback denied), feedbacks in sea ice upon the ocean (sea ice feedback denied), the albedo feedback, ice thickness–growth rate (insulation) feedback and the freezing temperature feedback. The methodology used to do this, the feedbacks studied and results for the ocean feedback denied are given in Section 4.2, the feedback study results for the Weddell and Amundsen Seas are presented in Sections 4.3 and 4.4, the feedback responses in the two regions are quantified and compared in Section 4.5 followed by a summary of the chapter in Section 4.6.

4.2 Methodology

The strength and sign of selected feedbacks in moderating the evolution of the sea ice–ocean system in response to perturbations in surface air temperature is investigated. For each feedback we consider the full model with perturbed +/– σ SAT and a feedback disabled (FD) run in response to the same +/– σ SAT forcing. The difference between the perturbed run and the FD run is the impact of the feedback response to the perturbation in SAT. Descriptions of the feedbacks along with an outline of how each feedback was denied are in Table 4.1. The 2 m surface air temperature (SAT) perturbations were chosen for the feedback studies because both regions demonstrated

large sensitivity to it in Chapter 3, and it is predicted to increase in the Southern Ocean in CMIP5 models over the next century (Christensen et al., 2013). Although snowfall also fits these two criteria, reanalysis values are not well trusted and predictions have higher uncertainty than surface air temperature (Bromwich et al., 2011; Jones et al., 2016).

The metrics are used as for the sensitivity studies, mean ice volume for both regions, timing of water column destratification for the Weddell Sea, and maximum mixed layer depth for the Amundsen Sea. All values are calculated after 8 years of simulation, at which point a steady state has been achieved (this typically only takes 2–3 years). An example of the feedback denial results is given for the ocean feedback in the next section before showing the results for all feedbacks.

4.2.1 Ocean Feedback on the Sea Ice

Here the ocean feedback denied results are shown in detail, in order to show the steps involved in summarising the results in sections 4.3, 4.4 and 4.5. This feedback was chosen to be shown in detail due to the numerous mentions in the literature of the importance of changes in the basal ocean heat flux for the Antarctic sea ice cover, e.g. (Martinson, 1990; Zhang, 2007). The full results for the other feedbacks are shown in Appendix A for reference, and the summary of all the feedback results are discussed in Sections 4.3, 4.4 and 4.5.

Figure 4.1 shows the feedback denial (FD) results in green for the Weddell Sea in response to +/–σ SATs, compared to the perturbed runs (+/–σ SATs in red/blue) and the original reference run (black line) after 8 years of simulation. In Figure 4.1, the feedback denied run (green line) in combination with + σ SATs run has an earlier rapid ice expansion and thickening, due to the earlier destratification of the water column compared to the + σ SAT perturbed simulation. There is also an earlier dip in ice concentration before this, due to the mixed layer entraining into the warmer deep waters earlier, and at a faster rate. The opposite statements are true for the –σ SAT FD simulation in Figure 4.1. In both FD simulations, once the mixed layer depth reaches the continental shelf we see that the ice concentration reaches the maximum value, and the ice thickness reaches the same maximum value as with the feedback enabled. At this point the negative feedback between the ice growth rate and the amount of warm water being entrained into ceases. The maximum and minimum ice thickness values only change by very small amounts.

In the Amundsen Sea FD results shown in Figure 4.2 there are much more dramatic changes in the ice cover in the FD simulations. In Figure 4.2, the feedback denied run in combination with + σ SAT (green line) in Figure 4.2 has much lower ice thickness all year round compared to the + σ SATs run (red). With the deeper mixed layer depth, the ice concentration and ice thickness now reach minimum values in the summer (i.e. open ocean). The opposite is true for – σ SAT (green line) in Figure 4.2, the ice thickness is greatly increased and the ice concentration minimum is increased relative to the – σ SAT simulation. We can also see in both simulations that the timing

Name of feedback denial simulation	Description of feedback	How the feedback is denied
Ocean denied	Brine rejection from sea ice growth causes mixed layer deepening. This results in more entrainment of warm deep water, increasing basal heating of the ice and reducing ice growth.	Mixed layer depth and properties from the reference run are prescribed.
Ice denied	Sea ice growth and melt results in brine and freshwater input into the mixed layer, resulting in mixed layer entrainment/shoaling. This typically reinforces the impact of atmospheric forcing on the mixed layer, e.g. on seasonal timescales surface cooling promotes mixed layer deepening and sea ice growth, which releases brine into the mixed layer and also causes mixed layer deepening.	The sea ice evolution (ice concentration and thickness) from the reference run is prescribed, along with the corresponding salt and heat fluxes.
Albedo feedback denied	The lower the ice concentration, the more shortwave radiation enters the mixed layer, promoting mixed layer warming and shoaling, causing the ice cover to reduce in concentration.	The ice concentration from the reference simulation is used in Equation 2.17 to determine the amount of shortwave radiation entering the mixed layer.
Insulation feedback denied	Thicker (thinner) ice decreases (increases) the conductive heat flux up through the ice (F_c), decreasing (increasing) the rate of ice thickening.	The reference ice thickness has been used within Equations 2.3 and 2.6 for F_c and the rate of change of ice concentration ($\frac{dA}{dt}$).
Freezing temperature feedback denied	Freshening the mixed layer increases the freezing temperature making it harder to melt ice and easier to freeze ice. In the model this relationship is governed by $T_f = 273.15 - 0.054S_{mix}$. Changes to the S_{mix} in this study are caused by changes to the seasonal cycle in sea ice volume. This is a part of the feedbacks involving changes to the stratification of the Southern Ocean, where freshening and cooling of the surface promote increasing sea ice.	The freezing temperature from the reference run is prescribed.

Table 4.1: Table outlining the feedbacks studied and how each feedback was denied.

at which the ice concentration starts to decrease in autumn is the same as the reference simulation, and is therefore dependent on the timing that the mixed layer depth penetrates the thermocline. The simulations show how changes in the mixed layer depth act as a negative feedback on the ice growth, acting to dampen the impact of the SAT perturbations on the volume of sea ice.

4.3 Weddell Sea Feedback Study Results

Feedback denial results for the Weddell Sea are shown in Figure 4.3. The distance between the red (blue) cross or dot and the red (blue) line shows the strength of the feedback. When the crosses or dots showing the destratification time/mean ice volume are inside the region bounded by the reference line and the corresponding red/blue line then the feedback is positive, and is negative otherwise.

The ocean FD results show that the ocean processes that are being switched off act as a small negative feedback on the ice volume. In the + σ SAT ocean FD run the prescribed water column destratification is earlier, lengthening the winter ice season. However, because the mixed layer deepening is earlier, this slows the rate of winter ice volume growth resulting in a decreased mean sea ice volume. Where the mixed layer depth was allowed to evolve in the sensitivity studies, the rate of ice growth determined the time of deepening, meaning that a longer sea ice season

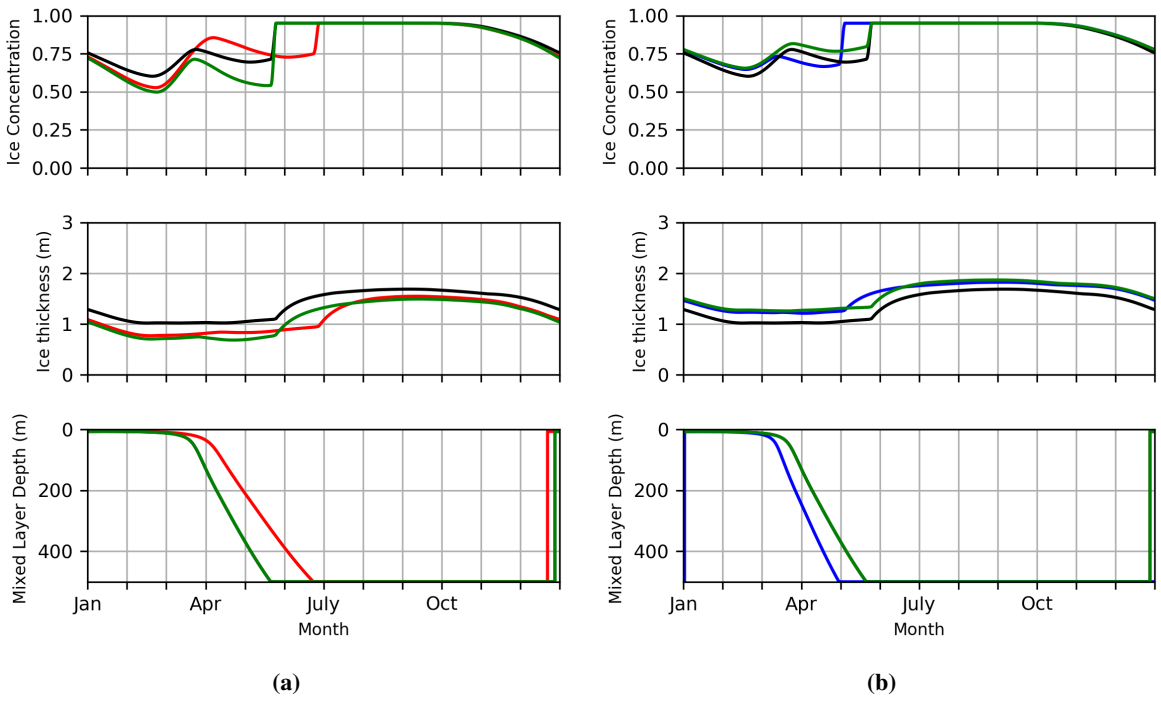

Figure 4.1: *Steady state ice concentration, ice thickness and mixed layer depth for the reference (black), + σ SAT (red), – σ SAT (blue), and the corresponding ocean denied simulations (green) for the Weddell Sea. (a) + σ SAT feedback denial simulation, and (b) – σ SAT feedback denial simulation.*

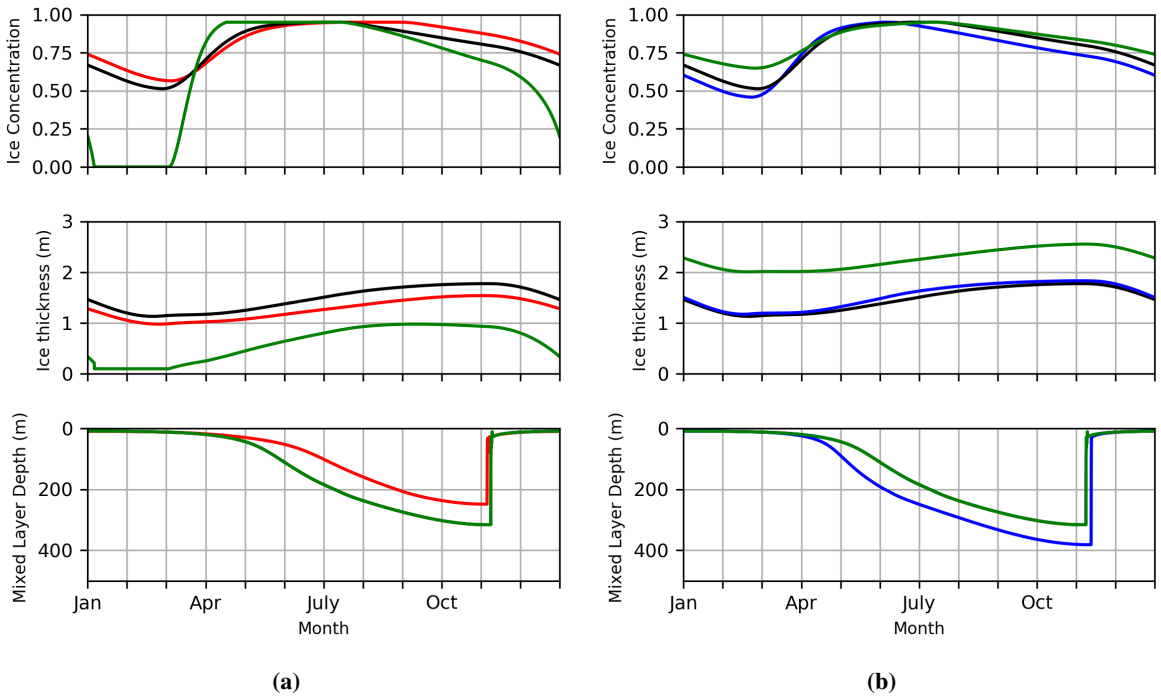

Figure 4.2: *Steady state ice concentration, ice thickness and mixed layer depth for the reference (black), + σ SAT (red), – σ SAT (blue), and the corresponding ocean denied simulations (green) for the Amundsen Sea. (a) + σ SAT feedback denial simulation, and (b) – σ SAT feedback denial simulation.*

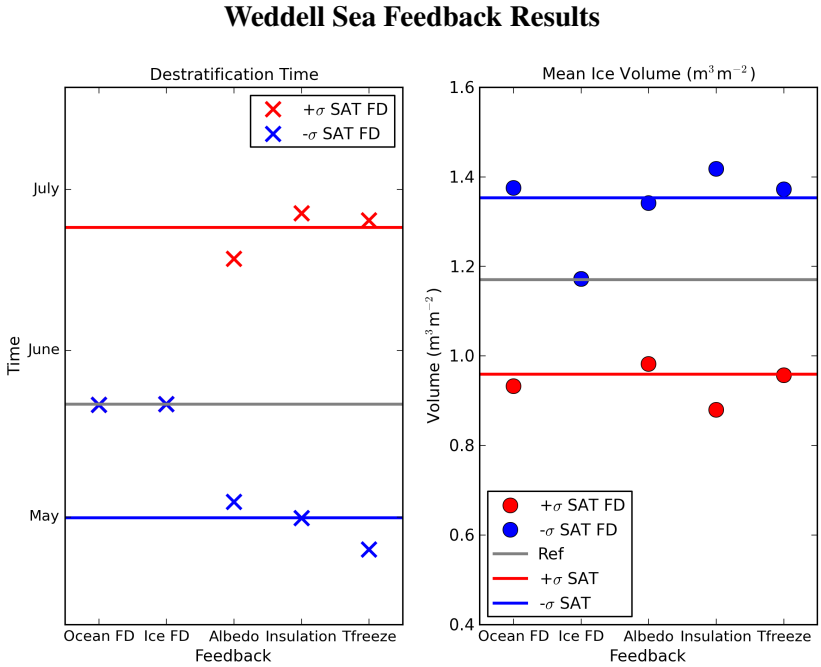

Figure 4.3: *Feedback study results for the Weddell Sea showing the destratification time and mean ice volume value for each simulation. All values are calculated from when the simulation has reached a steady state.*

corresponded with an increase in mean sea ice volume unlike what is seen when this feedback is removed. The opposite statements are true for the – σ SAT ocean FD run. Switching off the ocean response also prescribes the mixed layer salinity and therefore the freezing temperature.

Both ice FD runs have the same destratification time as the reference run. This illustrates that almost all of the mixed layer response to the perturbed surface air temperatures was due to the changes in the seasonal sea ice growth and melt changing the timing and magnitude of brine and freshwater fluxes into the mixed layer.

The albedo feedback acts as weak positive feedback on ice volume, and a slightly stronger positive feedback on the destratification time. In the + σ SAT FD run less shortwave radiation entering the mixed layer in the spring results in more summer ice. This increase is not seen as much in the winter ice volume due to negative feedbacks such as the ice thickness-insulation feedback reducing the rate of thickening for thicker ice. The opposite statements are true for the – σ SAT FD run.

The insulation feedback acts as a negative feedback on the mean ice volume and the destratification time. In the – σ SAT FD run, using the thinner ice thickness increases F_c and results in greater winter ice growth, increasing the mean ice volume and resulting in an earlier destratification time. The opposite is true for the + σ SAT FD run.

The freezing feedback only played a significant role in the – σ SAT FD run. As shown in Figure 3.1, using the higher reference freezing temperature reduces summer ice melt. Denying the freezing feedback increases the mean ice volume by a similar magnitude to the ocean FD, indicating that a significant proportion of the change in ice volume in the ocean FD run may be explained by changes in the freezing temperature. In the + σ SAT FD run for the Weddell Sea, however, the mixed layer temperature is roughly equal or greater than both the freezing temperature of the reference run and the warmer case, meaning there is little impact.

4.4 Amundsen Sea Feedback Study Results

Feedback denial results for the Amundsen Sea are shown in Figure 4.4. The results show the ocean FD to strongly buffer the mean ice volume. In – σ SAT FD run the prescribed mixed layer is shallower, resulting in an increase in mean sea ice volume. The opposite statements are true in the + σ SAT FD run. The large magnitude of response in the ice cover indicates that changes to the depth of the ocean mixed layer strongly buffer the impacts of perturbations in the atmospheric conditions on the sea ice volume. Note that the very small decrease in mean ice volume in the –σ run relative to the reference value means that this feedback has a positive sign for the –σ SAT FD run.

The ice FD results show that the maximum mixed layer depth are equal to the reference value

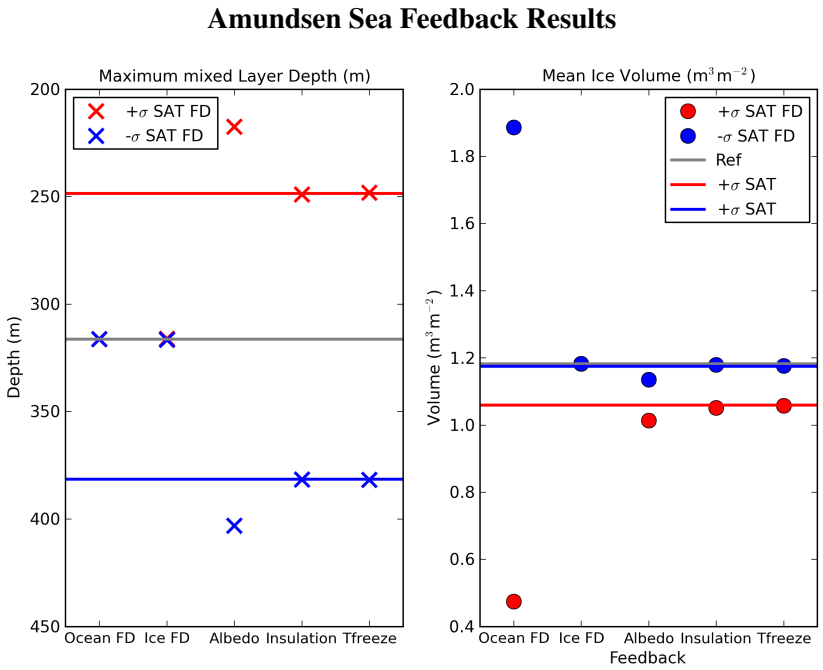

Figure 4.4: *Feedback study results for the Amundsen Sea showing the maximum mixed layer depth and mean ice volume value for each simulation. All values are calculated from when the simulation has reached a steady state.*

for both FD simulations. As with the Weddell results, this demonstrates how changes in the sea ice growth, and corresponding brine rejection, are responsible for the mixed layer response to the surface air temperature perturbation. Without the perturbations to the seasonal sea ice evolution the mixed layer remains at the reference value.

The albedo feedback acts as a negative feedback on the maximum mixed layer depth and the mean ice volume. The presence of warm CDW below the 200 m thermocline means that whenever the mixed layer deepens across this depth the amount of heat being mixed upwards increases, or decreases if the mixed layer shoals. In the + σ SAT FD run the amount of shortwave entering the mixed layer is increased in the spring, shoaling the mixed layer. In the – σ SAT FD run, the opposite changes to the shortwave occur. The changes to the mixed layer counteract the decrease in heat transferred to the ice from shortwave fluxes, meaning there is little change in the summer ice volume and a decrease in the winter ice volume is seen. In summary, the presence of the ocean mixing feedback makes the albedo results in the Amundsen Sea non-intuitive for two reasons: (i) the perturbations to the spring and summer ice concentration which are being used to remove the feedback are heavily determined by the ocean mixing feedback; and (ii) changes to the shortwave flux into the mixed layer influence the mixed layer depth, therefore making changes to ocean mixing an integral part of the feedback response.

The ice insulation feedback and the freezing temperature feedback show very little impact on the mixed layer depth or mean ice volume. The variation in freezing temperature between the reference and the +/– σ SAT runs is not as great as in the Weddell run, as shown in Figures

3.1 and 3.2 due to the ocean mixing feedback buffering changes to the ice volume. This means removing the freezing temperature feedback has little impact, and the changes in the ice volume when removing the ocean mixing feedback are nearly exclusively due to changes in ocean heat. However, larger freshening, e.g. from ice sheet melt or continental run off, may make this feedback more important near the continent.

4.5 Gamma: A Comparison the role of feedbacks in the Weddell and Amundsen Seas

Following the methodology in Goosse et al. (2018), the impact of each feedback on mixed layer depth/destratification time and mean ice volume has been quantified for each set of feedback

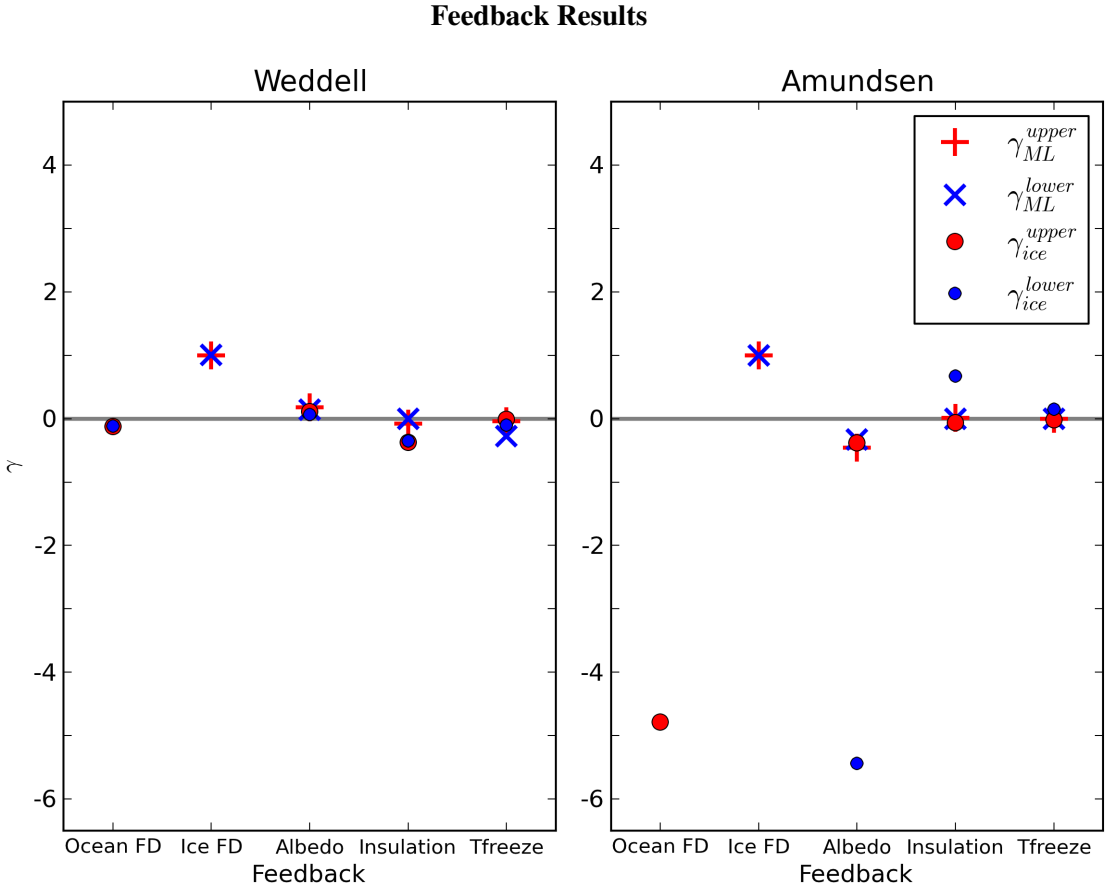

Figure 4.5: *Values of γ for each set of feedback runs, see equation 4.1 for calculation of γ, indicating the relative magnitude of impact of each feedback on the mixed layer depth/destratification time and mean ice volume for each region. γ_{ML} is calculated using the maximum mixed layer depth in the Amundsen Sea and using the destratification time in the Weddell Sea. γ_{ice} is calculated using the mean ice volume for both regions. Note there are no values for γ_{ML} for ocean FD and γ_{ice} for ice FD as the associated mixed layer/ice volume changes are prescribed as part of the process of removing the feedback. The γ_{ice}^{lower} value for the Ocean FD in the Amundsen is off the figure scale, with a value of 96.9.*

runs using

$$\gamma = \frac{(Pert - Ref) - (FD - Ref)}{(Pert - Ref)} = \frac{(Pert - FD)}{(Pert - Ref)}, \tag{4.1}$$

where γ indicates the sign and relative strength of each feedback for each perturbation and region, Ref is the reference run value (mixed layer depth/destratification timing/mean ice volume), $Pert$ is the perturbed (+/– σ SAT) run value, and FD is the corresponding +/– σ SAT feedback disabled (FD) run value. γ gives the magnitude of the feedback impact normalised by the response of the perturbation. A negative value of γ indicates a negative feedback, that acts to dampen any change in mixed layer depth/destratification timing/mean ice volume, meaning that removing the feedback results in amplifying the change. A positive value of γ indicates a positive feedback. γ = 0 indicates no feedback response (i.e. $Pert = FD$). γ =1 indicates a positive feedback, where all of the response to the perturbation is due to the feedback ($FD = Ref$) and γ = –1 indicates a negative feedback where $Pert - FD = -(Pert - Ref)$, meaning that enabling the feedback halves the resulting perturbation.

The use of γ allows the relative size of the feedbacks to be compared for the Weddell and Amundsen Seas relatively easily. The value of γ will be dependent on the reference values and perturbation applied, as discussed in Goosse et al. (2018). This is partially explored by investigating the +/– σ SAT response for each feedback. The use of a standard set of perturbations allows us to systematically compare the feedbacks. The feedbacks interact, and influence the impact of other feedbacks. This means that the values of γ corresponding to different feedbacks cannot be simply added to determine the combined feedback response. Figure 4.5 shows the results for both regions, γ_{ML} is calculated using the maximum mixed layer depth in the Amundsen and using the destratification time in the Weddell. γ_{ice} is calculated using the mean ice volume for both regions.

In the Weddell Sea, Figure 4.5 shows that the ice and mixed layer γ values for the feedbacks are mostly quite consistent for the +/– σ perturbations. In the Weddell Sea the impact of the ocean mixing feedback on the ice volume is relatively small. The timing of ice growth and the duration of the winter ice season changes (not reflected in γ_{ice}), however there is little change to the ice volume. This is because the mixed layer always destratifies, causing large amounts of water column cooling and ice growth. The ice FD results show that the ice feedback on the mixed layer is strong and positive, reflecting that faster ice growth results in faster destratification. Without the sea ice response to the perturbation the mixed layer remains unchanged, as shown by the γ_{ML} of 1. The albedo feedback in the Weddell Sea is relatively small, but has more intuitive results than the Amundsen (i.e. it is a positive feedback). The insulation feedback has the strongest impact on the ice volume, acting to buffer ice volume changes. The freezing temperature feedback is a weak negative feedback in the – σ SAT run, but negligible in the warmer run.

The results in Figure 4.5 clearly show how much stronger the impact of the ocean mixing feedback on the ice volume in the Amundsen Sea is than all the other feedbacks studied in both regions. The feedback becomes stronger as the mixed layer entrains deeper into the warm deep waters, making the feedback stronger in the – σ FD (off the scale in Figure 4.5 with a value of 96.9). This strong feedback means that the changes in ice concentration are relatively small in the sensitivity studies. It also means that the albedo feedback has little impact on the sea ice cover, and actually acts as a negative feedback in the Amundsen Sea. This is because the change in basal heating due to changes in mixed layer depth dominates the ice cover response. As seen in the Weddell the γ_{ML} values for the ice feedback on the mixed layer are 1, illustrating how changes in sea ice growth amplify the impact of the atmospheric perturbation on the mixed layer. Without the changes in sea ice growth the maximum mixed layer depth is unchanged.

The Amundsen Sea mixed layer responses γ_{ML} are fairly consistent in sign for each feedback for +/– σ perturbations, however the ice volume responses γ_{ice} are not. The albedo feedback is more negative for the – σ run due to the ocean mixing feedback interacting with the albedo feedback, and increasing in strength for deeper mixed layers. The insulation feedback has a very small magnitude in the Amundsen except for the – σ mean ice volume which is slightly positive. This is predominantly a result of the very small difference in mean ice volume between the reference and the – σ run which is used to calculate γ_{ice}^{lower}. In the Amundsen Sea the freezing temperature feedback has negligible impact on the sea ice cover as differences in the freezing temperature between the +/– σ SAT simulations are not large enough to lead to a significant change in ice volume.

4.6 Summary

Feedback studies were carried out using SAT perturbations and feedback denial experiments. The feedbacks investigated were: (i) the ocean feedback, whereby deepening of the mixed layer into warm, deep waters can increase the basal melt rate acting as a negative feedback on sea ice growth; (ii) the sea ice feedback, whereby the seasonal sea ice melt and growth cycle inputs freshwater and brine into the mixed layer, influencing the entrainment rate, typically amplifying the effect of atmospheric perturbations on the mixed layer (e.g. surface atmospheric warming causes both surface ocean warming and an increase in sea ice melt, both promoting mixed layer shoaling); (iii) the albedo feedback, whereby the ice concentration determines how much shortwave radiation enters the mixed layer so that a decrease in ice concentration increases the shortwave radiation flux to the mixed layer, causing shoaling and warming, promoting further decline in the sea ice concentration; (iv) the insulation feedback, whereby thicker sea ice has a lower conductive heat flux up through the ice, reducing the rate of ice thickening, acting as a negative feedback during ice growth; and (v) the freezing temperature feedback, whereby fresher

seawater freezes at a higher temperature, meaning that freshening from increased sea ice melt could in turn promote ice growth and act as a negative feedback.

In the Weddell Sea all the feedbacks were found to have a fairly minimal impact on the ice volume when compared to the magnitude of the sensitivity results. The sea ice feedback study showed that sea ice response to the atmospheric perturbation strongly amplified and controlled the mixed layer response. This suggests that whilst the strong surface cooling is the driver required to destratify the water column, it is the brine rejection from sea ice growth that strongly controls the rate and timing of mixed layer deepening. The same strong relationship was seen in the Amundsen. The albedo feedback is a small positive feedback in the Weddell Sea. The insulation feedback had the strongest impact on the sea ice volume, acting as a negative feedback on ice growth.

In the Amundsen Sea, the results from our feedback studies showed that the mixed layer response to atmospheric forcing acts as a strong buffer against the sea ice response to atmospheric perturbations, increasing/decreasing basal melting due to changes in entrainment of warm deep waters. Quantifying the impact of each of the feedbacks on the mixed layer and ice volume showed that the impact of the ocean feedback on the ice volume was by far the strongest. The impact of the ocean feedback was larger than the ice volume response to the +/– σ SAT perturbation, meaning that in the absence of the feedback, the ice response would be several times larger. The negative feedback was shown to strengthen as the mixed layer deepened further into the deep warm waters, opposing changes to the ice cover caused by surface warming. Zhang (2007) also showed that this change in ocean heating may outweigh the change in sea ice growth. This feedback interacts strongly with the other feedbacks investigated, due to the buffering of the ice concentration and ice volume changes in response to the perturbations, influencing the strength and behaviour of the other feedbacks. Changes to the mixed layer depth caused by other feedbacks also involve changes in mixing of deep waters, involving the ocean feedback. For example, the albedo feedback involves more or less shortwave radiation entering the mixed layer, which then shoals or deepens the mixed layer, engaging the ocean feedback.

Chapter 5:

USING THE COUPLED CICE-MIXED LAYER MODEL TO EXAMINE AT THE OCEAN–SEA ICE FEEDBACK IN THE AMUNDSEN SEA

In this section the Los Alamos sea ice model CICE is coupled to a mixed layer model and used to investigate the ocean feedback on the sea ice. The model configuration and set up is covered in Section 5.1, the model details are given in Section 5.2, the formulation of the model setup is elaborated in Section 5.3, a control run is presented in Section 5.4, the sensitivity of the model to atmospheric forcing is investigated in Section 5.5.3, and finally, the ocean feedback in the Amundsen Sea is investigated in Section 5.6, followed by a summary in section 5.8.

5.1 CICE Setup

CICE is a dynamic–thermodynamic model of sea ice. Largely the default CICE settings were used. The sea ice in each grid cell is divided between five ice thickness categories, one snow thickness category, and open water. The sea ice thermodynamics comes from Bitz and Lipscomb (1999), an update on the Maykut and Untersteiner (1971) sea ice surface energy balance, that is energy conserving and accounts for internal brine pockets in the sea ice. The ice dynamics are based on the elastic-viscous-plastic (EVP) rheology of Hunke and Dukowicz (1997); Hunke (2001); Hunke and Dukowicz (2002), a representation of the viscous–plastic rheology of sea ice dynamics (Hibler, 1979). Seven vertical layers are used, and one snow layer. The default radiation scheme is used, so penetrating solar radiation is equal to zero for snow covered sea ice, as most incoming sunlight is absorbed near the top surface. The standard Maykut and Untersteiner (1971)

conductivity is used. Linear remapping ice thickness distribution (ITD) approximation (Lipscomb and Hunke, 2004)A full description of the model can be found in the user manual (Hunke et al., 2015).

CICE was configured to run in stand-alone mode, on a 0.5° lat/long grid (176 by 176), with the north pole at the equator (roughly 55 km horizontal resolution). The Antarctic land mask and bathymetry are from interpolation of the RTOPO data set (Timmermann et al., 2010). The atmospheric forcing is from the ERA-Interim reanalysis (Dee et al., 2011). This consists of 6-hourly fields for 2 m air temperature, specific humidity and 10 m zonal and meridional wind, daily fields of downward short wave and long wave radiation, and monthly fields of precipitation (snow and rain). The model is initialised in January with no ice.

5.1.1 Mixed layer model

In the standard CICE stand alone configuration (which is used in Section 5.3.1), the mixed layer depth is set to a fixed value (in this case 20 m). The mixed layer salinity is prescribed and the mixed layer temperature is prognostic. The deep ocean temperature is prescribed from data. A mixed layer–ocean model has been incorporated into the Los Alamos sea ice model CICE (version 5.1, written in FORTRAN90), using the set up from Petty et al. (2014). Coupling CICE to a mixed layer model allows the mixed layer depth, temperature and salinity to evolve based on surface and deep ocean heat and salt fluxes. This enables us to examine the role of the ocean feedback on the sea ice, when more sophisticated sea ice physics is incorporated than in the simple model used in Chapters 2 to 4. Using a simple bulk mixed layer model allows a more complete understanding of the model components, and response in the feedback study. A very similar mixed layer model to the one used in the previous chapters and described in Chapter 2, using the same model set up as Petty et al. (2014). The ocean below the mixed layer is relaxed towards data based on observations, the profiles used for the Amundsen Sea study region are shown in Figure 5.1.

The ocean profiles used in the ML model are from the World Ocean Atlas 09 (WOA09) temperature (Lecarnini et al., 2010) and salinity (Antonov et al., 2010) . These are climatological fields of temperature and salinity, from in situ data collected, interpolated onto standard depth levels on a 1° grid. The annual climatological data has been interpolated onto the CICE grid, a weighted extrapolation procedure was used to fill any missing grid points near the coastline, then smoothed using a nine-point gaussian filter. A coarse vertical grid was used to represent the water column, depth values mapping to $z = (30, 50, 100, 150, 200, 300, 400, 600, 800, 1000)$ m levels. The WOA09 data is initialised at each of these levels in the T, S ocean grids at all grid points, T_{mix}, S_{mix} and T_s are initialised to the $z = 30$ m values. To balance any salt loss from relaxation of the deep ocean (below the mixed layer), the mixed layer salinity is restored back to the annual climatological (30 m) value, with a period of 1 year. This crudely represents the export of mixed

layer waters away form the shelf.

The mean for the Amundsen Sea is plotted for each month in Figure 5.1. The profiles are much more stratified, with a shallower thermocline, than those used in the idealised model, and to those indicated by observations in the region. Using these profiles means that there is no impact from variable ocean dynamics/advection, so as in the previous chapters, we are isolating the impact of surface processes alone and the subsequent responses. There is no horizontal interaction between grid cells in the mixed layer model.

5.2 Model description

This section summarises the description of the CICE-ML model given in Petty et al. (2014) of the coupled CICE-ML model. Any changes have been highlighted in the subsequent text.The main processes described below are highlighted in the schematic in Figure 5.2, taken from Petty et al. (2014).

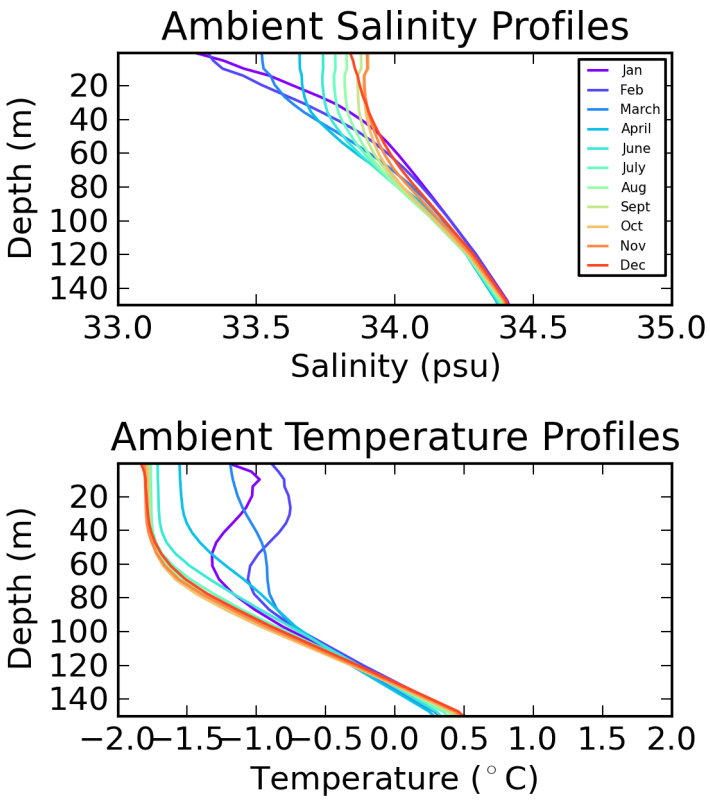

Figure 5.1: *Monthly ocean profiles for the Amundsen Sea study region, showing the top 150 m.*

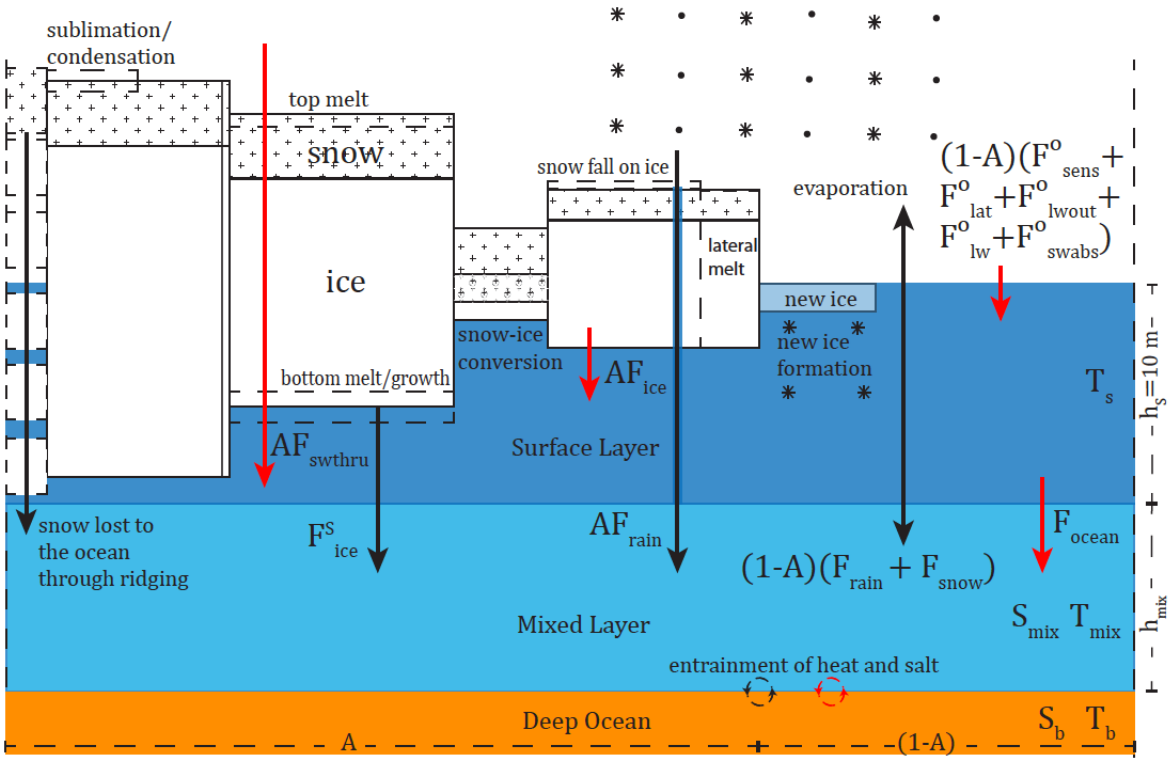

Figure 5.2: *Schematic of the main thermodynamic processes in the CICE-ML model, figure taken from Petty et al. (2014).*

5.2.1 Heat and salt fluxes

A simple two–layer ocean is used for the temperature calculations, a fixed depth (10 m) surface layer and a variable mixed layer depth below. The surface layer exchanges heat with the sea ice and atmosphere above, and the mixed layer below. This allows the ocean surface temperature to evolve more rapidly, as would be expected, which is important for simulating more realistic ice concentration fields. Without this surface layer present, the mixed layer (and therefore the surface) temperature may remain slightly above freezing when the mixed layer is deep, and entrain deep ocean heat that is instantaneously distributed throughout the whole mixed layer, unrealistically hindering the formation of sea ice in the winter. Small variations in the salinity have a smaller impact on the sea ice growth, so the sea surface salinity and the mixed layer salinity are treated as the same.

The heat flux from the ice and open–ocean fraction to the ocean surface layer are

$$F_{surface} = (1-A)(F^o_{sens} + F^o_{lat} + F^o_{lwout} + F^o_{lwin} + F^o_{swabs}) + A(F_{ice} + F_{swthru}), \quad (5.1)$$

where F^o_{sens} is the sensible heat flux between the atmosphere and the open ocean, F^o_{lat} is the latent heat flux between the atmosphere and the open–ocean surface, F^o_{lwout} is the black–body

heat flux and the open ocean surface to the atmosphere, F^o_{lwin} is the downward long–wave radiative heat flux, F^o_{swabs} is the downward short–wave radiative heat flux, calculated as a sum over four radiative categories (direct and diffuse, visible and near–infrared) with varying albedo parameterisations, F_{ice} is the heat flux from the ocean surface to the base of the ice (aggregated over all ice categories/thicknesses), and F_{swthru} is the short–wave radiative heat flux that passes through the ice and is absorbed by the ocean.

The ocean heat flux from the ocean surface layer to the mixed layer is calculated as

$$F_{ocean} = c_p \rho_w u_\star (T_S - T_{mix}), \tag{5.2}$$

where c_p is the specific heat capacity of water, ρ_w is the density of sea water, T_S is the ocean surface temperature and T_{mix} is the mixed layer temperature. The surface layer is assumed to be free draft, such that $u_\star$is the ocean surface friction velocity, calculated by a combination of the ice–ocean wind stress τ_i and the open water wind stress τ_0 as

$$u_\star = \sqrt{[A\,|\tau_i| + (1-A)\,|\tau_0|]/\rho_w}. \tag{5.3}$$

The net salt flux (m s^{-1}) into the mixed layer from the ice covered fraction A is calculated as

$$F^S_{ice} = [(1000 - S_{mix})F_{salt} - S_{mix}F_{fresh}]A]\rho_w, \tag{5.4}$$

where F_{salt} and F_{fresh} are the direct fluxes of salt and freshwater (kg m^{-2} s^{-1}), calculated as a combination of ice/snow growth/melt and snow lost to the mixed layer through pressure ridging.

Freshwater also enters the mixed layer from precipitation and evaporation. Precipitation includes both rainfall and snowfall (rain changes to snow if $T_a \leq 0°C$). The net surface salt flux is

$$F^S_{pe} = -\frac{S_{mix}}{\rho_w}[F_{rain} + (1-A)(F_{snow} + \frac{F^0_{lat}}{L_v})], \tag{5.5}$$

where F_{rain} and F_{snow} are prescribed rates of rainfall and snowfall, L_v is the latent heat of vaporisation. Rainfall on the sea ice fraction is assumed to percolate through the sea ice, and enter the mixed layer.

5.2.2 Power input

The surface buoyancy fluxes and wind drag drive convective mixing in the mixed layer. The rate of mechanical energy input from the surface fluxes is given by; (i) salt/freshwater flux from the sea ice growth/melt P_{salt}: (ii) salt/freshwater flux from precipitation and evaporation P_{pe}; (iii)

the heat flux between the ocean surface layer and the mixed layer P_{heat}; and (iv) wind shearing from the ice and open water fractions P_{wind}. The net power input P_{net} is the sum of these four input terms.

5.2.3 Mixed layer entrainment

As in Chapters 3 and 4, we use the idealised bulk mixed–layer energy balance model used in Petty et al. (2013), based on that of Kraus and Turner (1967) and Niiler and Kraus (1977). This assumes that temperature and salinity are homogenous throughout the mixed layer, and there is a full balance of turbulent kinetic energy (TKE). There is a very slight variation in the definition of d_{mix} for temperature and salinity, due to the ocean surface temperature layer (see Section 5.2.1 for details). However, the error this introduces should have a negligible impact on results in comparison to the general assumptions the bulk mixed layer model is built on. The entrainment rate of the mixed layer is given by the balance of the energy needed to entrain water from below with the energy given by the wind and the surface buoyancy fluxes, giving the entrainment rate as

$$w = \frac{dd_{mix}}{dt} = \frac{P_{net}}{d_{mix}\Delta b + c_m^2}, \tag{5.6}$$

where c_m is the bulk turbulent velocity scale representing the turbulent fluctuations of the mixed layer that will result in a frictional sink of TKE, and Δb is the difference in buoyancy across the base of the mixed layer, given by

$$\Delta b = g\alpha(T_{mix} - T_B) - g\beta(S_{mix} - S_B), \tag{5.7}$$

where T_B and S_B are the deep ocean temperature and salinity at the bottom of the mixed layer respectively, which are prognostic variables in this model.

When $w < 0$, the mixed layer detrains back to a stable state. The minimum mixed layer depth is set to 20 m. During detrainment the salinity and temperature are only influenced by the surface fluxes, leaving behind a layer of Winter Water below the new, shallower mixed layer base. The mixed layer depth is unable to exceed the seabed depth.

5.2.4 Temperature and salinity calculations

The changes in mixed layer temperature and salinity is calculated through a combination of surface heat/salt fluxes and entrainment heat/salt fluxes from the deep ocean

$$\frac{dT_{mix}}{dt} = \begin{cases} \frac{F_{ocean}}{\rho_w c_p d_{mix}} + \frac{w}{d_{mix}}(T_b - T_{mix}) & \text{for } w > 0 \\ \frac{F_{ocean}}{\rho_w c_p d_{mix}}, & \text{for } w \leq 0, \end{cases} \tag{5.8}$$

$$\frac{dS_{mix}}{dt} = \begin{cases} \frac{F^S_{ice}+F^S_{pe}}{d_{mix}} + \frac{w}{d_{mix}}(S_b - S_{mix}), & \text{for } w > 0 \\ \frac{F^S_{ice}+F^S_{pe}}{d_{mix}}, & \text{for } w \leq 0, \end{cases} \tag{5.9}$$

and an ocean surface temperature given by

$$\frac{dT_S}{dT} = \frac{F_{surface} - F_{ocean}}{c_p \rho_w h_s}. \tag{5.10}$$

The freeze/melt ice potential in the surface layer is calculated as

$$H^S_{frzmlt} = \frac{c_p \rho_w h_S (T_f - T_S)}{dT}, \tag{5.11}$$

where $T_f = 273.15 - 0.054 S_{mix}$ is the freezing temperature for seawater in the surface layer. it is ensured that $T_S \geq T_f$, such that any latent heat flux from ice formation is included in the heat flux calculations. If $T_{mix} \leq T_f$, the potential to form ice in the mixed layer (not melting because the mixed layer is separated from the ice by the surface layer) is calculated as the following

$$H^{mix}_{frzmlt} = \frac{c_p \rho_w h_S (T_f - T_{mix})}{dT}, \text{ for } T_{mix} < T_f, \tag{5.12}$$

in which case $T_{mix} = T_f$ to ensure that $T_{mix} \geq T_f$. H^{mix}_{frzmlt} is then returned to CICE as the net potential to grow/melt ice.

5.2.5 Representation of the deep ocean

At each horizontal (x, y) grid cell the temperature of salinity are given by

$$T_{ocean} = T(z_1), T(z_2), T(z_3), ..., T(z_N) \text{ and} \tag{5.13}$$

$$S_{ocean} = S(z_1), S(z_2), S(z_3), ..., S(z_N), \tag{5.14}$$

where z represents the vertical ocean grid index and $N$is the number of vertical levels chosen. The mixed layer temperature and salinity is assigned to the deep ocean grid within the mixed layer at each time step. As the mixed layer shoals, the signature of Winter Water is left behind in the deep ocean.

A linear interpolation scheme is used to update the values of S_B and T_B that are being entrained into the mixed layer, to account for the coarse ocean grid. If the mixed layer is very shallow or deep, then T_B and S_B are set to the top and bottom values. Below the mixed layer the T/S values are relaxed to their initial values, crudely representing the advection of Winter Water

and the replacement by mean summertime ocean water. The restoring timescale is 3 months, as we expect this this to mainly occur in the spring.

5.2.6 Ice dynamics

The sea ice model is forced with near surface winds, meaning that the atmospheric Ekman layer is accounted for. The ice-ocean drag is calculated as

$$\tau_{\mathbf{i}} = c_d \rho_w |\mathbf{U_W} - \mathbf{u}|[(\mathbf{U_W} - \mathbf{u})cos\theta_W + \mathbf{k} \times (\mathbf{U_W} - \mathbf{u})sin\theta_W], \tag{5.15}$$

where $\mathbf{u}$ is the ice velocity, $\mathbf{U_W}$ is the geostrophic ocean velocity (ocean currents are neglected here meaning that $\mathbf{U_W} = 0$, c_d is an ice–ocean drag coefficient, and θ_W (set to -15°) is the ocean turning angle between the geostrophic ocean currents and the ocean surface currents under the ice.

5.3 Formulation of the Sea Ice-Mixed Layer Model

In the following subsections the stages in the formulation of the sea ice-mixed layer model used to investigate the ocean feedback is presented. Examining the sequential changes from each of the stages helps to show the sensitivity and impact of each change to the model set up. The stages include the stand alone CICE, with the mixed layer fixed to 20 m (5.3.1), CICE coupled to a idealised mixed layer model (5.3.2), and finally a change to the snow ice parameterisation (5.3.3). In all of these simulations the model is forced with climatological atmospheric forcing (ERA-I temporally averaged between 1980 and 2016). The wind field is taken from 2005 instead of averaging to ensure that the wind field is spatially consistent. The seasonal averages of ice concentration, ice thickness and mixed layer depth are shown in Figures 5.3, 5.4 and 5.5, comparing the three model configurations. These values are calculated after the model is run with the climatological atmospheric forcing for 10 years, the seasonal averages are then calculated from the final year.

5.3.1 Fixed mixed layer model

In the CICE stand alone set up, the mixed layer depth is set to a fixed value of 20 m. The seasonal averages for ice concentration and ice thickness are shown in Figures 5.3 and 5.4, with comparisons to the later two versions of the model.

The maximum ice extent is reached in winter (JJA), and is maintained throughout spring (SON), but the ice concentration values away from the se ice edge starts to decrease from 1.0 in winter to 0.75-0.8.

The minimum ice thickness occurs in Spring (Autumn) and maximum in Spring (SON). Typical maximum values in the Weddell Sea of 1.5-2 m, apart from on the western side of the peninsula where values reaching 3 m or more. There is a persistent patch of thick ice (greater than 3 m) to the west of the Antarctic peninsula and in the Bellingshausen Sea all year round.

5.3.2 Mixed layer model coupled to CICE

The 1D mixed layer model used in Chapters 3-4 was coupled to the CICE model, as described in Section 5.2. The seasonal averages of ice thickness and concentration are broadly similar to the fixed mixed layer simulation, shown in Figures 5.3 and 5.4. There is a slight decrease in maximum sea ice extent in JJA and SON. Ice concentration is generally slightly lower if significantly different, the largest differences being near the ice edge. From looking at the mixed

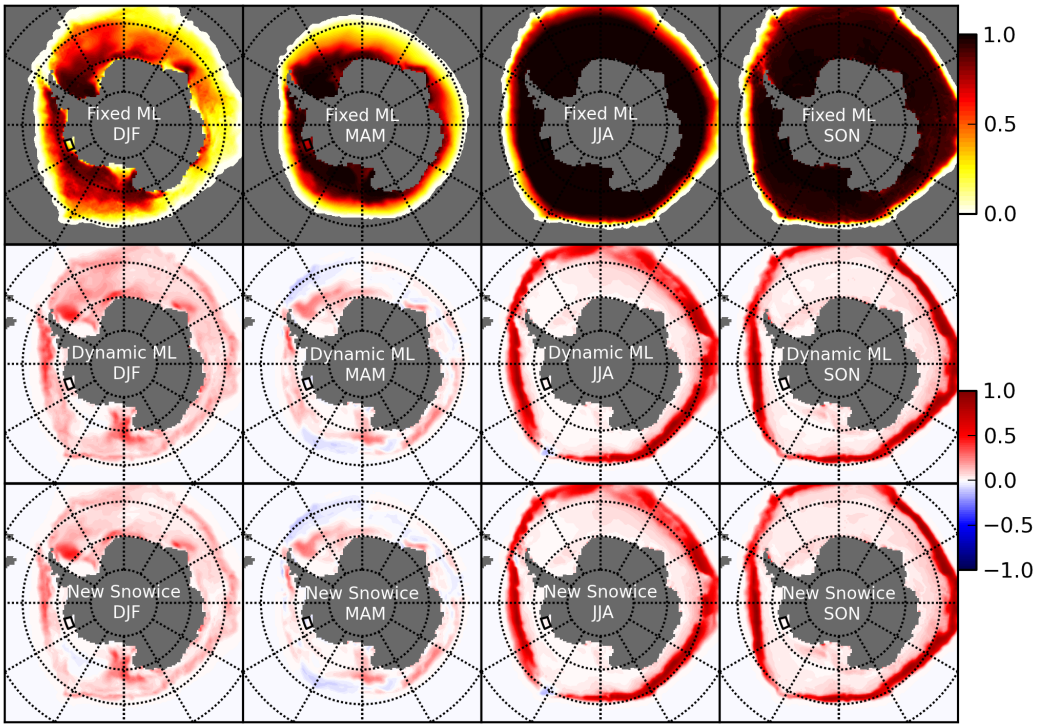

Figure 5.3: *Seasonal averages for sea ice concentration. Summer (DJF) is the December, January and February average. Autumn (MAM) is the March, April and May average. Winter (JJA) is the June, July and August average. Spring (SON) is the September, October and November average. The region used for the Amundsen Sea averaging is indicated by a black box. Top row is the fixed mixed layer depth configuration, second row is the fixed mixed layer minus the dynamic mixed layer averages (Fixed ML–Dynamic ML), and the bottom row is the averages for fixed mixed layer run minus the changed snow ice parameterisation run averages (Fixed ML – New snowice).*

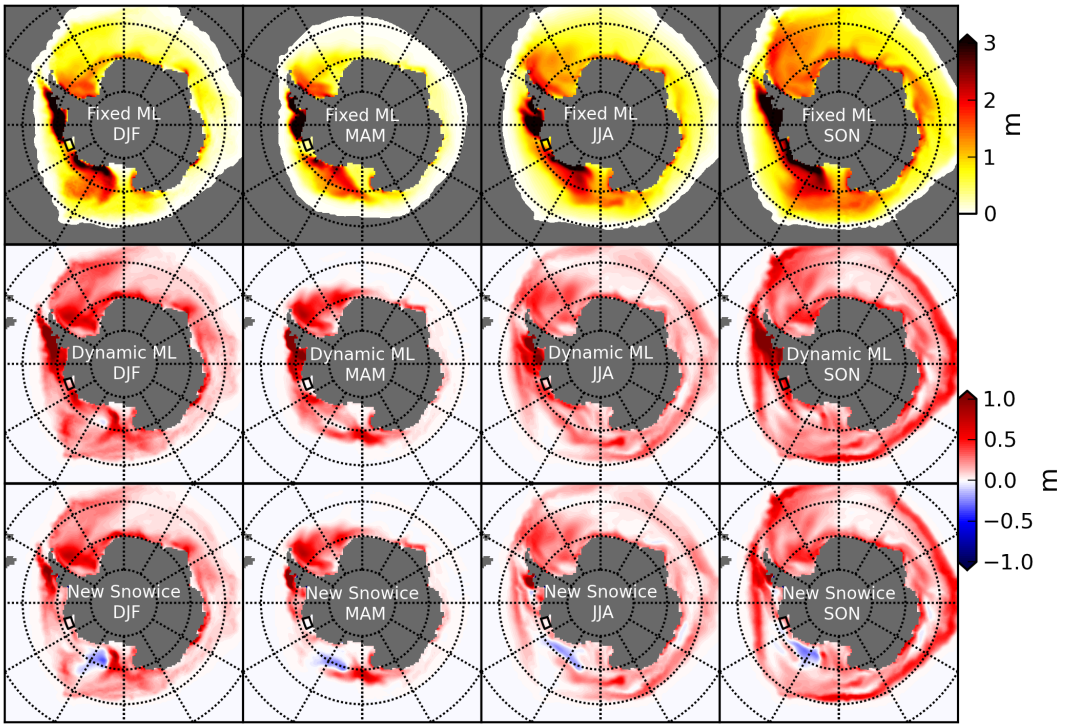

Figure 5.4: *Seasonal averages for sea ice thickness. Summer (DJF) is the December, January and February average. Autumn (MAM) is the March, April and May average. Winter (JJA) is the June, July and August average. Spring (SON) is the September, October and November average. The region used for the Amundsen Sea averaging is indicated by a black box. Top row is the fixed mixed layer depth configuration, second row is the fixed mixed layer minus the dynamic mixed layer averages (Fixed ML–Dynamic ML), and the bottom row is the averages for fixed mixed layer run minus the changed snow ice parameterisation run averages (Fixed ML – New snowice).*

layer depths in Figure 5.5, this seems to reflect the change in mixed layer depth at these latitudes where the ACC is located. The ice concentration is decreased where the mixed layer becomes deeper, changing from about 50 m to 100-200 m. This may reflect an increase in basal melting of the sea ice due to upward mixing of warmer circumpolar deep waters. However nearer to the coast, the deeper mixed layers present in the Weddell Sea and the Ross Sea have not had a significant impact on the ice concentration.

The ice thickness has been generally decreased, particularly in the region of the thick ice to the west of the peninsula. This may be due to the presence of warm circumpolar deep waters higher in the water column in these regions due to the proximity to the ACC. This indicates that basal melting is a significant process in these regions.

Ice concentration is lower in all seasons, with a smaller coverage of complete ice concentration. We can see this particularly in the Weddell Sea sector away from the coast. The

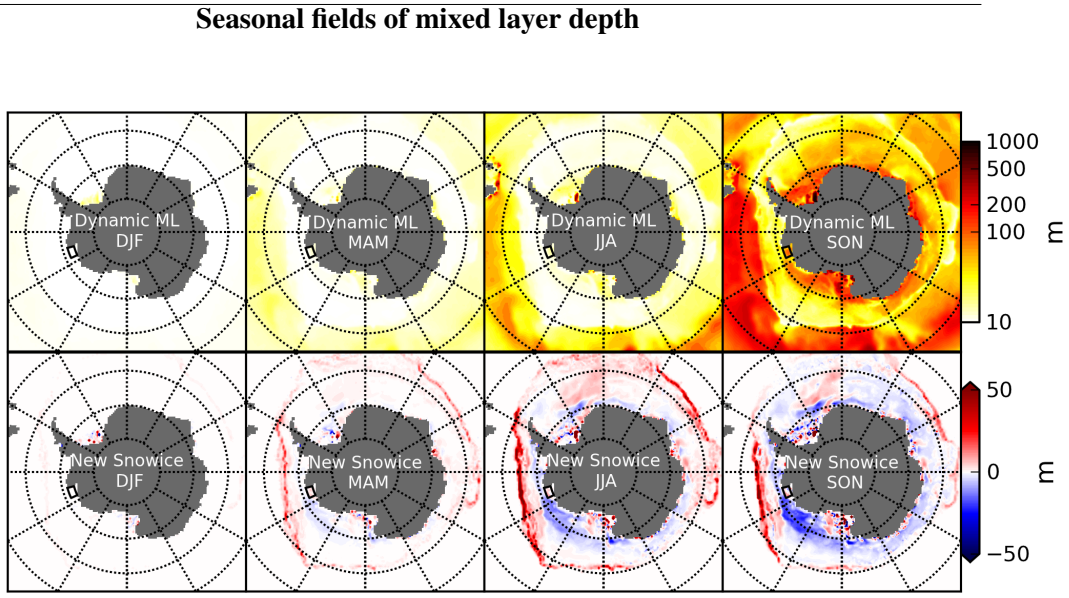

Figure 5.5: *Seasonal averages for mixed layer depth. Summer (DJF) is the December, January and February average. Autumn (MAM) is the March, April and May average. Winter (JJA) is the June, July and August average. Spring (SON) is the September, October and November average. The region used for the Amundsen Sea averaging is indicated by a black box. Top row is the dynamic mixed layer depth configuration, second row is the dynamic mixed layer values minus the new snow ice parameterisation run (Dynamic ML – New snowice).*

region of thick ice on the Western side of Antarctica is smaller. Values in the Weddell Sea are slightly lower, now reaching thicknesses of 1-1.5 m. This is because the presence of a coupled mixed layer means that heat is now being mixed from below, causing a reduction in sea ice thickness. In areas of very thin ice this results in a reduction in concentration.

Maximum mixed layer depths are seen in Autumn with mixed layers up to 1000 m seen in the Eastern part of the Weddell Sea, and in the Ross Sea. The ocean profiles are much more stratified than the ones used in the idealised sea ice–mixed layer model (see Section 2.3.2), with a much shallower pycnocline. This means that the mixed layer depths reached in the Amundsen Sea are much shallower than the 310 m maximum mixed layer depth reached in the idealised model simulations (see Section 2.3.3).

5.3.3 Change in the snow ice parameterisation

In the versions of the CICE sea ice model being used in the previous two subsections, conservation of mass was assumed in the snow to snow ice conversion. The old mass of snow was assumed to be equal to the new mass of snow ice formed. However, this neglects the seawater flooding the snow, and therefore underestimates the amount of snow ice being formed.

This was altered following the same assumptions as the parameterisation used in the idealised sea ice–mixed layer model, see equation 2.13. It is now assumed that the thickness of snow

removed is equal to the thickness of snow ice formed. This means that a greater thickness of snow ice is formed per unit of flooded snow. Note that in the mushy layer configuration of CICE this is actually accounted for already.

Compared to the previous version we get much thicker ice in the Amundsen and Bellingshausen Seas. We also see a large change just to the west of the Ross Sea. In these regions we have higher snowfall rates, leading to the greatest rates of snow ice formation, meaning that this is where we would expect the largest impact from the change. This is increasing the amount of persistent thick ice in this region. Ice thickness everywhere is slightly increased in Spring (SON), by about 10 cm.

Ice thickness is increased in the study region in the Amundsen Sea by 0.5 m in spring (SON). Ice concentration values are largely unchanged from the previous version (with the old snow ice parameterisation), as are mixed layer depths.

5.4 Description of the Control Run

In this section the model is run with ERA-I forcing from 1980 to 2016, using the final set up of the model from the previous section. To spin up and initialise the model, the forcing from 1980 is run for 10 years. The ice concentration and thickness values are compared to available observations and the interannual variability in the Amundsen Sea is examined. The climatology of the simulation (1980-2016) was calculated in order to create seasonal averages for the time period.

5.4.1 Ice Concentration

The seasonal averages from the Special Sensor Microwave Imager (SSM/I) data product (Cavalieri et al., 1996, updated yearly) is shown in Figure 5.6. The data has been averaged between 1980-2016 to create comparable plots to the control run. Note that the bottom two rows show difference values for simulations using climatological forcing, and repeated 2005 forcing. These results are discussed in Section 5.5.

The SSMI data shows a clear seasonal cycle. The minimum sea ice extent is in summer (DJF) increasing gradually throughout Autumn and Winter. From Winter to Spring the sea ice extent remains similar, but the concentration in the sea ice pack starts to decreases slightly, then there is a rapid decrease from Spring to Summer.

In Figure 5.6 we can see that the mean seasonal values of ice concentration values are broadly similar to the observed values. The winter (JJA) and spring (SON) values are very similar. The SSM/I values are greater to the East of the peninsula in Summer (DJF) and Autumn (MAM), and the model values are greater in the Ross Sea during these months. The SSMI/I values are also

greater in the study region (boxed) in these months.

5.4.2 Ice Thickness

The seasonal ice thickness values from the control run are shown in Figure 5.8. A clear seasonal cycle is shown, with the maximum values in spring and minimum in autumn. Thickness values are generally below 1 m, with thicker values between 2-3 m near the coast in winter/spring.

Ice thickness observations are limited both spatially and temporally for the Southern Ocean. We do not currently have observations of decadal trends like we do for ice concentration, and in situ observations have significant gaps both spatially and temporally (Worby et al., 2008). Despite the availability of satellite data, the presence of thick snow covering the sea ice in the Southern Ocean makes gaining a reliable value for sea ice thickness is tricky. The difficulty in using radar altimetry for the Southern Ocean is due to the variation in snow penetration of the radar, meaning that the ice freeboard and therefore the ice thickness has a large uncertainty (Giles et al., 2008). However, the freeboard can be identified by laser altimeters, then assuming that the sea ice freeboard is at sea level and using estimates for the snow thickness, snow density and ice density an estimate of ice thickness can be obtained (Kurtz and Markus, 2012; Ozsoy-cicek et al., 2013). Kurtz and Markus (2012) provides a Southern Ocean wide estimate of ice thickness using ICESAT data.

The estimates shown in Figure 5.7 are restricted to the collection periods of ICESAT, which not exactly match up to the periods used in the ice thickness averages in Figure 5.8, however it does still provide an estimate of realistic values. However, the comparison shows that broadly the values are in agreement in the magnitude and patterns of regions of thick ice. Ice thickness reaches a maximum of about 2 m close to the coast, and mostly about 0.5-1 m further away.

5.4.3 Mixed Layer Depth

The seasonal mixed layer depths are shown in the top row of Figure 5.9. The maximum mixed layer depths are seen during the Spring, as the sea ice extent has reached its maximum. The deepest mixed layer depths are near the coast, particularly in the Weddell Sea and the Ross Sea where the mean mixed layer depths reaches 500 m. In the Amundsen Sea study region the mean mixed layer depth reaches just over 100 m. Observations of mixed layer depth in the Southern Ocean are limited both spatially and temporally making the results difficult to compare to observations.

Seasonal fields of ice concentration

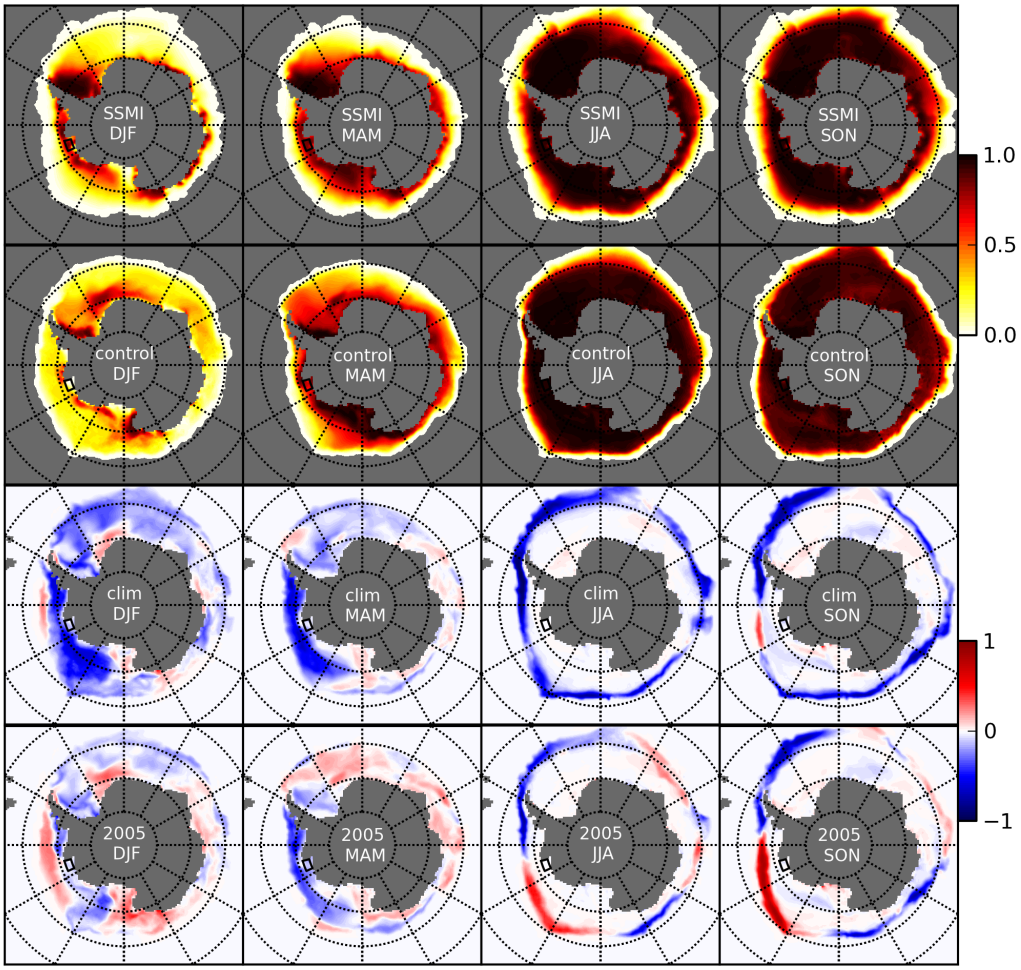

Figure 5.6: *Seasonal averages of satellite observations of ice concentration between 1980-2015 in the top row. Seasonal averages of ice concentration for the control simulation run between 1980-2016 shown in the second row from the top. Differences in the seasonal averages of ice concentration between the control and the simulation with climatological forcing in the third row (control–clim). Difference between the repeated 2005 atmospheric forcing and the control run in the bottom row (control–2005).*

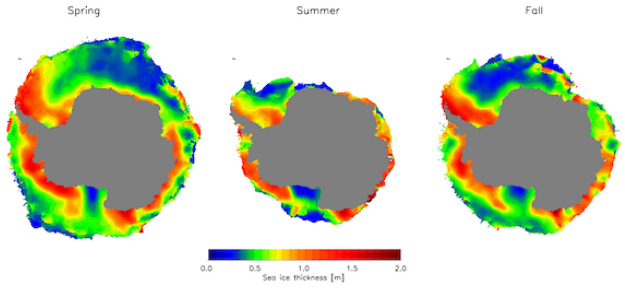

Figure 5.7: *Figure taken from Kurtz and Markus (2012) showing seasonal ice thickness values. See Kurtz and Markus (2012) for more details about the data.*

Seasonal fields of ice thickness

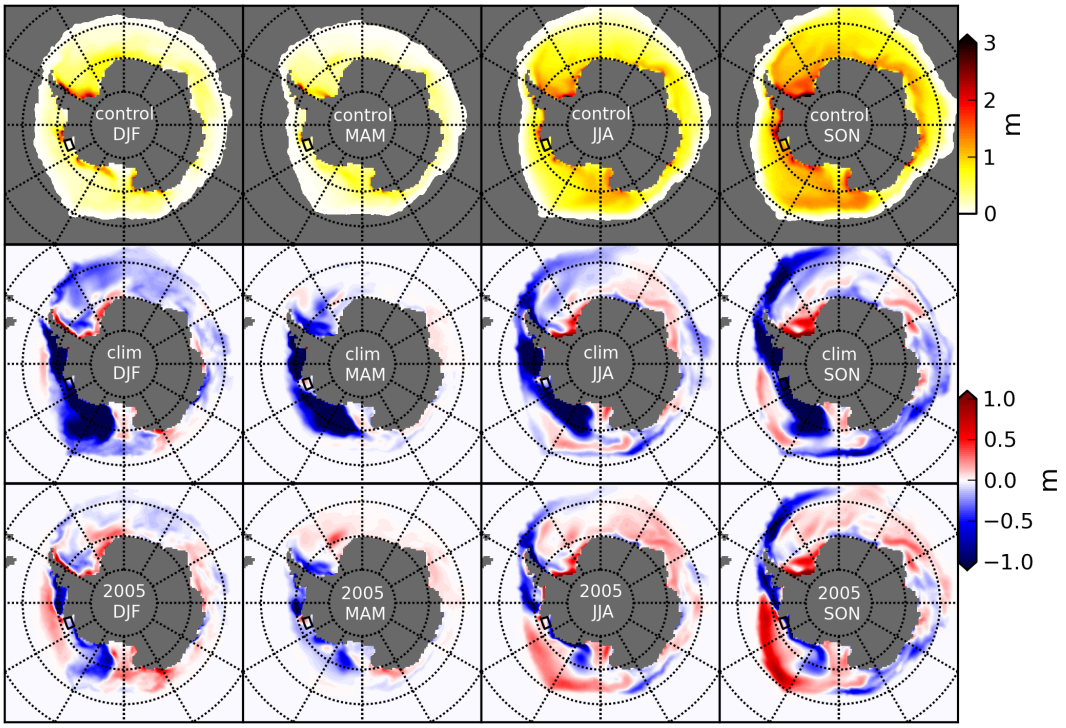

Figure 5.8: *Seasonal averages of ice thickness in the control simulation run between 1980-2016 shown in the top row. Differences in the seasonal averages of ice thickness between the control and the simulation with climatological forcing in the second row (control–clim). Difference between the repeated 2005 atmospheric forcing and the control run in the bottom row (control–2005).*

5.4.4 Amundsen Sea - interannual variability

The timeseries for the Amundsen Sea is shown in Figure 5.10, showing the interannual variability for the region over the period. The back boxed region indicated in Figures 5.6, 5.8 and 5.9 is used for spatial averaging, the same as in the idealised modelling work presented in the previous chapters.

Apart from the first couple of years, the ice concentration always reaches a maximum of 1 in the winter. The summer/autumn ice concentration minimum varies considerably, between an ice concentration of 0, to values of 0.8 in 1999/2000. In general low/high sea ice years are grouped in years of 3-4.

Ice thickness in both winter and summer varies considerably. The maximum annual values vary from just over 1.5 m, down to 0.7 m. The minimum varies between no ice, up to values of just under 1 m. The periods of thinner/thicker ice mirror years of greater/lower summer ice concentration.

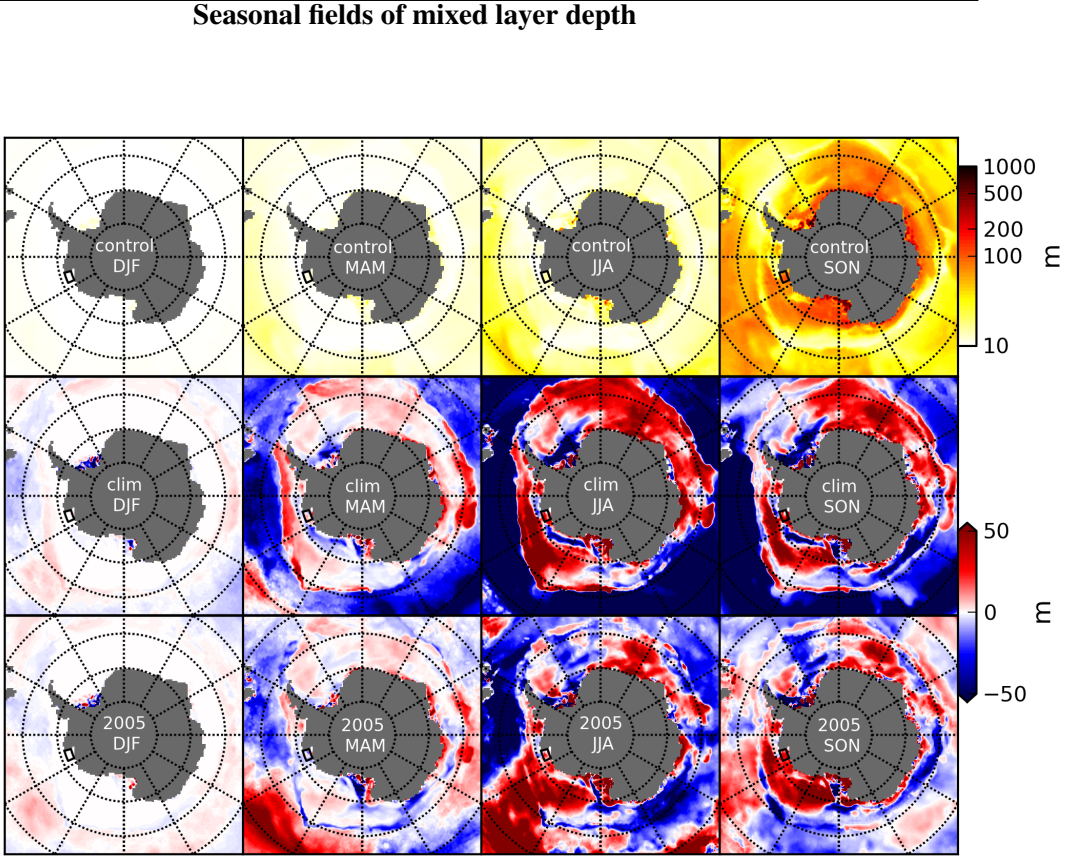

Figure 5.9: *Seasonal averages of mixed layer depth in the control simulation run between 1980-2016 shown in the top row. Differences in the seasonal averages of mixed layer depth between the control and the simulation with climatological forcing in the second row (control–clim). Difference between the repeated 2005 atmospheric forcing and the control run in the bottom row (control–2005).*

The maximum mixed layer depth varies from up to 160 m in 1981 to minimum values of 50 m in 2006 and 2011. There is no clear relationship between the maximum mixed layer depth and the ice thickness/concentration. Mixed layer depths are shallower than those simulated in the idealised model in Section 2.3.3, this is because the ocean profiles used here are more stratified than the ones used in the idealised simulation, see Figure 5.1.

5.5 Impact of Atmospheric Forcing

In this section the impact of the atmospheric forcing being used is examined. First using climatological forcing is compared to the control run in Section 5.5.1, then to using repeated atmospheric forcing from a particular year in Section 5.5.2 and finally the cause of the difference between the climatological and repeated forcing simulations are examined in more detail in Section 5.5.3.

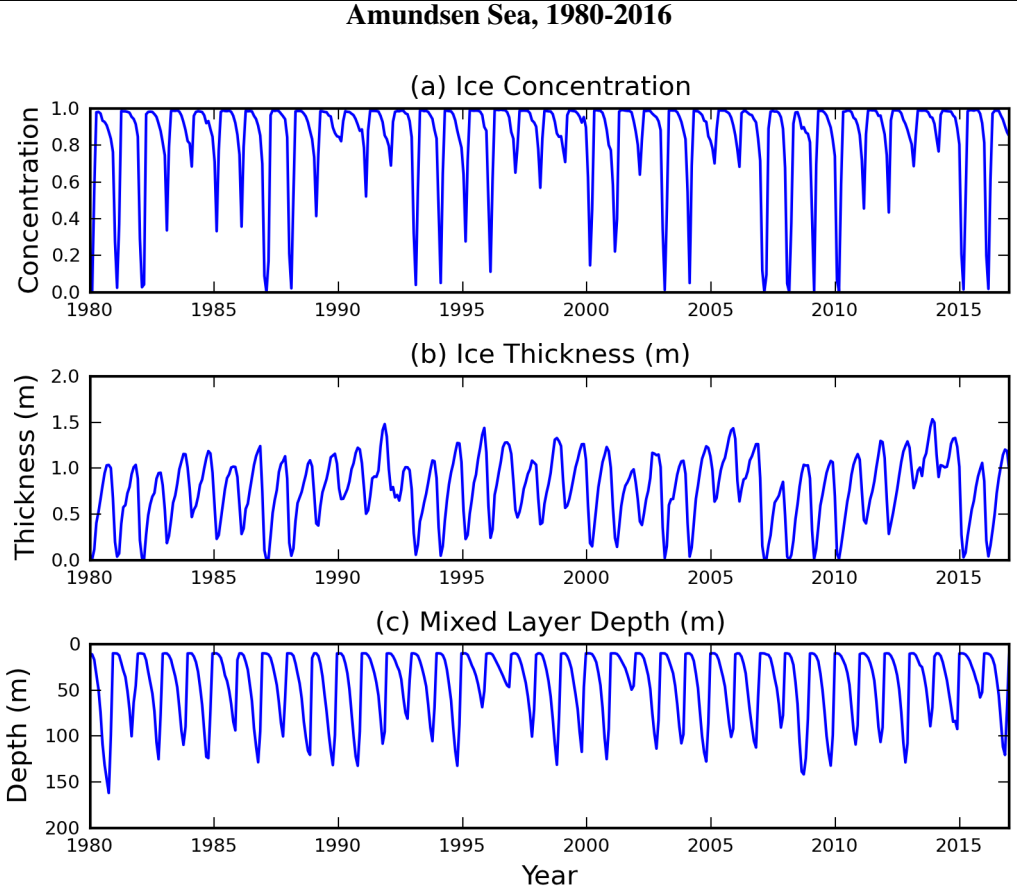

Figure 5.10: *Interannual variability for the Amundsen Sea, showing ice concentration, ice thickness and mixed layer depth.*

5.5.1 Climatological atmospheric forcing

The difference in ice concentration, ice thickness and mixed layer depth between the climatological and control run is shown in Figures 5.6, 5.8 and 5.9. All differences are shown as control run–climatological forcing run.

Looking at the difference between the climatological and control run ice concentration (Figure 5.6 third row from top) we can see that the climatology generally has greater ice concentration values, particularly in the summer, and the maximum ice extent is very slightly reduced. In the climatological run the ice concentration is now more a function of latitude, there is no longer a tongue of higher concentration ice moving eastward from the peninsula. The ice thickness (Figure 5.8, middle row) is significantly reduced in the run with climatological forcing in all seasons. There is now no persistent thick ice (of greater than 3 m) in the Amundsen-Bellingshausen region. There is thick ice very close to the continent in Winter/Spring in the Bellingshausen Sea and on the northwestern portion of the Weddell Sea. Typical winter values are 1-1.5 m for most regions. The mixed layer depths (Figure 5.9, middle row) are shallower than the climatological mixed layer depths, particularly in the Ross and the Weddell

Seas. This is likely because of the thinner sea ice in the simulation.

5.5.2 Repeated annual atmospheric forcing

The model was forced with repeated annual (2005) forcing (the year that has been used for the wind fields in the climatology), and initialised from 2005 in the control run to reduce spin up time. This was done in order to see how much of the difference between the control run and the climatological run might be caused by interannual variability in the atmospheric forcing. The differences in ice concentration, ice thickness and mixed layer depth from the control run seasonal averages are shown in bottom rows of Figures 5.6, 5.8 and 5.9. All differences are shown as control run–2005 repeated forcing run.

The ice concentration and thickness are much more similar to average of the control run, and we no longer have the thick ice build up to the west of the peninsula, although it is still slightly thicker than the control run average. Investigating using other years resulted in similar results, with less thick ice building up to the west of Antarctica, and between the Amundsen and Ross Seas. The results indicate that the very thick ice in climatological run is caused by the averaging of the atmospheric forcing.

5.5.3 Isolating the source of the discrepancy

The ice thickness when using the climatological atmospheric forcing is thicker than observed values (Kurtz and Markus, 2012), and is much thicker than the average of the 1980–2016 simulation (see Figure 5.8), by contrast this not the case when using repeated forcing from 2005. In order to understand what the cause of the thick ice is, the model was run with the forcing for 2005, with one atmospheric field (surface air temperature, specific humidity, snowfall, precipitation, shortwave radiation and longwave radiation) at a time swapped for the climatological forcing. The difference in ice thickness from the simulation with all of the 2005 forcings is shown in Figure 5.11. Doing this clearly shows that the averaging of the surface air temperature was responsible for the cause of the extremely thick ice (3+ m in the Amundsen-Bellingshausen Seas region). The temporal averaging smoothed out the storms/cyclones which loop around the coast in this region and produced a more zonal temperature distribution. This removes the large amplitude winter temperature variability in the region (in the order of 20°C, see Figures 5.12, 5.13 and 5.14). This means when using the climatological forcing there are no short lived melting events during winter months. This ice is able to build up and persist all year around, which is not what has been observed to occur in the region.

Seasonal vales of ice thickness

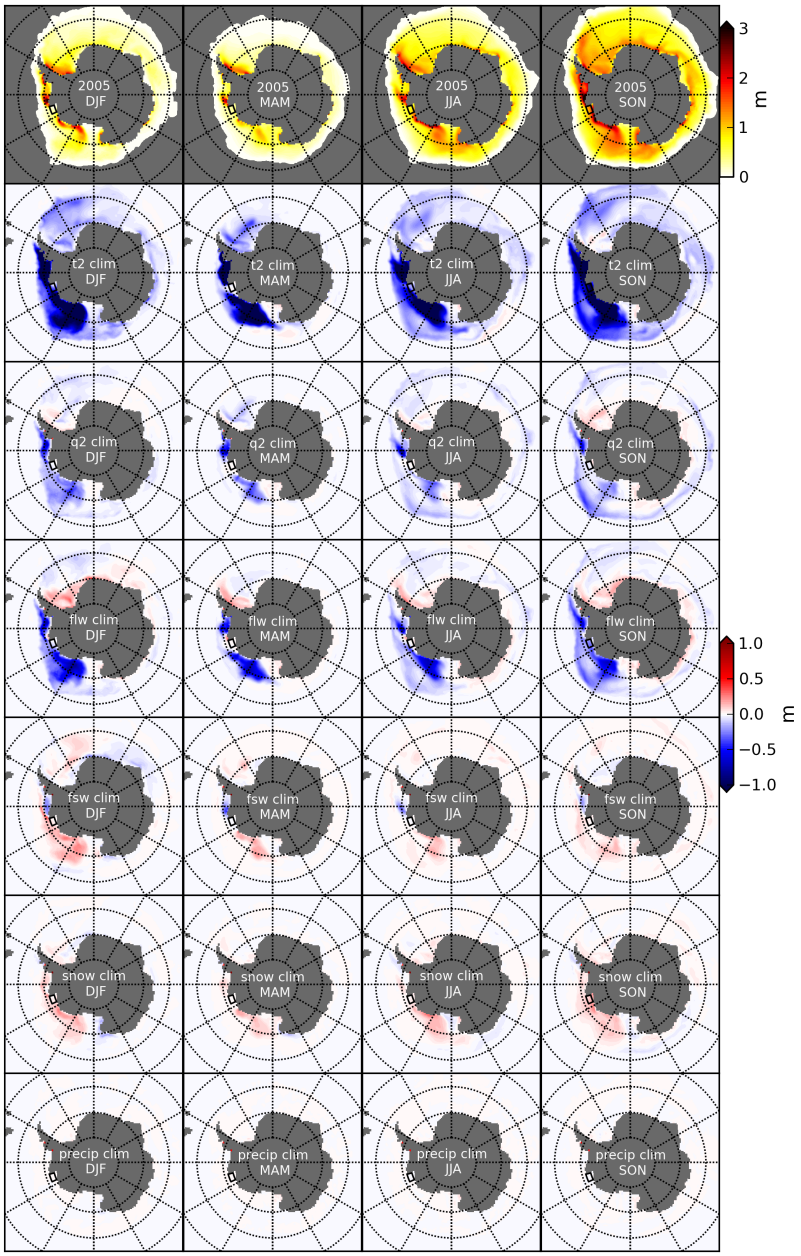

Figure 5.11: *Seasonal averages of ice thickness. Top row is ice thickness values when using repeated atmospheric forcing from 2005. Other rows (from top to bottom) are the top row minus the average when the climatological forcing values for surface air temperature, specific humidity, longwave radiation, shortwave radiation, snowfall has been used.*

5.6 Ocean Feedback Study

The feedback analysis using the idealised model in Chapter 4 (see Figure 4.5) showed the ocean feedback to be the strongest in the Amundsen Sea, and stronger than any of the feedbacks investigated in the Weddell Sea. Therefore, it was chosen as the feedback to test in the CICE-ML model set up, focusing on the Amundsen Sea region, where the feedback response was largest.

5.6.1 Establishing the reference and perturbed runs

As a result of the large differences between the climatology forced run and the control run, we chose not to perform feedback studies relative to the climatology forced run. This meant that a different approach to the idealised model study in Chapter 4 was required.

In our idealised feedback studies we explored the feedback response to changes in surface air temperature, Here, we have not varied surface air temperature in isolation as we did in the idealised studies. This is because we did not want to create inconsistent forcing fields, as that may create a significant amount of the response. In the idealised studies we were able to use a climatology, which removed some of the tight coupling between the atmospheric variables. However, as noted in the previous section, using the climatological forcing results in unrealistic simulations and we instead decided to use the atmospheric forcing from particular years in their entirety and compare the differences between years.

The Amundsen Sea field mean temperatures for all of the years between 1979–2016 were ranked based on the difference from the smoothed climatology. Years picked as warm, typical and cold are shown in Figures 5.13, 5.12 and 5.14. The model was initialised using the 1980-2016 simulation, and then each of the selected years were repeated until a steady state was reached. The field mean values for ice concentration, ice thickness and mixed layer depth are shown in Figure 5.15.

From Figure 5.15 we can see that there is no clear relationship between warmer/cold years and mixed layer depth. Therefore, in order to focus on the ice–ocean mixed layer depth feedback, we chose, rather than using warm and cold years for the atmospheric perturbations, to use *deep*, *typical*, and *shallow* mixed layer depth, to investigate the role the difference in mixed layer depth evolution has in explaining the difference in ice evolution between the different years.

5.6.2 Ocean feedback disabled simulations

The year 2010 was chosen as producing a typical mixed layer depth and 2005 and 2016 were chosen as shallow and deep mixed layer depth case studies (perturbed runs). The mixed layer depth and properties from 2010 were prescribed in combination with 2005/2016 forcing and initialisation (ocean feedback denied runs). The difference in the sea ice between the perturbed

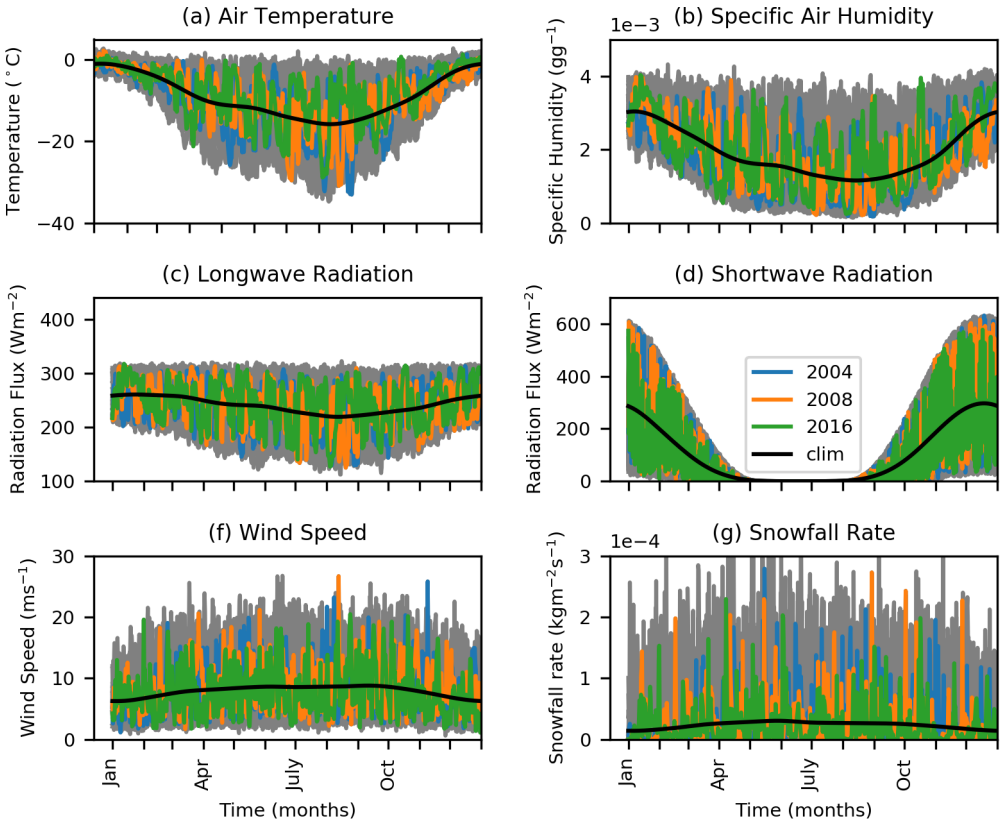

Figure 5.12: *Atmospheric forcings for the Amundsen Sea. All years plotted in grey, smoothed climatology in black. The three years closest to the climatological surface air temperature values are in orange, green and blue.*

run and the ocean feedback denied (FD) run is the impact of the mixed layer depth and properties on the sea ice.

5.6.2.1 Imposing a deeper mixed layer

Figure 5.16 shows the results form using the 2005 atmospheric forcing (initialised from 2005 repeated simulation) in combination with the deeper mixed layer properties from 2010 prescribed. This results in less ice compared to the 2005 simulation. The ice thickness is reduced by about 15-20 cm all year round. The ice concentration still reaches 1 in the winter, but is reduced in the summer months. This follows the theory from the idealised modelling work (see Chapter 4), that a deeper mixed layer results in more ocean heat being mixed upwards, increasing basal melting of the sea ice. The thermocline is at a depth of 60-80 m, so significantly more ocean heat would be mixed up when forcing the 2005 set up with the 2010 mixed layer.

The γ value (using mean ice volume values) is 1.461, see Section 4.5 for the definitions of γ. This indicates a positive feedback on the sea ice volume, where the response of the mean sea ice volume to the feedback is larger than the perturbation (in this case the change in surface forcing from 2010 to 2005).

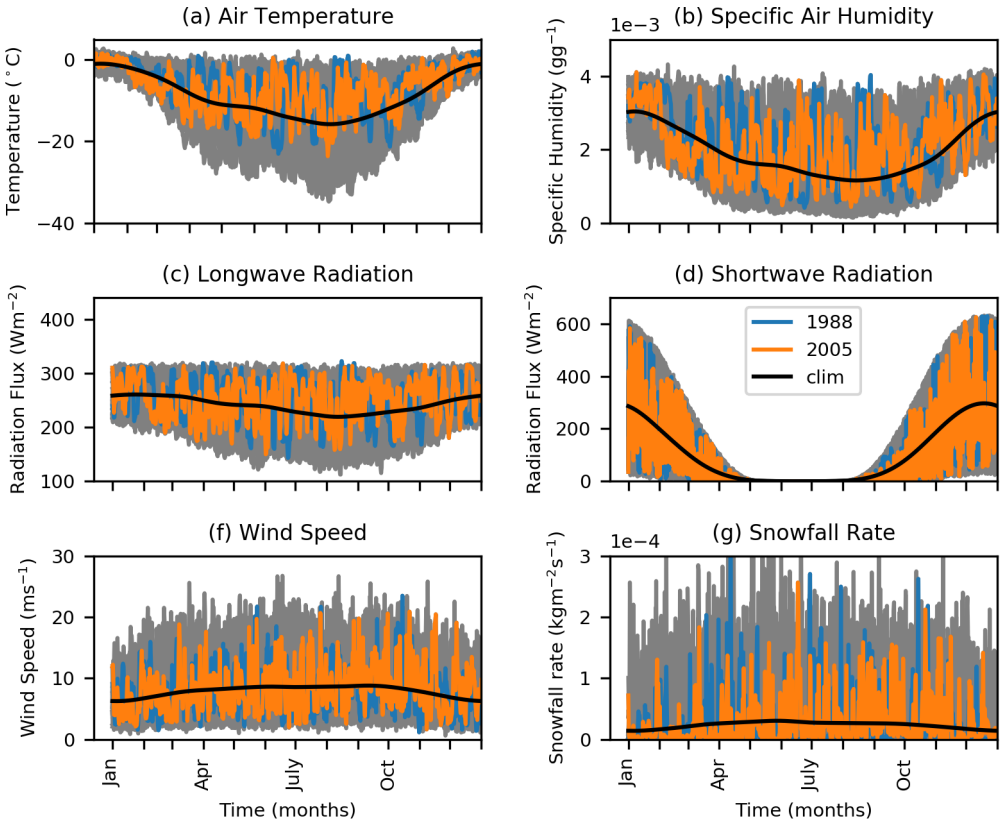

Figure 5.13: *Atmospheric forcings for the Amundsen Sea. All years plotted in grey, smoothed climatology in black. The two warmest years are in blue and orange.*

5.6.2.2 Imposing a shallower mixed layer

Figure 5.17 shows the results form using the 2016 atmospheric forcing (initialised from 2016 repeated simulation) in combination with the shallower mixed layer from 2010 prescribed. Forcing 2016 with a shallower mixed layer from 2010 results in less ice compared to 2016. This contraindicates the previous hypothesis, where a shallower winter mixed layer results in less basal melting of the sea ice.

The ice thickness is reduced from February to November by 10-20 cm. In December and January it is increased slightly. The ice concentration is increased in December through to February, but it is reduced in the February to April sea ice expansion phase.

The γ value (calculated with mean ice volume) is -0.198, see Section 4.5 for the definitions of γ. This indicates a relatively weak, negative feedback. The feedback strength is much weaker than the response of the mean sea ice volume to the change in surface forcing from 2010 to 2016.

5.6.2.3 Mixed layer and freezing temperatures

Looking at the mixed layer and freezing temperatures in Figure 5.18, we can see that throughout the winter that $T_{mix} - T_f$, which determines the rate of basal melting, is approximately

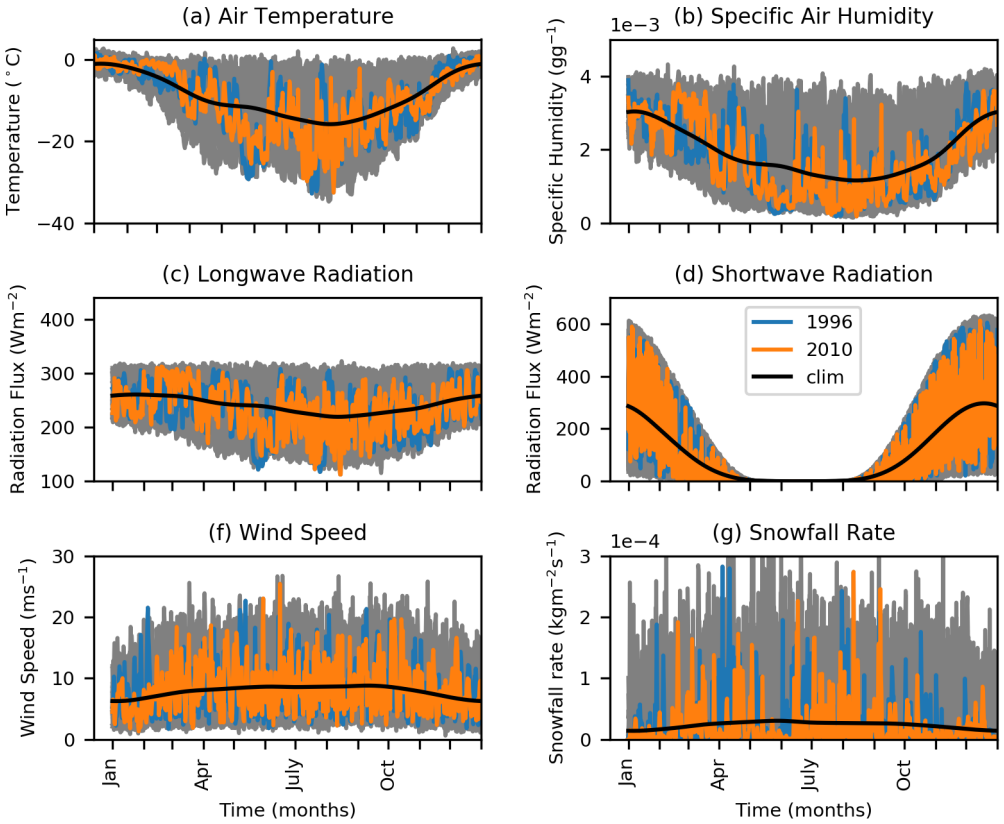

Figure 5.14: *Atmospheric forcings for the Amundsen Sea. All years plotted in grey, smoothed climatology in black. The two coldest years in blue and orange.*

zero for all simulations regardless of mixed layer depth. The main differences between the three runs is the mixed layer temperature from December through to March. with the maximum difference (due to the maximum in mixed layer temperature) occurring in February. 2010 has the lowest $T_{mix} - T_f$ values, this means that forcing 2005 and 2016 would reduce the rapid ice volume increase during February to March, and will result in decreasing the ice volume in the 2005 and 2016 FD runs with the 2010 mixed layer. The difference in the sea ice state then results in the differences between the FD and the perturbed runs throughout the winter.

The difference in evolution of the mixed layer temperature between the CICE model and the 1D model explain the difference in behaviour of this feedback. In the 1D model the amplitude of the seasonal cycle in the mixed layer temperature were much smaller (see Figure 3.2). In the CICE simulations, the mixed layer temperature increases significantly during the summer. This is in part due to the summer ambient profiles being significantly warmer in the upper 100 m during January and February, which is not the case in the 1D model set up. In the CICE model this setup results in a significant increase in $T_{mix} - T_f$ that impacts the rate of sea ice melt throughout December to February then the growth throughout February to April, and this is the behaviour that is most evident in the Ocean FD experiment results in Figures 5.16 and 5.17.

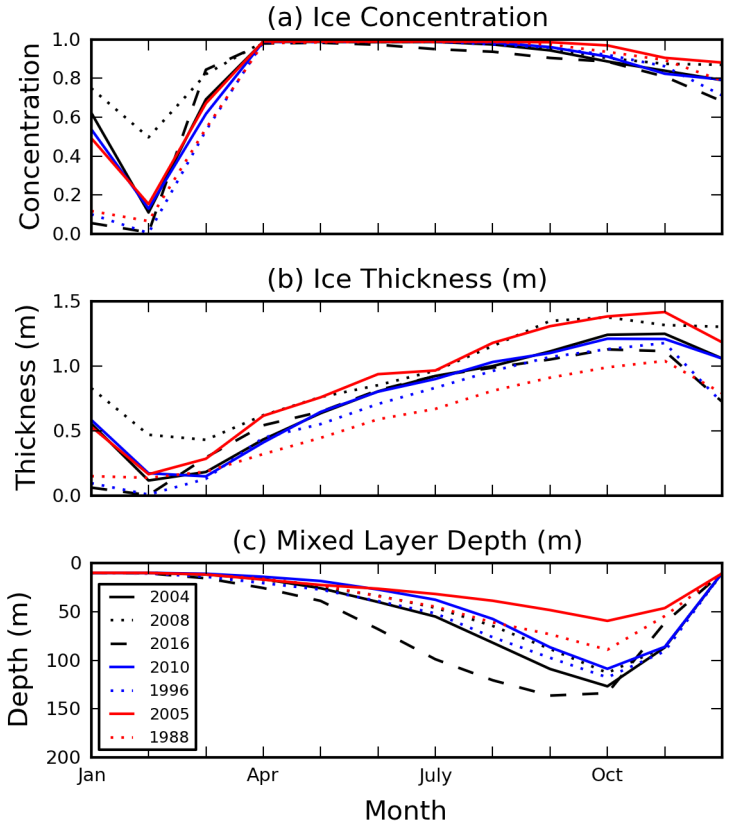

Figure 5.15: *Values of ice concentration, ice thickness and mixed layer depth for the Amundsen Sea. The simulations are forced using different years of atmospheric forcing repeated. Values are taken after 9 years fo simulation.*

5.7 The Role of Atmospheric Forcing

The results from the ocean feedback simulations did not give clear results due to the set up of the simulations, using atmospheric forcing from particular years as opposed to a climatology. Therefore in this section the relationship between the atmospheric forcing fields and the sea ice state and mixed layer depth is examined. The forcings for years with high/low sea ice cover, and deep/shallow mixed layer depth were averaged. This should show some relationships between the atmospheric forcings and the sea ice cover and mixed layer depth, and indicate whether the behaviour is as seen in the idealised model results in Chapter 3.

5.7.1 High and low sea ice years

Years with a summer minimum sea ice concentration value above 0.5 were classed as *high sea ice years* (24 years), and the rest were classed as *low sea ice years* (12 years). The atmospheric forcing fields were then averaged for those years and compared to the climatological averages for 1980-2016, the results are shown in Figure 5.20. The results show that on average high sea ice years are colder in winter as well as having slightly lower humidity and incoming longwave

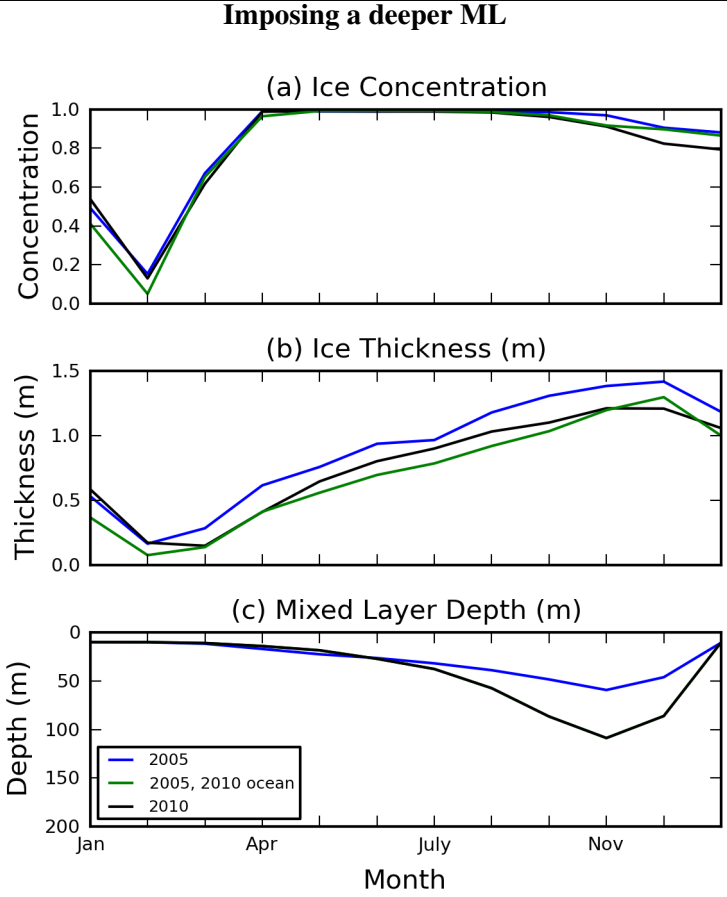

Figure 5.16: *Values of ice concentration, ice thickness and mixed layer depth for the Amundsen Sea. The green line shows the feedback denial simulation, where the model is forced with atmospheric forcing from 2005 but with the deeper mixed layer from 2010 prescribed. The bblue and black lines show the simulations forced with 2005 (blue) and 2010 (black) atmospheric forcing. Values are taken after 9 years fo simulation.*

radiation flux. Little difference in the shortwave radiation flux, wind speed and snowfall rate can be seen from the climatology. The opposite can be true for low sea ice years, but by a much smaller magnitude. The differences in the atmospheric forcings here are much smaller than the standard deviations used in Chapter 2. This suggests that the variability of the forcings seen in high/low sea ice years is also large, which is why the averages are close to the climatology. However the choice of definition of high/low sea ice years may impact this result.

5.7.2 Deep and shallow mixed layer years

Years with a maximum mixed layer depth below 100 m were classified as *deep mixed layer years* (27 years), and all other were classified as *shallow mixed layer years* (9 years). Shallow mixed layer years are on average warmer, moister and have a larger longwave radiation flux up until August, after which the opposite is true. These forcing changes contribute to a lower surface ocean heat loss, and therefore slower rate of mixed layer deepening. Deep mixed layer years are

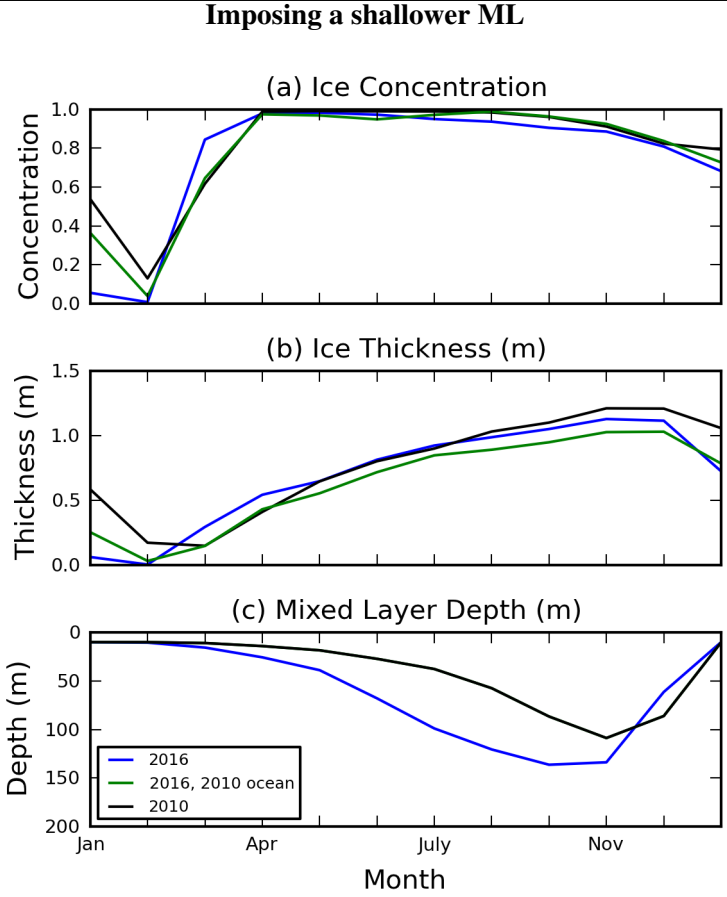

Figure 5.17: *Values of ice concentration, ice thickness and mixed layer depth for the Amundsen Sea. The green lines show the feedback denial simulation, where the model is forced with atmospheric forcing from 2016 but with the shallower mixed layer from 2010 prescribed. The blue and black lines show the simulations forced with 2016 (blue) and 2010 (black) atmospheric forcing.*

on average have forcing similar to the climatological average, however this is likely a reflection of the criterion used to define deep mixed layer years. The differences in the atmospheric forcings here are much smaller than the standard deviations used in Chapter 3. This suggests that the variability of the forcings seen in high/low sea ice years is also large, which is why the averages are close to the climatology. However the choice of definition of high/low sea ice years may impact this result.

5.8 Summary

In this chapter the CICE-ML model has been used to investigate the ocean feedback on the sea ice cover in the Amundsen Sea (AS), the feedback found to be the strongest out of all the feedbacks studied in the idealised modelling work in the Amundsen and Weddell Seas. Initially the impact of each step of the formulation of the CICE-ML model on the sea ice cover was investigated. This involved the impact of changing from a fixed mixed layer depth to a coupled mixed layer model, where the surface and deep ocean heat and salt fluxes are calculated. This

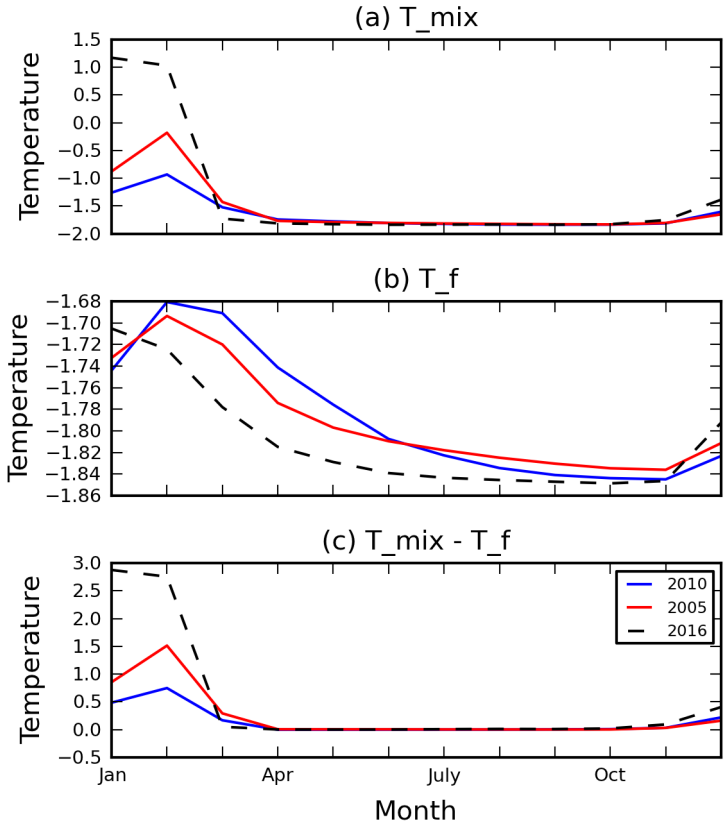

Figure 5.18: *Mixed layer temperature and freezing temperature values for the Amundsen Sea in simulations with atmospheric forcing from 2010, 2005 and 2016.*

resulted in a general decrease in sea ice thickness across the Southern Ocean, due to an increase in the basal heat flux. The snow ice parameterisation was corrected, to account for the weight of sea water flooding the submerged snow forming the snow ice. This resulted in a greater thickness of snow ice being formed, thickening the sea ice in regions of greater snowfall rates on the western side of the peninsula and the Amundsen and Bellingshausen Seas.

The impact of the atmospheric forcing on the simulation was investigated. The control run, which used ERA-I atmospheric forcing from 1980 to 2016, produced ice concentration and ice thickness values broadly similar to observations. However, when using climatological atmospheric forcing the ice to the west of the peninsula was much thicker (1-2 m difference) than observations. From looking at an individual years forcing, and swapping in one climatological atmospheric field at a time, it became clear that averaging the surface air temperature resulted in sea ice that was too thick. This is due to the averaging out of large amplitude oscillations in temperature due to the passing of storms around the coast, which particularly impact the sea ice cover in the western side of Antarctica. The higher temperature events in winter cause some melting, and prevent the build up of thick ice that persists all year round when using the climatological temperature fields. Due to the unrealistic ice cover produced when using the climatological forcing, the sensitivity of the ice was investigated using individual years,

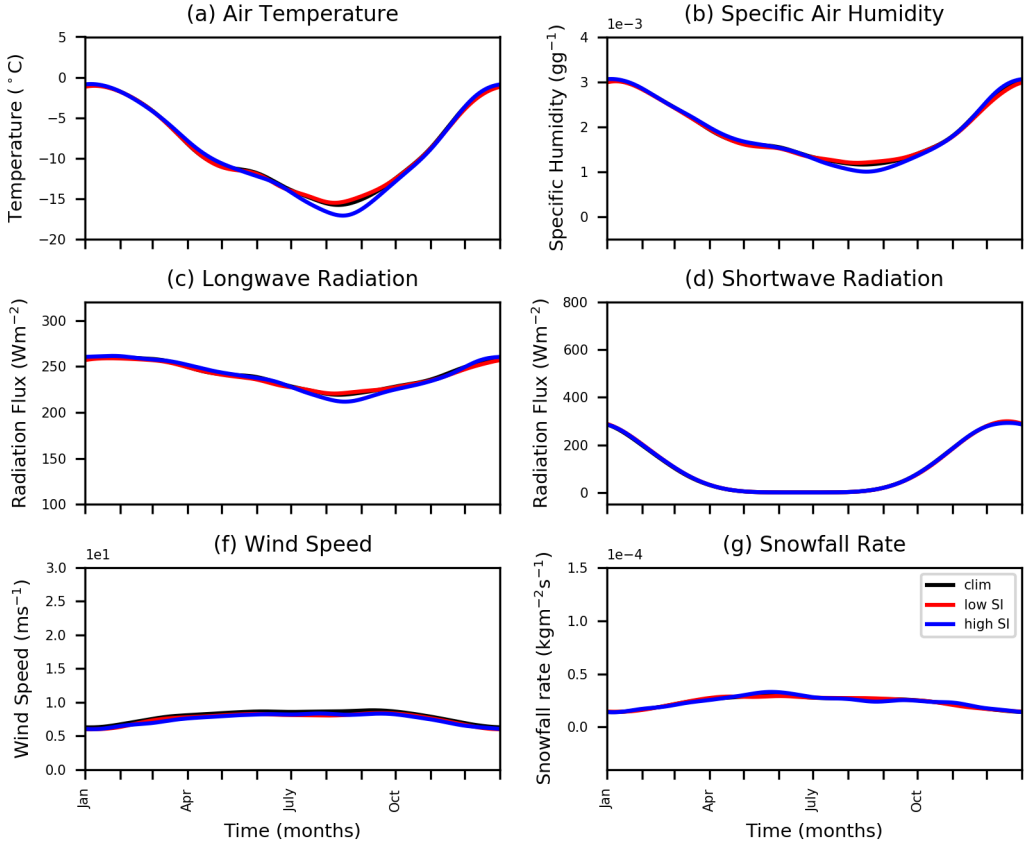

Figure 5.19: *Atmospheric fields averaged for years with high and low sea ice cover, compared to the climatological average between 1980-2016. Low sea ice years are defined as having a minimum summer sea ice concentration below 50%, and the others are defined as high sea ice years.*

as opposed to perturbations to the climatological surface air temperature, as was done in the idealised model sensitivity studies in Chapter 3. Warmer, typical and cooler years in the AS were picked, and forced on the model until a steady state was reached. The simulations showed that warmer/colder atmospheric conditions in the AS did not correlate with more/less ice in the AS.

Finally the ocean feedback on the sea ice in the AS was investigated. Due to the lack of correlation between warmer/cooler years and more/less sea ice, the choice of which years to choose as the reference and perturbation simulations was done using the mixed layer depth evolution as opposed to the change in atmospheric forcing. 2010 was picked as a typical mixed layer depth from the years investigated. 2016 as a deep mixed layer depth year, and 2005 as a shallow mixed layer depth year. 2005 and 2016 were run with 2010 mixed layer prescribed, in order to isolate the impact of the difference in mixed layer between the years. The values of γ were quite different for the two sets if simulations. In the idealised model it was found that in the AS, a deeper mixed layer increased the basal melting, reducing the mean volume of sea ice. However, in the coupled CICE-ML model, over winter the difference between the mixed layer and freezing was approximately zero compared to the rest of the annual cycle. This meant that

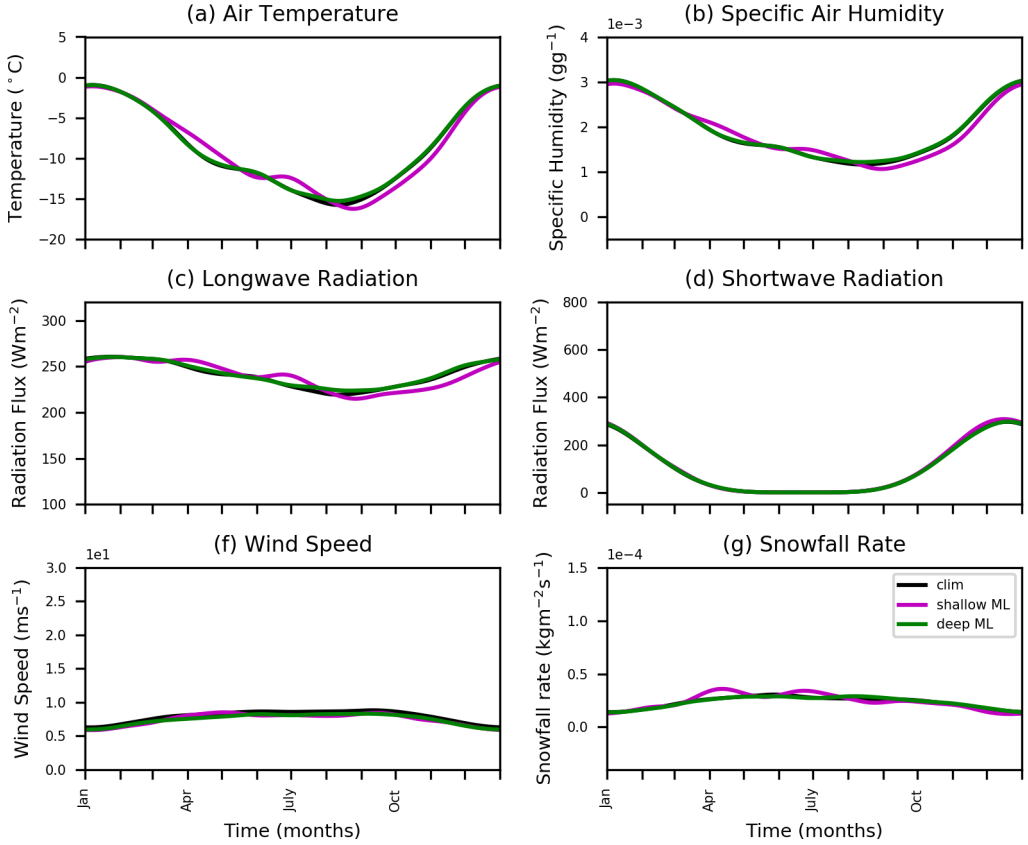

Figure 5.20: *Atmospheric fields averaged for years with high and low sea ice cover, compared to the climatological average between 1980-2016. Shallow mixed layer years are defined as having a winter mixed layer depth shallower than 100 m, and the others years are defined as deep sea ice years.*

the difference in temperatures over the first portion of the year dictated the response of the sea ice to the change in mixed layer depth and properties. Further work would be required in order to conclusively explain the difference in behaviour between the idealised model and CICE-ML model results.

Chapter 6:

CONCLUDING REMARKS

The main objective of this thesis was to explore the role of sea ice–ocean feedbacks in the continental shelf seas using models. In particular, to investigate the importance of sea ice–ocean feedbacks on the evolution of sea ice and the ocean mixed layer in two contrasting regions of the Antarctic continental shelf ocean: the Amundsen Sea, which has warm shelf waters; and the Weddell Sea, which has cold and saline shelf waters. Of particular interest is whether the feedbacks amplify or dampen the response to atmospheric perturbations, and the relative magnitude of the feedbacks. In this chapter, the main conclusions of the thesis will be outlined, alongside discussion of the approach, implications of the results, and the potential for future work on this topic.

6.1 The impact of atmospheric forcing on the sea ice and ocean mixed layer in the continental shelf seas

An idealised sea ice–mixed layer model was developed in order to isolate sea ice–ocean feedbacks and compare their relative importance and magnitude in the two regions. The use of an idealised model enabled easier isolation of the feedbacks through manipulating the boundary conditions, and greater clarity in the subsequent interpretation of the results. However, care must be taken when extrapolating the findings due to the simplicity of the assumptions the model is built on. In particular our model excludes explicit representation of all horizontal transport processes, which are only crudely captured through relaxation of ice and ocean properties to climatological conditions. An analysis of circum–Antarctic sea ice–ocean interactions and feedbacks necessitates a more spatially dependent model.

The model was developed to include snow ice formation, detailed in Chapter 2, which are important for investigating the sea ice sensitivity to the precipitation rate. The model is able to simulate realistic annual sea ice and mixed layer evolution, similar to results in Petty et al. (2013),

with the Amundsen Sea partially destratifying (mixed layer depth of 310 m), and the Weddell Sea completely destratifying to the continental shelf (500 m). The ice concentration and thickness are within the range of realistic values from observations. In both regions the ice thickness varies between 1–1.8 m in each year, and between roughly 50% to 95% ice concentration (the maximum ice concentration) in the Amundsen Sea, and 60% to 95% in the Weddell Sea. In the Amundsen Sea most of the sea ice in the simulation was composed of snow ice, and between one to two thirds of the sea ice cover in the Weddell Sea simulations. Although, an Amundsen Sea sea ice cover that is almost entirely snow ice may be extreme, it is likely that a significant proportion of the sea ice cover here is snow ice, and observations are limited. However, this potential bias in the reference state may to some degree influence the sensitivity and feedback responses. Without a more comprehensive observational data set of snow ice, it is difficult to assess if/how much of an overestimation of the snow ice fraction this is. In the Weddell Sea, the mixed layer destratified every winter. This may be an overestimation of mixing, however, the limited observations available do suggest a deep winter mixed layer in the region of the Weddell Sea studied here. Despite these potential biases, the model produced realistic results for the two regions that were within the bounds suggested by observations, as described in Chapter 2. In the interannual variability, no significant trends were apparent in either region.

In Chapter 3 the sensitivity of the sea ice cover and mixed layer evolution in response to each of the six atmospheric forcing variables: surface air temperature (SAT), specific humidity, shortwave radiation, longwave radiation, wind speed and snowfall rate was investigated. Each variable was varied individually by +/– one standard deviation (σ), apart from snowfall rate where the 16th and 84th percentiles were used. The response was quantified by the change in the destratification time of the water column and mean ice volume in the Weddell Sea, and the maximum mixed layer depth and mean ice volume in the Amundsen Sea. This allowed the sensitivity to observed variability of the two regions' atmospheric conditions to be explored, and allowed the magnitude of feedback responses in Chapter 4 to be compared to the sensitivity responses to observed atmospheric variability.

Varying one atmospheric variable at a time allowed the impact of each atmospheric variable to be isolated and examined. In reality the variables would covary to some degree, but singling out each variable enabled a clearer understanding the response to each variable in isolation. The observed interannual variability indicates that the impact of the atmospheric variables may compensate each other to some degree, as the observed inter annual variability in Chapter 2 was less than the responses seen in the sensitivity studies in Chapter 3.

The two regions displayed very different sensitivity to surface atmospheric conditions. In the Weddell Sea the water column completely destratified during winter in all sensitivity scenarios, however the timing becomes earlier/later depending on whether the rate of sea ice growth is increased/decreased. Decreased winter sea ice growth and a shorter period of complete

destratification could decrease the rate of formation of Antarctic Bottom Water, as is currently being observed (Purkey et al., 2019).

In the Amundsen Sea, changes to the surface energy balance that promote ice growth and ocean cooling also promote mixed layer deepening. Changes to entrainment of warm deep waters oppose the direct impact of the atmospheric perturbation on the ice cover through changes in the rate of basal ice melting. These competing processes are evident in the sensitivity responses, and have been found in other modelling studies (Martinson, 1990; Zhang, 2007). A shallower mixed layer could also result in more warm CDW on the continental shelf, resulting in increased melting of the ice shelves.

The conditions in the Southern Ocean are predicted to get warmer and wetter (Christensen et al., 2013). The magnitude and regional variation in this is uncertain. The sensitivity results suggested that reliable precipitation datasets are crucial to simulating realistic Antarctic sea ice cover. An increase in snowfall could promote an increase in the sea ice volume due to two processes: (i) an increase in snow ice formation; and (ii) freshening the surface ocean and decreasing the entrainment of warm deep waters. The formation of snow ice releases less brine into the ocean than the same volume of congelation ice from basal freezing, this effectively contributes to surface freshening.

The sensitivity study examining both increased surface air temperature (SAT) and snowfall indicated that the impact of the two added relatively linearly, with the increased snowfall counteracting some of the impact of warming on the sea ice volume due to an increase in snow ice formation and an increase in stratification which decreased the basal melting in the Amundsen Sea. The sensitivity studies showed that the sensitivity to continued warming and increased snowfall by $+\sigma$ in the Weddell Sea response was dominated by sensitivity to SAT, resulting in a decrease in sea ice, and slower destratification, whereas the Amundsen Sea response was dominated by sensitivity to increasing snowfall, resulting in more sea ice due to snow ice formation and a shallower mixed layer due to surface ocean warming and freshening. Part of this difference in response is due to the greater variability seen in the ERA-Interim snowfall rate in the Amundsen Sea.

6.2 The role of sea ice–ocean feedbacks in the continental shelf seas

A study of five feedbacks was carried out in the Weddell and Amundsen Seas using an idealised sea ice–mixed layer model. The feedback studies were carried out in response to surface air temperature perturbations of $+/-\sigma$, using feedback denial simulations. Although denying the action of a feedback is unphysical it allowed a clear demonstration of the action of the feedback, and insight into the role that each feedback plays in response to perturbed surface air temperature. The novelty of the study is the systematic investigation of a number of sea

ice–ocean feedbacks in two different regimes, using the same framework. The variable γ was used to quantify the feedbacks, following the framework of Goosse et al. (2018), which normalises the feedback responses using the original perturbation responses. γ is defined as the difference in the response to the perturbation with and without the feedback denied, divided by the response to the perturbation (with the feedback) relative to the reference run, see Section 4.5 and Equation 4.1. This has allowed a direct comparison of the role each feedback plays in each regime, and a comparison of the linearity of the feedback responses to $+/-\sigma$ SAT perturbations.

The feedbacks investigated were: (i) the ocean feedback, whereby deepening of the mixed layer into warm, deep waters can increase the basal melt rate acting as a negative feedback on sea ice growth; (ii) the sea ice feedback, whereby the seasonal sea ice melt and growth cycle inputs freshwater and brine into the mixed layer, influencing the entrainment rate, typically amplifying the effect of atmospheric perturbations on the mixed layer (e.g. surface atmospheric warming causes both surface ocean warming and an increase in sea ice melt, both promoting mixed layer shoaling); (iii) the albedo feedback, whereby the ice concentration determines how much shortwave radiation enters the mixed layer so that a decrease in ice concentration increases the shortwave radiation flux to the mixed layer, causing shoaling and warming, promoting further decline in the sea ice concentration; (iv) the insulation feedback, whereby thicker sea ice has a lower conductive heat flux up through the ice, reducing the rate of ice thickening, acting as a negative feedback during ice growth; and (v) the freezing temperature feedback, whereby fresher seawater freezes at a higher temperature, meaning that freshening from increased sea ice melt could in turn promote ice growth and act as a negative feedback.

Through the ocean and sea ice feedback denial experiments, two parts of the ice growth–entrainment feedback were studied. The impact of changes in the sea ice growth/melt annual cycle on the mixed layer evolution, and the impact of changes in the mixed layer depth and properties on the sea ice cover. The results show that in both regions the sea ice response to the SAT perturbation strongly controlled the mixed layer responses due to changes in the timing, and magnitude, of the brine and freshwater fluxes from the sea ice growth/melt cycle. However, the results for the ocean feedback on the sea ice cover varied more between the two regions. In the Amundsen Sea changes in the depth of the winter mixed layer, and therefore the entrainment of warm deep water, strongly buffered changes in the sea ice volume, opposing the direct impact of the surface air temperature perturbation. This was shown to be the strongest feedback. In the Weddell Sea, due to the water column always destratifying because of the atmospheric conditions and weak stratification the impact on the ice volume were relatively small. The difference in the impact of the mixed layer variations in the two regions is reflected in the more linear response of the Weddell Sea sea ice cover to perturbations in the atmospheric forcing variables in Chapter 3.

How these two regions would be expected to respond to atmospheric warming would therefore be very different. The Weddell Sea is likely to show a decrease in sea ice, resulting in

later destratification, and possibly more importantly, a decrease in the rate of AABW formation in the Weddell Sea. In the Amundsen Sea, changes in entrainment may buffer changes to the sea ice cover, possibly even overshooting if the decrease in basal heating outweighed the decrease in sea ice growth.

In the Weddell Sea all the feedbacks were found to have a fairly minimal impact on the ice volume when compared to the magnitude of the sensitivity results. The albedo feedback is a small positive feedback in the Weddell Sea. The insulation feedback had the strongest impact on the sea ice volume, acting as a negative feedback on ice growth. The ocean feedback interacts strongly with the other feedbacks investigated in the Amundsen Sea, due to the buffering of the ice concentration and ice volume changes in response to the perturbations, influencing the strength and behaviour of the other feedbacks. Changes to the mixed layer depth caused by other feedbacks also involve changes in mixing of deep waters, involving the ocean feedback. For example, the albedo feedback involves more or less shortwave radiation entering the mixed layer, which then shoals or deepens the mixed layer, engaging the ocean feedback. The freezing temperature feedback had a negligible impact on the sea ice cover response to the SAT perturbations in both regions. Care must be taken when extrapolating these results due to the simplicity of the assumptions the model is built on. However, these results could aid the assessment of climate model performance in the Southern Ocean, and give insight into the extent to which the sea ice–ocean feedbacks as opposed to atmospheric forcing play a part in the discrepancy between climate model results and Antarctic sea ice observations.

An extension of this work could be to examine the action of this feedback in response to a greater range of perturbations. This would allow us to build up a better picture of the behaviour of γ for different size perturbations, to examine if there are values where γ for the ocean feedback changes sign or rapidly changes magnitude, and to examine this behaviour. This could also be done using other atmospheric forcing variables for the perturbations, such as shortwave or longwave radiation. Another extension of this study could be to quantify the sensitivity of γ to using the same perturbations, but changing the initial state, such as the stratification of the ambient ocean profile in the Amundsen Sea. This would provide a fuller understanding of the role of this ocean feedback may play depending on the magnitude of surface warming and changes in stratification due to snowfall changes/ice shelf melting, and demonstrate under what circumstances the behaviour of the feedback may change. The oceanic observations of temperature and salinity in both regions are limited both in space and time. More observations of the ocean properties of temperature and salinity for the two regions would help to better constrain the ambient profiles used in the idealised work, and the variability in these conditions in the two regions, which will influence the ocean feedbacks on the sea ice cover. Due to the magnitude of the ocean feedback in the Amundsen Sea, changes in this feedback may have significant consequences.

Due to the model used in the study, there were no feedbacks from the sea ice to the atmosphere in response to the perturbations. This had the benefit of making it easier to solely isolate the impact of changes in the surface conditions on the sea ice and ocean mixed layer. In reality, however, there would be positive feedbacks from the atmosphere that would amplify any warming (Pithan and Mauritsen, 2014), possibly altering the magnitude of the response of the sea ice and mixed layer, and therefore possibly the feedback responses. This was outside the study area of this thesis. It would however provide a challenging, but worthwhile extension of this work. A simple atmospheric boundary layer model coupled to the sea ice–mixed layer model could be used to examine the relative magnitude of the atmospheric feedbacks compared to the oceanic feedbacks and how they interact.

6.3 Ocean feedback study in the Amundsen Sea using the coupled CICE mixed layer model

CICE was coupled to a mixed layer (ML) model in order to study the ocean feedback in the Amundsen Sea, as this was found to be the strongest feedback in the feedback studies with the idealised model in Chapter 4. The purpose of this study was to examine the impact of more sophisticated sea ice physics on the feedback, as well as simulating the Amundsen Sea in the context of the whole of the Southern Ocean. Initially the impact on the sea ice cover of coupling the mixed layer model to CICE and modifying the snow ice parameterisation in CICE was examined. Using climatological atmospheric forcing it was shown to produce sea ice that was too thick all year round to the west of the Antarctic peninsula due to the averaging of surface air temperature. Therefore the atmospheric forcing from individual years that were identified as warm, cold, and typical years in the Amundsen Sea were used as the reference and perturbed years. However, forcing the model with those years of forcing, no correlation between warmer years and a shallower mixed layer and less sea ice, or vice versa, was seen. Therefore, to investigate the ocean feedback in the Amundsen Sea the reference and perturbed simulations were chosen based on mixed layer depth. In the coupled CICE–ML model, over winter the difference between the mixed layer and freezing temperature was approximately zero compared to the rest of the annual cycle. This meant that the difference in temperatures over the first portion of the year dictated the response of the sea ice to the change in mixed layer depth and properties.

A significant part of the difference in response may be due to the difference in the ambient ocean profiles being used. Therefore, a logical next step to compare the behaviour of the idealised model compared to perform simulations with the idealised model, using the same ambient ocean profiles and years of forcing as used in the coupled CICE–ML model and compare the results. This would then enable the impact of the difference in sea ice physics to be isolated. Direct

comparison of the idealised model and the CICE–ML model feedback studies is complicated by so many differences in the methodology. Another clear extension after this would be to use CICE coupled to a full ocean model, and to examine the impact of a more sophisticated representation of the ocean on the role and magnitude of the ocean feedback. Maps of the value of γ could also be created as well as looking at area average values, as there will likely be significant spatial variability in the strength of the feedback within the Amundsen Sea depending on the ocean temperature and salinity profiles.

As well, as carrying out a similar study for the Weddell Sea, to compare the behaviour to the idealised model. The findings of this thesis highlights the tight coupling between the ocean and sea ice in the continental shelf seas of Antarctica. A greater spatial and temporal coverage of observations of the sea ice and ocean properties in the future will help to better assess the current state of the Antarctic climate system. Therefore, aiding future modelling modelling studies to more accurately unravel the role sea ice–ocean feedbacks in our current and future climate.

Appendix A:

FEEDBACK DENIAL SIMULATION FIGURES

The following figures show the feedback denial results for the ice feedback denial (FD), ice thickness–ice growth FD, albedo FD, and freezing temperature FD. See Chapter 4 and Table 4.1 for more details about the methodology and descriptions of the feedbacks. Black lines indicate the reference simulations, red lines indicate +σ surface air temperatures (SAT) simulations, blue lines indicate -σ SAT, and green lines indicate the corresponding feedback denied simulations. The results are plotted after 8 years of simulation, by which time the simulations have reached a steady state annual cycle. These figures are presented as additional information for the results presented in Chapter 4.

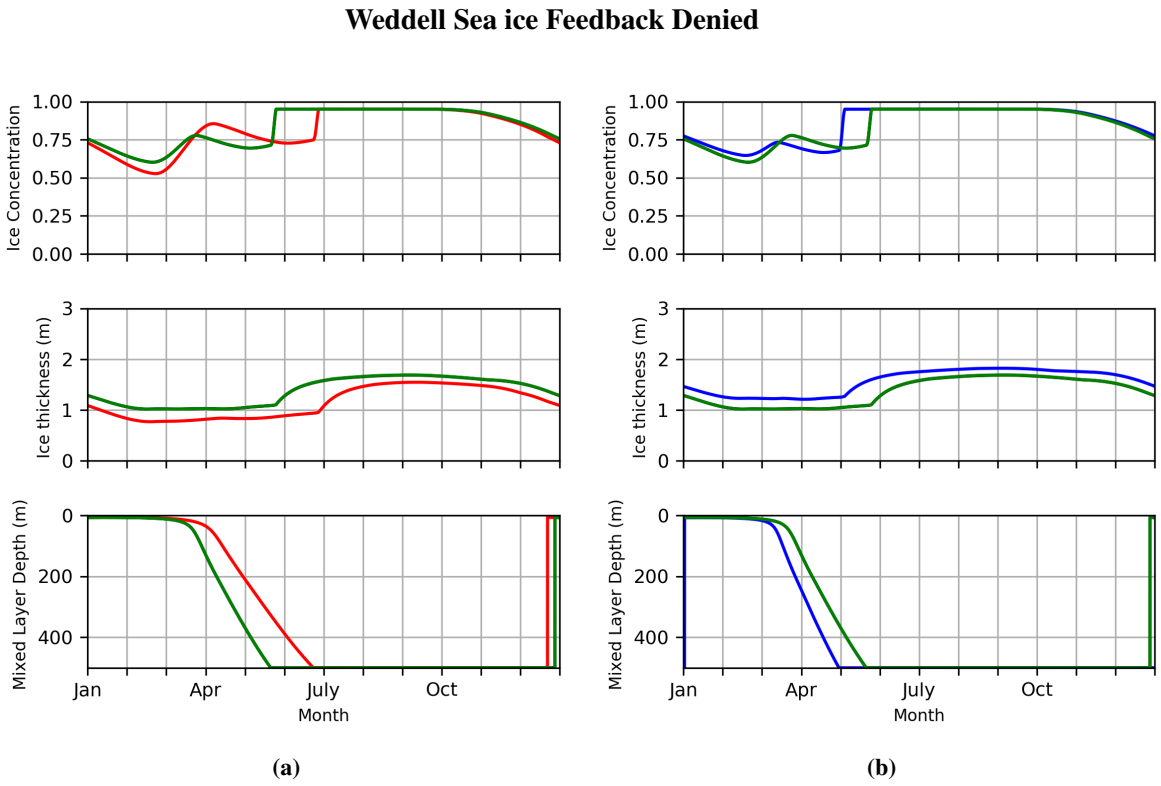

Figure A.1: *Steady state ice concentration, ice thickness and mixed layer depth for the reference (black), + σ SAT (red), – σ SAT (blue), and the corresponding ice denied simulations (green) for the Weddell Sea. (a) + σ SAT feedback denial (FD) simulation, and (b) – σ SAT feedback denial (FD) simulation.*

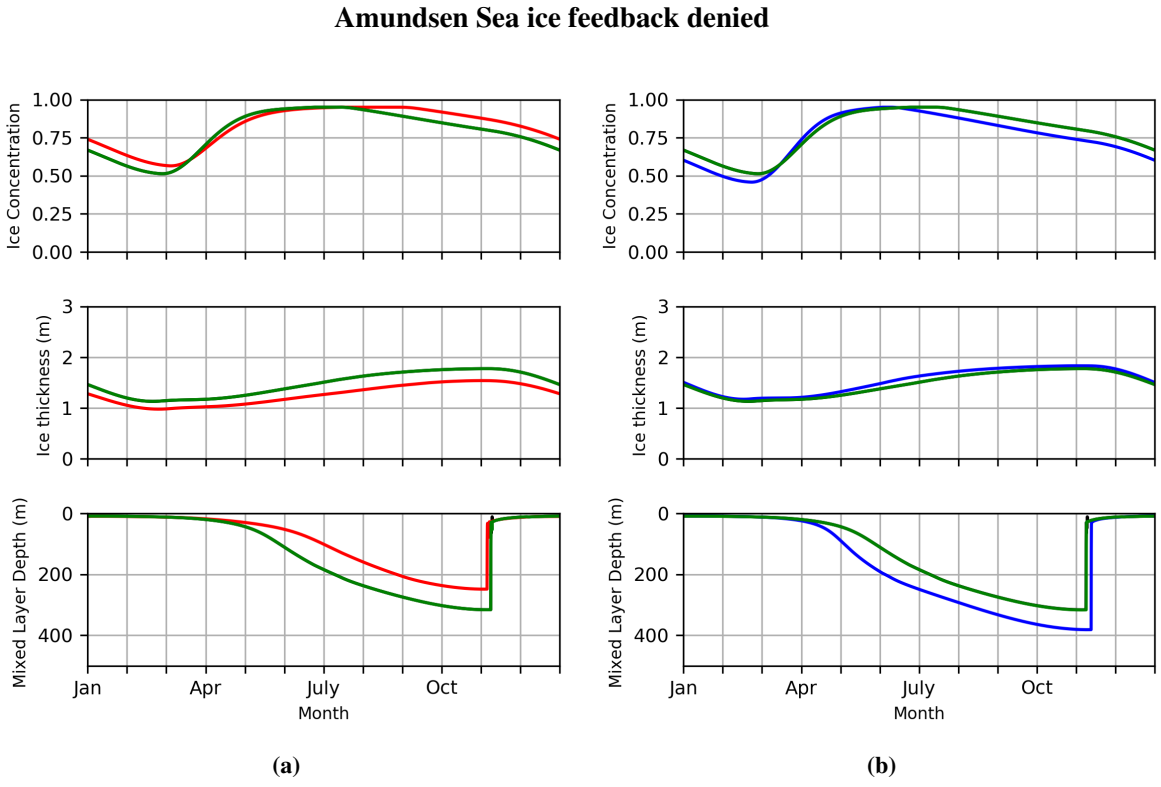

Figure A.2: *Ice feedback denial results for the Amudsen Sea, (a) + σ SAT FD, and (b) – σ SAT FD. See Figure A.1 caption for details.*

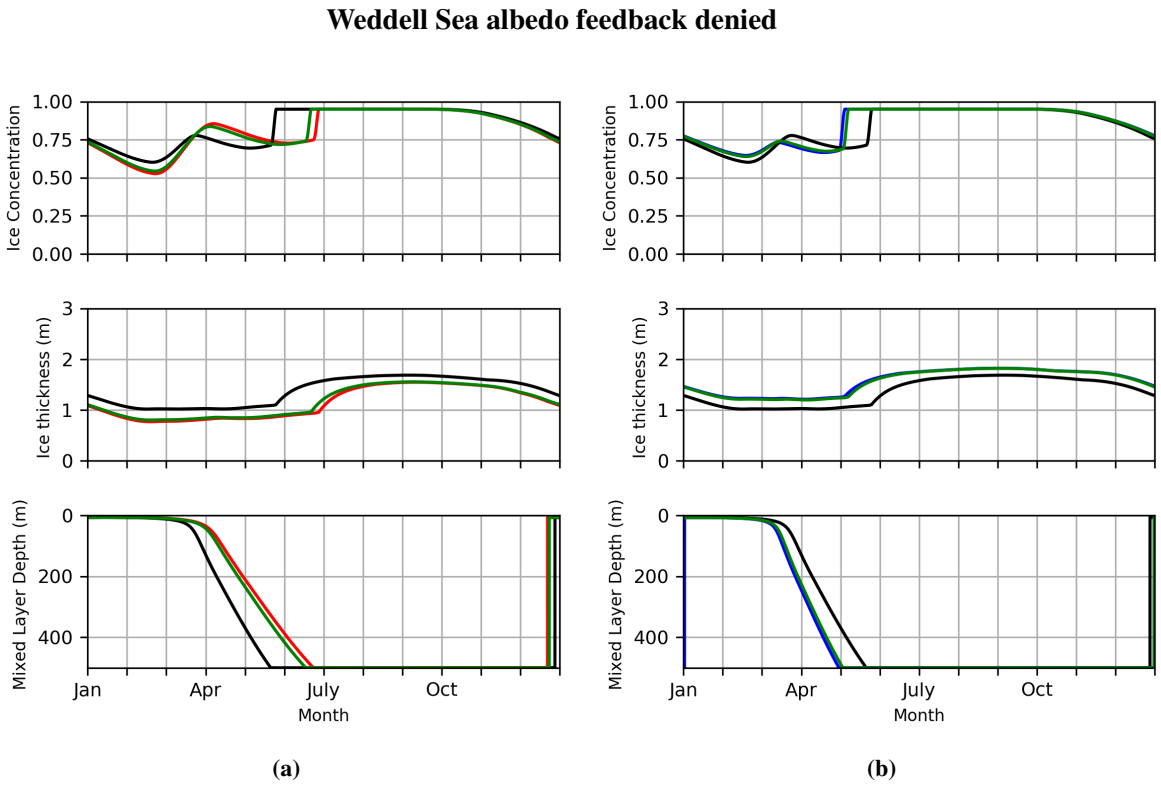

Figure A.3: *Albedo feedback denial results for the Weddell Sea, (a) + σ SAT FD, and (b) – σ SAT FD. See Figure A.1 caption for details.*

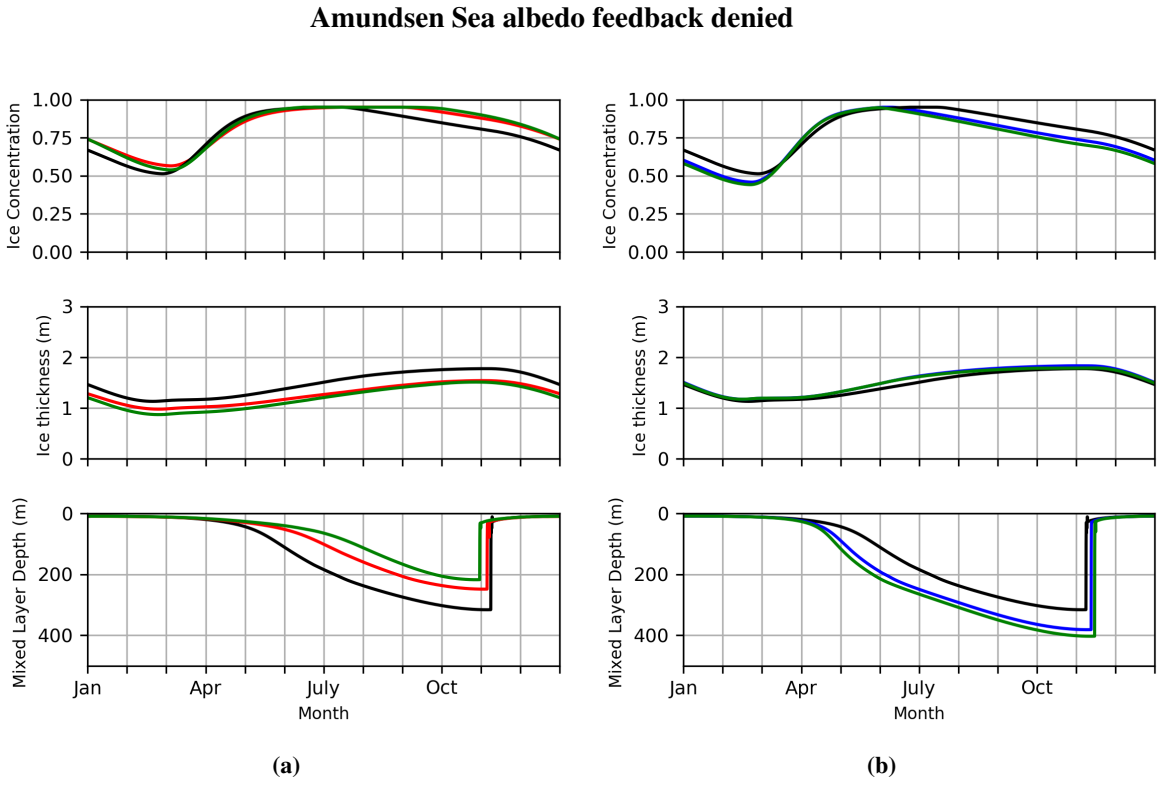

Figure A.4: *Albedo feedback denial results for the Amundsen Sea, (a) + σ SAT FD, and (b) – σ SAT FD. See Figure A.1 caption for details.*

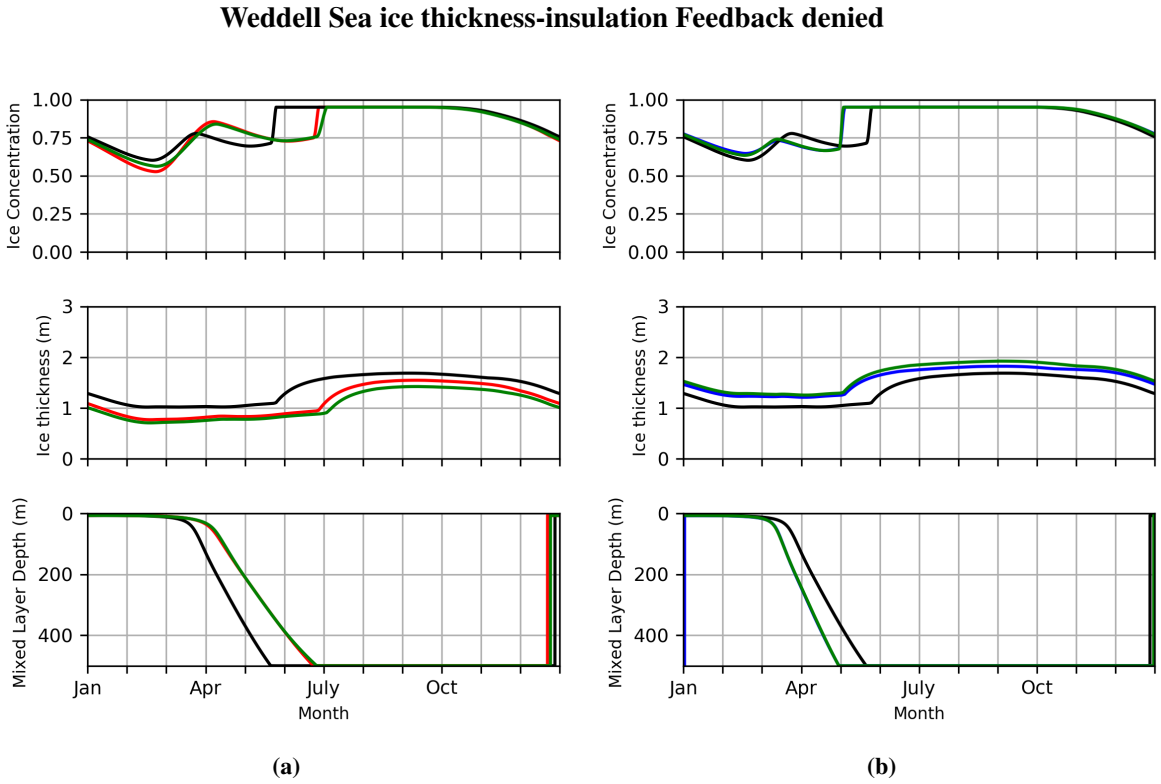

Figure A.5: *Ice thickness–insulation feedback denial results for the Weddell Sea, (a) + σ SAT FD, and (b) – σ SAT FD. See Figure A.1 caption for details.*

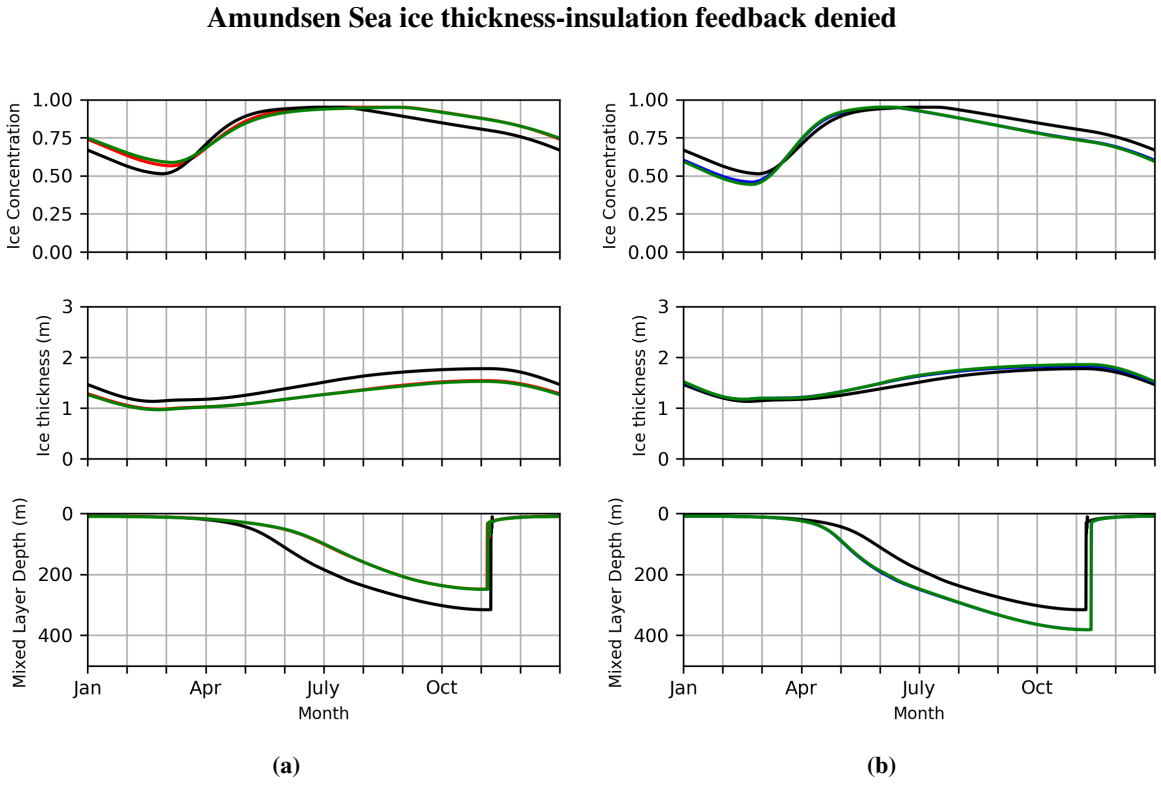

Figure A.6: *Ice thickness-insulation feedback denial results for the Amundsen Sea, (a) + σ SAT FD, and (b) – σ SAT FD. See Figure A.1 caption for details.*

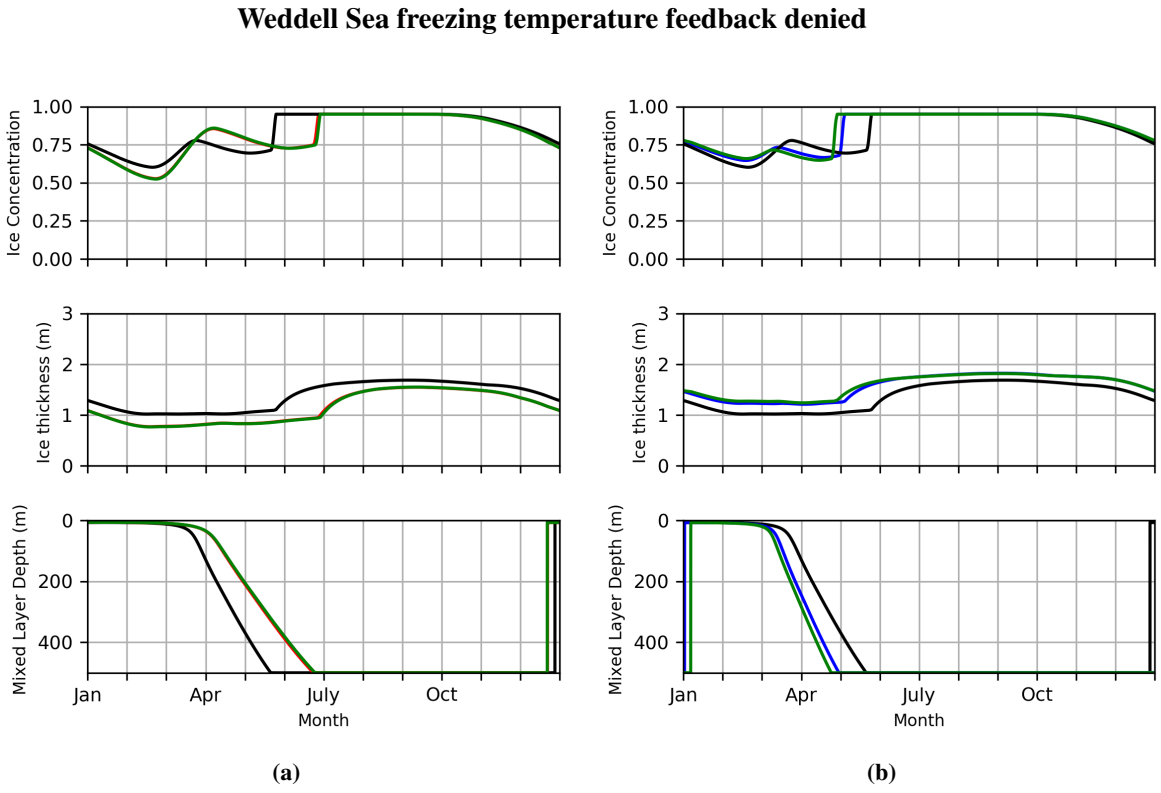

Figure A.7: *Freezing temperature feedback denial results for the Weddell Sea, (a) + σ SAT FD, and (b) – σ SAT FD. See Figure A.1 caption for details.*

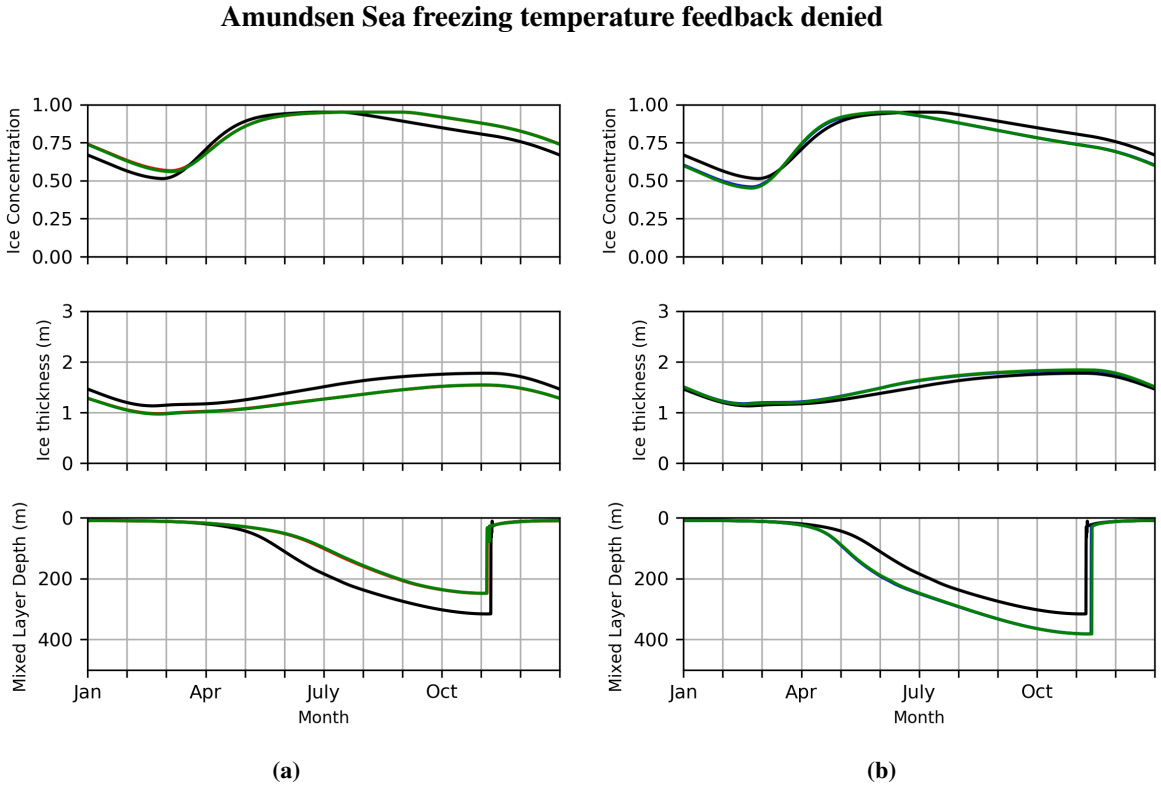

Figure A.8: *Freezing temperature feedback denial results for the Weddell Sea, (a) + σ SAT FD, and (b) – σ SAT FD. See Figure A.1 caption for details.*

REFERENCES

Abernathey, R. P., P. I. Cerovecki, P. R. Holland, E. Newsom, M. Mazlo, and L. D. Talley, 2016: Water-mass transformation by sea ice in the upper branch of the Southern Ocean overturning. *Nat. Geosci.*, **9**, 596–601, doi:10.1038/ngeo2749.

Anderson, R. F., S. Ali, L. I. Bradtmiller, M. Q. Nielson, S H H. Fleisher, B. E. Anderson, and L. H. Burckle, 2009: Wind–driven upwelling in the Southern Ocean and the deglacial rise in atmospheric CO2. *Science*, **323**, 1443, doi:10.1126/science.1167441.

Antonov, J. I., D. Seidov, T. P. Boyer, R. A. Locarnini, A. V. Mishonov, H. E. Garcia, O. K. Baranov, M. M. Zweng, and D. R. Johnson, 2010: *World Ocean Atlas 2009, Volume 2: Salinity*. NOAA Atlas NESDIS 68, U.S. Government Printing Office, Washington D.C., 184 pp.

Assmann, K. M., A. Jenkins, D. R. Shoosmith, D. P. Walker, S. S. Jacobs, and K. W. Nicholls, 2013: Variability of Circumpolar Deep Water transport onto the Amundsen Sea continental shelf through a shelf break trough. *J. Geophys. Res.*, **118**, 6603–6620, doi:10.1002/2013JC008871.

Bamber, J. L., R. E. M. Riva, V. B. L. A., and A. M. LeBrocq, 2009: Reassessment of the potential sea-level rise from a collapse of the West Antarctic Ice Sheet. *Science*, **324**, 901–903, doi:10.1126/science.1169335.

Bintanja, R., G. J. van Oldenborgh, S. S. Drijfhout, B. Wouters, and C. A. Katsman, 2013: Important role for ocean warming and increased ice–shelf melt in Antarctic sea-ice expansion. *Nat. Geosci.*, **6**, 376–379, doi:10.1038/NGEO1767.

Bitz, C. M., P. R. Gent, R. A. Woodgate, M. M. Holland, and R. Lindsay, 2006: The influence of sea ice on ocean heat uptake in response to increasing CO_2. *J. Climate*, **19**, 2437–2450., doi:10.1175/JCLI4294.1.

Bitz, C. M. and W. H. Lipscomb, 1999: An energy–conserving thermodynamic model of sea ice. *J. Geophys. Res.*, **104**, 15669–15677, doi:10.1029/1999JC900100.

Bitz, C. M. and L. M. Polvani, 2012: Antarctic climate response to stratospheric ozone depletion in a fine resolution ocean climate model. *Geophys. Res. Lett.*, **39**, L20705, doi:10.1029/2012GL053393.

Bromwich, D. H., J. P. Nicolas, and A. J. Monaghan, 2011: An assessment of precipitation changes over Antarctica and the Southern Ocean since 1989 in contemporary global reanalyses. *J. Climate*, **24**, 4189–4209, doi:10.1175/2011JCLI4074.1.

Bronselaer, B., M. Winton, S. M. Griffies, W. J. Hurlin, K. B. Rodgers, O. V. Sergienko, R. J. Stouffer, and J. L. Russell, 2018: Change in future climate due to Antarctic meltwater. *Nature*, **564**, 53–58, doi:10.1038/s41586-018-0712-z.

Cavalieri, D. J., C. L. Parkinson, P. Gloersen, and H. J. Zwally, 1996, updated yearly: Sea Ice Concentrations from Nimbus-7 SMMR and DMSP SSM/I-SSMIS Passive Microwave Data, Version 1. *Boulder, Colorado USA. NASA National Snow and Ice Date Center Distributed Achive Archive Center.*, doi:10.5067/8GQ8LZQVL0VL.

Christensen, J. H., K. Krishna Kumar, E. Aldrian, S. I. An, I. F. A. Cavalcanti, M. de Castro, W. Dong, P. Goswami, A. Hall, J. K. Kanyanga, A. Kitoh, J. Kossin, N. C. Lau, J. Renwick, D. B. Stephenson, X. S. P., and T. Zhou, 2013: Climate Phenomena and their Relevance for Future Regional Climate Change. *Climate Change 2013: The Physical Science Basis. Contribution of Working Group I to the Fifth Assessment Report of the Intergovernmental Panel on Climate Change*.

Clem, K. R. and R. L. Fogt, 2013: Varying roles of ENSO and SAM on the Antarctic Peninsula climate in austral spring. *J. Geophys. Res. Atmos*, **118**, 11481–11492, doi:10.1002/jgrd.50860.

Colling, A., 1994: *Ocean Circulation (The Open University)*. Butterworth Heinemann, The Open University, Milton Keynes, England.

Collins, M., R. Knutti, J. Arblaster, J.-L. Dufresne, T. Fichefet, P. Friedlingstein, X. Gao, W. J. Gutowski, T. Johns, G. Krinner, M. Shongwe, C. Tebaldi, W. A. J., and M. Wehner, 2013: *Long-term Climate Change: Projections, Commitments and Irreversibility. In: Climate Change 2013: The Physical Science Basis. Contribution of Working Group I to the Fifth Assessment Report of the Intergovernmental Panel on Climate Change*. Cambridge University Press, Cambridge, United Kingdom and New York, NY, USA.

Cunningham, S., S. Alderson, B. King, and M. Brandon, 2003: Transport and variability of the Antarctic Circumpolar Current in Drake Passage. *J. Geophys. Res.*, **108(C5)**, 8084, doi:10.1029/2001JC001147.

de Lavergne, C., J. B. Palter, E. D. Galbraith, R. Bernardello, and I. Marinov, 2014: Cessation of deep convection in the open Southern Ocean under anthropogenic climate change. *Nat. Climate Change*, **4**, 278–282, doi:10.1038/nclimate2132.

Dee, D. P., S. M. Uppala, A. J. Simmons, P. Berrisford, P. Poli, S. Kobayashi, U. Andrae, M. A. Balmaseda, G. Balsamo, P. Bauer, P. Bechtold, A. C. M. Beljaars, L. van de Berg, J. Bidlot, N. Bormann, C. Delsol, R. Dragani, M. Fuentes, A. J. Geer, L. Haimberger, S. B. Healy, H. Hersbach, E. V. Hólm, L. Isaksen, P. Kållberg, M. Köhler, M. Matricardi, A. P. McNally, B. M. Monge-Sanz, J.-J. Morcrette, B.-K. Park, C. Peubey, P. de Rosnay, C. Tavolato, J.-N. Thépaut, and F. Vitart, 2011: The ERA-Interim reanalysis: configuration and performance of the data assimilation system. *Q.J.R. Meteorol. Soc*, **137**, 553–597, doi:10.1002/qj.828.

Ding, Q., D. S. Steig, E J.and Battisti, and M. Kuttel, 2011: Winter warming in West Antarctica caused by central Pacific warming. *Nature Geosci.*, **4**, 398–403, doi:10.1038/ngeo1129.

Doddridge, E. W. and J. Marshall, 2017: Modulation of the seasonal cycle of Antarctic sea ice extent related to the Southern Annular Mode. *Geophys. Res. Lett.*, **44**, 9761–9768, doi:10.1002/2017GL074319.

Donohue, K. A., K. L. Tracey, D. R. Watts, M. P. Chidichimo, and T. K. Chereskin, 2016: Mean Antarctic Circumpolar Current transport measured in Drake Passage. *Geophys. Res. Lett.*, **43**, 11760–11767, doi:10.1002/2016GL070319.

Durack, P. J. and S. E. Wijffels, 2010: Fifty–year trends in global ocean salinities and their relationship to broad scale warming. *J. Climate*, **23**, 4342–4362, doi:10.1175/2010JCLI3377.1.

Dutrieux, P., J. De Rydt, A. Jenkins, P. R. Holland, H. K. Ha, S. H. Lee, E. J. Steig, Q. Ding, E. P. Abrahamsen, and M. Schröder, 2014: Strong sensitivity of Pine Island ice-shelf melting to climatic variability. *Science*, **343**, 174–178, doi:10.1126/science.1244341.

Fahrbach, E., O. Boebel, O. Klatt, and A. Wisotzki, 2011: Warming of deep and abyssal water masses along the Greenwich meridian on decadal time scales: The Weddell gyre as a beat buffer. *Deep Sea Research II*, **58**, 2509–2523, doi:10.1016j.dsr2.2011.06.007.

Fahrbach, E., G. Rohardt, M. Schröder, and V. Strass, 1994: Transport and structure of the Weddell Gyre. *Ann. Geophys.*, **12**, 840–855, doi:10.1007/s00585-994-0840-7.

Fan, T., C. Deser, and D. P. Schneider, 2014: Recent Antarctic sea ice trends in the context of Southern Ocean surface climate variations since 1950. *Geophys. Res. Lett.*, **41**, 2419–2426, doi:10.1002/2014GL059239.

Ferreira, D. and J. Marshall, 2015: Antarctic Ocean and sea ice response to ozone depletion: a two-time-scale problem. *J. Climate*, **28**, 1206–1226, doi:10.1175/JCLI-D-14-00313.1.

Fichefet, T. and M. A. Morales Maqueda, 1999: Modelling the influence of snow accumulation and snow–ice formation on the seasonal cycle of the Antarctic sea–ice cover. *Clim. Dyn.*, **15**, 251–268.

Foldvik, A. and T. Gammelsrød, 1988: Notes on Southern Ocean hydrography, sea–ice and bottom water formation. *Palaeogeogr. Palaeoclimatol. Palaeoecol.*, **67**, 3–17, doi:10.1016/00310182(88)901198.

Foldvik, A., T. Gammelsrød, S. Østerhus, E. Fahrbach, G. Rohardt, M. Schröder, K. W. Nicholls, L. Padman, and R. A. Woodgate, 2004: Ice shelf water overflow and bottom water formation in the southern Weddell Sea. *J. Geophys. Res.*, **109**, C02015, doi:10.1029/2003JC002008.

Foster, T. D. and E. C. Carmack, 1976: Frontal zone mixing and Antarctic Bottom Water formation in the southern Weddell Sea. *Deep-Sea Res.*, **34**, 301–317, doi:10.1016/0011-7471(76)90872-X.

Francis, D., C. Eayrs, J. Cuesta, and D. Holland, 2019: Polar cyclones at the origin of the reoccurence of the Maud Rise polynya in the austral winter 2017. *Journal of Geophysical Research: Atmospheres*, **124**, 5251–5267, doi:10.1029/2019JD030618.

Gent, P. R., 2016: Effects of southern hemisphere wind changes on the meridional overturning circulation in ocean models. *Ann. Rev. Mar. Sci.*, **8**, 79–94, doi:10.1146/annurev-marine-122414-033929.

Giles, K. A., S. W. Laxon, and A. P. Worby, 2008: Antarctic sea ice elevation from satellite radar altimetry. *Geophys. Res. Lett.*, **35**, 872–875, doi:10.1029/2007GL031572.

Gille, S. T., 2002: Warming of the Southern Ocean since the 1950s. *Science*, **295**, 12751277, doi:10.1126/science.1065863.

— 2008: Decadal-scale temperature trends in the Southern Hemisphere Ocean. *J. Climate*, **21**, 4749–4765, doi:10.1175/2008JCLI2131.1.

Gillett, N. P. and D. W. J. Thompson, 2003: Simulation of recent southern hemisphere climate change. *Science*, **302**, 273–275, doi:10.1126/science.1087440.

Goosse, H., J. E. Kay, K. C. Armour, A. Bodas-Salcedo, D. Chepfer, H. Docquier, A. Jonko, P. J. Kushner, O. Lecomte, F. Massonnet, H.-S. Park, F. Pithan, G. Svensson, and M. Vancoppenolle, 2018: Quantifying climate feedbacks in polar regions. *Nat. Comm.*, **9**, 1919, doi:10.1038.s41467–018–04173–0.

Goosse, H. and V. Zunz, 2014: Decadal trends in the Antarctic sea ice extent ultimately controlled by ice–ocean feedback. *The Cryosphere*, **8**, 453–470, doi:10.5194/tc-8-453-2014.

Gordon, A. L., 1978: Deep Antarctic convection west of Maud Rise. *J. Phys. Ocean.*, **8**, 600–612, doi:10.1175/1520-0485(1978)008¡0600:DACWOM¿2.0.CO;2.

— 1982: Weddell deep water variability. *Journal of Marine Research*, **40**, 199–217.

— 1998: Western Weddell Sea thermohaline stratification. *Amer. Geophys. Union*, **75**, 215–240.

— 2007: A possible link between the Weddell Polynya and the Southern Annular Mode. *J. Climate*, **20**, 2558–2571, doi:10.1175/JCLI4046.1.

Gordon, A. L., B. A. Huber, H. H. Hellmer, and A. FField, 1993: Deep and bottom water of the Weddell Sea's western rim. *Science*, **262**, 95–97, doi:10.1126/science.262.5130.95.

Gruber, N., P. Landschüyzer, and N. S. Lovenduski, 2019: The variable southern ocean carbon sink. *Ann. Rev. Mar. Sci.*, **11**, 159–186, doi:10.1146/annurev- marine- 121916- 063407.

Haid, V., D. Iovino, and S. Masinna, 2017: Impacts of freshwater changes on Antarctic sea ice in an eddy–permitting sea–ice–ocean model. *The Cryosphere*, **11**, 1387–1402, doi:10.5194/tc-11-1387-2017.

Hall, A. and M. Visbeck, 2002: Synchronous variability in the southern hemisphere atmosphere, sea ice, and ocean resulting from the annular mode. *J. Climate*, **15**, 3043–3057, doi:10.1175/1520-0442(2002)015¡3043:SVITSH¿2.0.CO;2.

Haumann, N., F A. Gruber, I. Münnuch, M. Frenger, and S. Kern, 2016: Sea-ice transport driving Southern Ocean salinity and its recent trends. *Nature*, **537**, 82–92, doi:10.1038/nature191012.

Hibler, W. D., 1979: A dynamic thermodynamic sea ice model. *J. Phys. Ocean.*, **9**, 817–846.

Holland, D., 2001a: Explaining the Weddell Polynya: A large ocean eddy shed at Maud Rise. *Science*, **292**, 1697–1700, doi:10.1126/science.1059322.

Holland, D. M., 2001b: Transient sea-ice polynya forced by oceanic flow variability. *Progress in Oceanography*, **48(4)**, 403–460, doi:10.1016/S0079-6611(01)00010-6.

Holland, M. M., L. Landrum, Y. Kostov, and J. Marshall, 2016: Sensitivity of Antarctic sea ice to the Southern Annular Mode in coupled climate models. *Clim. Dyn.*, **49**, 1813–1831, doi:10.1007/s00382-016-3424-9.

Holland, M. M., L. Landrum, M. Raphael, and S. E. Stammerjohn, 2017: Springtime winds drive Ross Sea variability and change the following autumn. *Nat. Commum.*, **8**, 731, doi:10.1038/s41467-017-00820-0.

Holland, P. R., 2014: The seasonality of Antarctic sea ice trends. *Geophys. Res. Lett.*, **41**, 4230–4237, doi:10.1002-/2014GL060172.

Holland, P. R., N. Bruneau, C. Enright, M. Losch, N. T. Kurtz, and R. Kwok, 2014: Modeled trends in Antarctic sea ice thickness. *J. Climate*, **27**, 3784–3801, doi:10.1175/JCLI-D-13-00301.1.

Holland, P. R. and R. Kwok, 2012: Wind-driven trends in Antarctic sea-ice drift. *Nat. Geosci.*, **5**, 872–875, doi:10.1038/ngeo1627.

Holmes, C. R., P. R. Holland, and T. J. Bracegirdle, 2019: Compensating biases and a noteworthy success in the CMIP5 representation of Antarctic sea ice processes. *Geophys. Res. Lett.*, **46**, 4299–4307, doi:10.1029/2018GL081796.

Hosking, J. S., A. Orr, G. J. Marshall, J. Turnerr, and T. Phillips, 2013: The influence of the Amundsen–Bellingshausen Seas low on the climate of West Antarctica and its representation in coupled climate model simulations. *J. Climate*, **26**, 6633–6648, doi:10.1175/JCLI-D-12-00813.1.

Hunke, E. C., 2001: Viscous-plastic sea ice dynamics with the EVP model: Linearization issues. *J. Comput. Phys.*, **170**, 18–38.

Hunke, E. C. and J. K. Dukowicz, 1997: An elastic viscous plastic model for sea ice dynamics. *J. Phys. Ocean.*, **27**, 1849–1867.

— 2002: The Elastic-Viscous-Plastic sea ice dynamics model in general orthogonal curvilinear coordinates on a sphere–Effect of metric terms. *Mon. Wea. Rev.*, **130**, 1848–1865.

Hunke, E. C., W. H. Lipscomb, N. Turner, A K. Jeffery, and S. Elliott, 2015: CICE: the Los Alamos Sea Ice Model Documentation and Software Users Manual Version 5.1, LA-CC-06-012, Los Alamos National Laboratory, Los Alamos NM 87545.

Jacobs, S., A. Jenkins, H. Hellmer, C. Giulivi, F. Nitsche, B. Huber, and R. Guerrero, 2012: The Amundsen Sea and the Antarctic Ice Sheet. *Oceanography*, **25(3)**, 154–163, doi:10.5670/oceanog.2012.90.

Jacobs, S. S., H. H. Hellmer, and A. Jenkins, 1996: Antarctic Ice Sheet melting in the Southeast Pacific. *Geophys. Res. Lett.*, **23**, 957–960, doi:10.1029/96GL00723.

Jacobs, S. S., A. Jenkins, C. F. Giulivi, and P. Dutrieux, 2011: Stronger ocean circulation and increased melting under Pine Island Glacier ice shelf. *Geophys. Res. Lett.*, **113**, 519–523, doi:10.101038/ngeo1188.

Jeffries, M. O., H. R. Krouse, B. Hurst-Cushing, and T. Maksym, 2001: Snow ice accretion and snow cover depletion on Antarctic first–year sea ice floes. *Annals of Glaciology*, **33**, 51–60, doi:10.3189/172756401781818266.

Jeffries, M. O., A. P. Worby, K. Morris, and W. F. Weeks, 1997: Seasonal variations in properties, and structural isotopic composition of sea ice and snow cover in the Bellingshausen and Amundsen Seas. *J. Glaciol.*, **43(143)**, 138–151, doi:10.1016/j.dsr2.2016.03.008.

Jena, B., M. Ravichandran, and J. Turner, 2019: Recent reoccurence of large open-ocean polynya on the Maud Rise seamount. *Geophys. Res. Lett.*, **46**, 4320–4329, doi:10.1029/2018GL081482.

Johnson, G. C. and S. C. Doney, 2006: Recent western South Atlantic bottom water warming. *Geophys. Res. Lett.*, **33**, L14614, doi:10.1029/2006GL026769.

Jones, R. W., I. A. Renfrew, A. Orr, B. G. M. Webber, and D. M. holland, 2016: Evaluation of four global reanalysis products using in situ observations in the Amundsen Sea Embayment, Antarctica. *J. Geophys. Res.*, **121**, doi:10.1002/2015JD024680.

Jutras, M., M. Vancoppenolle, A. Laurençoa, F. Viviera, G. Carnatc, G. Madeca, C. Rousseta, and J.-L. Tison, 2016: Thermodynamics of slush and snow–ice formation in the Antarctic sea–ice zone. *Deep Sea Research II*, doi:10.1016/j.dsr2.2016.03.008.

Karsten, R. and J. Marshall, 2002: Constructing the residual circulation of the ACC from observations. *J. Phys. Ocean.*, **32**, 33153327, doi:10.1175/1520-0485(2002)032¡3315:CTRCOT¿2.0.CO;2.

Khatiwala, S., F. Primeau, and T. Hall, 2009: Reconstruction of the history of anthropogenic CO_2 concentrations in the ocean. *Nature*, **462**, 346–349, doi:10.1038/nature08526.

Khatiwala, S., T. Tanhhua, S. Mikaloff-Fletcher, M. Gerber, H. D. Doney, S C. Graven, N. Gruber, G. A. McKinley, A. Murata, A. F. Ríos, and C. L. Sabine, 2013: Global ocean storage of anthropogenic carbon. *Biogeosciences*, **10**, 22169–2192, doi:10.5194/bg-10-2169-2013.

Kirkman, C. H. and C. M. Bitz, 2010: The effect of the sea ice freshwater flux on Southern Ocean temperatures in CCSM3: deep ocean warming and delayed surface warming. *J. Climate*, **24**, 2224–2237, doi:10.1175/2010JCLI3625.1.

Kraus, E. B. and J. S. Turner, 1967: A one-dimensional model of the seasonal thermocline II. The general theory and its consequences. *Tellus*, **19**, 98–106, doi:10.1111/j.2153-3490.1967.tb01462.x.

Kuhlbrodt, T., A. Griesel, M. Montoya, A. Levermann, M. Hofmann, and S. Rahmstorf, 2007: On the driving processes of the atlantic meridional overturning circulation. *Rev. Geophys.*, **45**, RG2001, doi:10.1029/2004RG000166.

Kurtz, N. T. and T. Markus, 2012: Satellite observations of Antarctic sea ice thickness and volume. *J. Geophys. Res.*, **117**, doi:10.1029/2012JC008141.

Kwok, R., J. C. Comiso, T. Lee, and P. R. Holland, 2016: Linked trends in the South Pacific sea ice edge and Southern Oscillation Index. *Geophys. Res. Lett.*, **43**, 10,295–10,302, doi:10.1002/2016GL070655.

Lange, M. A., S. F. Schlosser, A P. Ackley, P. Wadhams, and G. S. Dieckmann, 1990: ^{18}O concentrations in sea ice of the Weddell Sea, Antarctica. *Journal of Glaciology*, **36(124)**, 315–323, doi:10.3189/002214390793701291.

Large, W. G., J. C. McWilliams, and S. C. Doney, 1994: Oceanic vertical mixing: A review and a model with nonlocal boundary layer parameterization. *Rev. Geophys.*, **32**, 363–403, doi:10.1029/94RG01872.

Lecarnini, R. A., A. V. Mishonov, J. I. Antonov, T. P. Boyer, H. E. Garcia, O. K. Baranova, M. M. Zweng, and D. R. Johnson, 2010: *World Ocean Atlas 2009, Volume 1: Temperature*. NOAA Atlas NESDIS 68, U.S. Governmnet Printing Office, Washington D.C.

Lecomte, O., H. Goosse, C. Fichefet, T. de Lavergne, A. Barthélemy, and V. Zunz, 2017: Vertical ocean heat redistribution sustaining sea–ice concentration trends in the Ross Sea. *Nat. Comm.*, **8**, 258, doi:10.1038/s41467-017-00347-4.

Lindsay, R. W., R. Kwok, de Steur L., and W. Meier, 2008: Halo of ice deformation observed over the Maud Rise seamount. *Geophys. Res. Lett.*, **35**, L15501, doi:10.1029/2008GL034629.

Lipscomb, W. H. and E. C. Hunke, 2004: Modeling sea ice transport using incremental remapping. *Mon. Weather. Rev.*, **132**, 1341–1354.

Liu, J. and J. A. Curry, 2010: Accelerated warming of the Southern Ocean and its impacts on the hydrological cycle and sea ice. *Proc. Natl. Acad. Sci. U.S.A.*, **107(34)**, 14,987–14,992, doi:10.1073/pnas.1003336107.

Maksym, T., 2019: Arctic and Antarctic sea ice change: contrasts, commonalities and causes. *Annual Review of Marine Science*, **11**, 187–213, doi:10.1146/annurev-marine-010816-06-610.

Maksym, T., S. E. Stammerjohn, S. Ackley, and R. Massom, 2012: Antarctic sea ice- A polar opposite? *Oceanography*, **25(3)**, 140–150.

Marshall, G. J., 2003: Trends in the southern annular mode from observations and reanalyses. *J. Climate*, **16**, 4134–4143, doi:10.1175/1520-0442(2003)016¡4134:TITSAM¿2.0.CO;2.

Martinson, D. G., 1990: Evolution of the Southern Ocean winter mixed layer and sea ice: open ocean deepwater formation and ventilation. *J. Geophys. Res.*, **95**, 11,641–11,654, doi:10.1029/JC095iC07p11641.

Massom, R. A., H. Eicken, C. Haas, M. O. Jeffries, M. R. Drinkwater, M. Sturm, A. P. Worby, X. Wu, V. I. Lytle, S. Ushio, K. Morris, P. A. Reid, S. Warren, and I. Allison, 2001: Snow on Antarctic sea ice. *Rev. Geophys.*, **39(3)**, 413–445.

Massonnet, F., P. Methiot, T. Fichefet, H. Goosse, C. K. Beatty, M. Vancoppenolle, and T. Lavergne, 2013: A model reconstruction of the Antarctic sea ice thickness and volume changes over 19802008 using data assimilation. *Ocean Modelling*, **64**, 67–75, doi:10.1016/j.ocemod.2013.01.003.

Matear, T. J., R J. andn O'Kane, J. S. Risbey, and M. Chamberlain, 2015: Sources of heterogeneous variability and trends in Antarctic sea-ice. *Nat. Comms.*, **6**, 8656, doi:10.1038/ncomms9656.

Maykut, G. A. and D. K. Perovich, 1987: The role of shortwave radiation in the summer decay of a sea ice cover. *J. Geophys. Res.*, **92(C7)**, 7032–7044.

Maykut, G. A. and N. Untersteiner, 1971: Some results from a time-dependent thermodynamic model of sea ice. *J. Geophys. Res.*, **76(6)**, 1550–1575, doi:10.1029/JC076i006p01550.

Mellow, G. L. and T. Yamada, 1982: Development of a turbulence closure model for ggeophysical fluid problems. *Rev. Geophys.*, **20**, 851–875.

Mercer, J. H., 1978: West Antarctic ice sheet and CO_2 greenhouse effect: a threat of disaster. *Science*, **271**, 321–325, doi:10.1038/271321a0.

Meredith, M. P. and J. C. King, 2005: Rapid climate change in the ocean west of the Antarctic Peninsula during the second half of the 20th century. *Geophys. Res. Lett.*, **32**, 1550–1575, doi:10.1029/2005GL024042.

Meredith, M. P., A. C. Naveira Garabato, A. P. Gordon, and G. C. Johnson, 2008: Evolution of the Deep and Bottom Waters of the Scotia Sea, Southern Ocean. *J. Climate*, **21**, 3327–3343, doi:10.1175/2007JCLI2238.1.

Meredith, M. P., A. C. Naveira-Garabato, and R. Hogg, A M. Farneti, 2012: Sensitivity of the overturning circulation in the Southern Ocean to decadal changes in wind forcing. *J. Climate*, **25**, 99–110, doi:10.1175/2011JCLI4204.1.

Morrison, A. . and A. M. Hogg, 2013: On the relationship between Southern Ocean overturning and ACC transport. *J. Phys. Ocean.*, **43**, 140–148, doi:10.1175/JPO-D-12-057.1.

Muench, R. D., J. H. Morison, L. Padman, D. Martinson, P. Schlosser, B. Huber, and R. Hohmann, 2001: Maud Rise revisited. *J. Geophys. Res.*, **106**, 2423–2440, doi:10.1029/2000JC000531.

Nicholls, K. W., L. Boehme, M. Biuw, and M. A. Fedak, 2008: Wintertime ocean conditions over the southern Weddell Sea continental shelf, Antarctica. *Geophys. Res. Lett.*, **35**, L21605, doi:10.1029/2002JC001713.

Nicholls, K. W., S. Østerhus, K. Makinson, T. Gammelsrod, and E. Fahrbach, 2009: Ice–ocean processes over the continental shelf of the southern Weddell Sea, Antarctica: A review. *Rev. Geophys.*, **47**, RG3003, doi:10.1029/2007RG000250.

Nicholls, K. W., L. Padman, M. Schröeder, R. A. Woodgate, A. Jenkins, and S. Østerhus, 2003: Water mass modification over the continental shelf north of Ronne Ice Shelf, Antarctica. *Geophys. Res. Lett.*, **108**, 3260, doi:10.1029/2002JC001713.

Nicholls, K. W., C. J. Pudsey, and P. Morris, 2004: Summertime water masses off the northern Larsen C Ice Shelf. *Geophys. Res. Lett.*, **31**, L09309, doi:10.1029/2004GL035742.

Niiler, P. and E. B. Kraus, 1977: One–dimensional models of the upper ocean. *Modeling and prediction of the upper layers of the ocean.*, **E. B. Kraus, Ed., Pergamon Press**, 143–172.

Olbers, D. and M. Visbck, 2005: A model of the zonally averaged stratification and overturning in the Southern Ocean. *J. Phys. Ocean.*, **35**, 1190–1205, doi:10.1175/JPO2750.1.

Orsi, A. H., G. C. Johnson, and J. L. Bullister, 1999: Circulation, mixing, and production of Antarctic Bottom Water. *Progress in Oceanography*, **43**, 55–109, doi:10.1016/S0079-6611(99)00004-X.

Ozsoy-cicek, B., S. F. Ackley, H. Xie, and H. J. Zwally, 2013: Sea ice thickness retrieval algorithms based on in situ surface elevation and thickness values for application to altimetry. *J. Geophys. Res.*, **118**, 3807–3822, doi:10.1002/jgrc.20252.

Parkinson, C. L., 2019: A 40-y record reveals gradual Antarctic sea ice increases followed by decreases at rates far exceeding the rates seen in the Arctic. *PNAS*, **116**, 14414–14423, doi:10.1073/pnas.1906556116.

Parkinson, C. L. and D. J. Cavalieri, 2008: Arctic sea ice variability and trends, 1979–2006. *J. Geophys. Res. Oceans.*, **113**, C07003, doi:10.1029/2007JC004558.

— 2012: Antarctic sea ice variability and trends, 1979-2010. *The Cryosphere*, **6**, 871–880, doi:10.5194/tc-6-871-2012.

Parkinson, C. L. and J. C. Comiso, 2013: On the record low Arctic sea ice cover: combined impact of preconditioning and an August storm. *Geophys. Res. Lett.*, **40**, 1356–1361, doi:10.1002/grl.50349, 2013.

Pauling, A. G., C. B. Bitz, I. J. Smith, and P. J. Langhorne, 2016: The response of the Southern Ocean and Antarctic sea ice to freshwater from ice shelves in an earth system model. *J. Climate*, **29**, 1655–1672, doi:10.1175/JCLI-D-15-0501.1.

Pellichero, V., J.-B. Sallée, C. C. Chapman, and S. M. Downes, 2018: The Southern Ocean meridional overturning in the sea-ice sector is driven by freshwater fluxes. *Nat. Commun.*, **9**, 1789, doi:10.1038/s41467-018-04101-2.

Pellichero, V., J.-B. Sallée, S. Scmidtko, F. Roquet, and J.-B. Charrassin, 2017: The ocean mixed layer under Southern Ocean sea-ice: seasonal cycle and forcing. *Geophys. Res. Oceans.*, **122**, 1608–1633, doi:10.1002/2016JC011970.

Perovich, D. K., K. F. Jones, B. Light, H. Eicken, T. Markus, J. Stroeve, and R. Lindsay, 2011: Solar partitioning in a changing Arctic sea-ice cover. *Annals of Glaciology*, **52(57)**, 192–196, doi:10.3189/172756411795931543.

Petty, A. A., D. L. Feltham, and P. R. Holland, 2013: Impact of atmospheric forcing on Antarctic continental shelf water masses. *J. Phys. Ocean.*, **43**, 920–940, doi:10.1175/JPO-D-12-0172.1.

Petty, A. A., P. R. Holland, and D. L. Feltham, 2014: Sea ice and the ocean mixed layer over the Antarctic shelf seas. *The Cryosphere*, **8**, 761–783, doi:10.5194/tc-8-761-2014.

Pithan, F. and T. Mauritsen, 2014: Arctic amplification dominated by temperature in contemporary climate models. *Nat. Geosci.*, **7**, 181–184, doi:10.1038/NGEO2071.

Polvani, L. M., D. W. Waugh, G. J. P. Correa, and S.-W. Son, 2011: Stratospheric ozone depletion: The main driver of twentieth-century atmospheric circulation changes in the Southern Hemisphere. *J. Climate*, **24**, 795–812, doi:10.1175/2010JCLI3772.1.

Powell, D. C., T. Markus, and A. Stössel, 2005: Effects of snow depth forcing on Southern Ocean sea ice simulations. *J. Geophys. Res.*, **124(3)**, doi:10.1029/2003JC002212.

Price, J. F., R. A. Weller, and Y. Han, 1986: Development of a simple upper–ocean and sea–ice model. *J. Phys. Ocean.*, **91**, 8411–8427.

Purkey, S. G. and G. C. Johnson, 2010: Warming of global abyssal and deep Southern Ocean waters between the 1990s and 2000s: Contributions to global heat and sea level rise budgets. *J. Climate*, **23**, 6336–6351, doi:10.1175/2010JCLI3682.1.

— 2013: Antarctic Bottom Water warming and freshening: Contributions to sea level rise, ocean freshwater budgets, and global heat gain. *J. Climate*, **26**, 6105–6122, doi:10.1175/JCLI-D-12-00834.1.

Purkey, S. G., G. C. Johnson, L. D. Talley, B. M. Sloyan, S. E. Wijffels, W. Smethie, S. Sabine Mecking, and K. Katsumata, 2019: Unabated Bottom Water warming and freshening in the South Pacific Ocean. *J. Geophys. Res.*, **124**, 1778–1794, doi:10.1029/2018JC014775.

Raphael, M. N., J. Marshall, G J. n Turner, R. I. Fogt, D. Schnieder, D. A. Dixon, J. S. Hosking, J. M. Jones, and W. R. Hobbs, 2016: The Amundsen Sea Low: Variability, change, and impact on Antarctic climate. *Bull. Amer. Meteor. Soc.*, **97**, 111–121, doi:0.1175/BAMS-D-14-00018.1.

Reid, P. and R. A. Massom, 2015: Successive Antarctic sea ice extent records during 2012, 2013 and 2014. *Bull. Am. Meteorol. Soc.*, **96(7)**, 163–164, doi:10.1029/2000JC000720.

Renfrew, I. A., J. C. King, and T. Markus, 2002: Coastal polynyas in the southern Weddell Sea. *J. Geophys. Res.*, **106**, C3, 3063, doi:10.1029/2000JC000720.

Rignot, E., J. Mouginot, B. Scheuchl, M. van den Broeke, M. J. van Wessem, and M. Morlighem, 2019: Four decades of Antarctic Ice Sheet mass balance from 19792017. *PNAS*, **116(4)**, 1095–1103, doi:10.1073/pnas.1812883116.

Rintoul, S. R. and A. C. Naveira Garabato, 2013: *Dynamics of the Southern Oean circulation*, volume 103 of *International Geophysics*. Academic Press, 471–492 pp.

Roach, L. A., S. M. Dean, and J. A. Renwick, 2018: Consistent biases in Antarctic sea ice concentration simulated by climate models. *The Cryosphere*, **12(1)**, 365–383, doi:10.5194/tc-12-365-2018.

Robertson, R., M. Visbeck, A. Gordon, and E. Fahrbach, 2002: Long–term temperature trends in the deep waters of the Weddell Sea. *Deep Sea Research II*, **49**, 4791–4806.

Schneider, D. P. and D. B. Reusch, 2016: Antarctic and Southern Ocean surface temperatures in CMIP5 models in the context of the surface energy budget*. *J. Climate*, **29**, 16891716, doi:10.1175/ JCLI-D-15-0429.15.

Schodlok, M. P., D. Menemenlis, E. Rignot, and M. Studinger, 2012: Sensitivity of the ice shelf ocean system to the sub–ice shelf cavity shape measured by NASA IceBridge in Pine Island Glacier, West–Antarctica. *Annals of Glaciology*, **53**, 156–162, doi:10.3189/2012AoG60A073.

Scott, F. and D. L. Feltham, 2010: A model of the three-dimensional evolution of Arctic melt ponds on first–year and multiyear sea ice. *JGR: Oceans*, **115**, C12064, doi:10.1029/2010JC006156.

Semtner, A. J., 1976: A Model for the thermodynamic growth of sea ice in numerical investigations of climate. *J. Phys. Ocean.*, **6**, 379–389, doi:10.1029/2010GL044301.

Sen Gupta, A. and M. H. England, 2006: Coupled ocean–atmosphere–ice response to variations in the southern annular mode. *J. Climate*, **19**, 4457–4486, doi:10.1175/JCLI3843.1.

Seviour, W. J. M., F. Codron, E. W. Doddridge, D. Ferreira, A. Gnanadesikan, M. Kelley, Y. Kostov, J. Marshall, L. M. Polvani, J. L. Thomas, and D. W. Waugh, 2019: The Southern Ocean sea surface temperature response to ozone depletion: a multimodel comparison. *J. Climate*, **32**, 5107–5121, doi:10.1175/JCLI-D-19-0109.1.

Seviour, W. J. M., A. Gnanadesikan, D. Waugh, and M.-A. Pradal, 2017: Transient rsponse of the Southern Ocean to changing ozone: regional responses and physical mechanisms. *J. Climate*, **30**, 2463–2480, doi:10.1175/JCLI-D-16-0474.1.

Seviour, W. J. M., A. Gnanadesikan, and D. W. Waugh, 2016: The transient response of the Southern Ocean to stratospheric ozone depletion. *J. Climate*, **29**, 7383–7396, doi:10.1175/JCLI-D-16-0198.1.

Shepherd, A., E. R. Ivins, G. A. V. R. Barletta, M. J. Bentley, S. Bettadpur, K. H. Briggs, D. H. Bromwich, R. Forsberg, N. Galin, M. Horwath, S. Jacobs, I. Joughin, M. A. King, J. T. Lenaerts, J. Li, S. R. Ligtenberg, A. Luckman, S. B. Luthcke, M. McMillan, R. Meister, G. Milne, J. Mouginot, A. Muir, J. P. Nicolas, J. Paden, A. J. Payne, H. Pritchard, E. Rignot, H. Rott, L. S. Sørensen, T. A. Scambos, B. Scheuchl, E. J. Schrama, B. Smith, A. V. Sundal, J. H. van Angelen, W. J. van de Berg, M. R. van den Broeke, D. G. Vaughan, I. Velicogna, J. Wahr, P. L. Whitehouse, D. J. Wingham, D. Yi, D. Young, and H. J. Zwally, 2012: A reconciled estimate of ice-sheet mass balance. *Science*, **338**, 1183–1189, doi:10.1126/science.1228102 pmid:23197528.

Shepherd, A., D. Wingham, and E. Rignot, 2004: Warm ocean is eroding West Antarctic Ice Sheet. *The Cryosphere*, **31**, L23402, doi:10.1029/2004GL021106.

Sigmond, M. and J. C. Fyfe, 2010: Has the ozone hole contributed to increased Antarctic sea ice extent. *Geophys. Res. Lett.*, **37**, L18502, doi:10.1175/1520-0485(1976)006,0379:AMFTTG.2.0.CO;2.

— 2014: The Antarctic sea ice response to the ozone hole in climate models. *J. Climate*, **27**, 1336–1342, doi:10.1175/JCLI-D-13-00590.12.

Skinner, L. C., S. Fallon, C. Waelbroeck, E. Michel, and S. Barker, 2010: Ventilation of the deep Southern Ocean and deglacial CO_2 rise. *Science*, **328**, 1147, doi:10.1126/science.1183627.

Speer, K., S. Rintoul, and B. Sloyan, 2000: The diabatic Deacon cell. *J. Phys. Ocean.*, **30**, 3212–3222, doi:0.1175/1520-0485(2000)030¡3212:TDDC¿2.0.CO;2.

Stammerjohn, S. E., M. D. G., R. C. Smith, X. Yuan, and D. Rind, 2008: Trends in Antarctic annual sea ice retreat and advance and their relation to El Niiño–Southern Oscillation and Southern Annular Mode variability. *J. Geophys. Res. Oceans*, **113**, C03S90, doi:10.1029/2007JC004269.

Stammerjohn, S. E., R. Massom, D. Rind, and D. Martinson, 2012: Regions of rapid sea ice change: An inter–hemispheric seasonal comparison. *Geophys. Res. Lett.*, **39**, L06501, doi:10.1029/2012GL050874.

Steig, E. J., Q. Ding, D. S. Battisti, and A. Jenkins, 2012: Tropical forcing of Circumpolar Deep Water inflowand outlet glacier thinning in the Amundsen Sea Embayment. *Annals of Glaciology*, **53**, 19–28, doi:10.3189/2012AoG60A110.

Stuecker, M. F., C. M. Bitz, and K. C. Armour, 2017: Conditions leading to the unprecedented low Antarctic sea ice extent during the 2016 austral spring season. *Geophys. Res. Lett.*, **44**, 9008–9019, doi:10.1002/2017GL074691.

Swart, N. C. and J. C. Fyfe, 2013: The influence of recent Antarctic ice sheet retreat on simulated sea ice area trends. *J. Climate*, **29**, 1655–1672, doi:10.1175/JCLI–D–15–0501.1.

Talley, L. D., 2013: Closure of the global overturning circulation through the Indian, Pacific and Southern Ocean: schematics and transports. *Oceanography*, **26**, 880–897, doi:10.5670/oceanog.2013.07.

Tang, C. L., 1991: A two–dimensional thermodynamic momdel for sea ice advance and retreat in the Newfoundland marginal ice zone. *J. Geophys. Res.*, **96**, 4723–4737.

Taylor, K. E., R. J. Stouffer, and G. A. Meehl, 2012: An overview of CMIP5 and the experiment design. *Bulletin of the American Meteorology Society*, **83**, 485–498, doi:10.1175/BAMS-D-11-00094.1.

Thoma, M., A. Jenkins, D. Holland, and S. Jacobs, 2008: Modelling Circumpolar Deep Water intrusions on the Amundsen Sea continental shelf, Antarctica. *grl*, **35**, L18602, doi:10.1029/2008GL034939.

Thompson, D. W. J. and S. Solomon, 2002: Interpretation of recent southern hemisphere climate change. *Science*, **296**, 895–899, doi:10.1126/science.1069270.

Thompson, D. W. J., S. Solomon, P. J. Kushner, M. H. England, K. G. Grise, and D. J. Karoly, 2011: Signatures of the Antarctic ozone hole in Southern Hemisphere surface climate change. *Nature Geoscience*, **4**, 741–749, doi:10.1038/NGEO1296.

Thompson, D. W. J., J. M. Wallace, and G. C. Hegerl, 2000: Annular modes in the extratropical circulation. Part II: Trends. *J. Climate*, **13**, 1018–1036, doi:10.1175/1520-0442(2000)013¡1018:AMITEC¿2.0.CO;2.

Timmermann, R. and A. Beckmann, 2004: Parameterization of vertical mixing in the Weddell Sea. *Ocean Modell.*, **6**, 83–100.

Timmermann, R., A. Le Brocq, T. Deen, E. Domack, P. Dutrieux, B. Galton-Fenzi, H. Hellmer, A. Humbert, D. Jansen, A. Jenkins, A. Lambrecht, K. Makinson, F. Niederjasper, F. Nitsche, O. Nøst, L. H. Smedsrud, and W. H. F. Smith, 2010: A consistent data set of Antarctic ice sheet topography, cavity geometry, and global bathymetry. *Earth Syst. Sci. Data*, **2**, 261–273, doi:10.5194/essd–2–261–2010.

Timmermann, R. and M. Losch, 2005: Erratum: Using the Mellow–Yamada mixing scheme in seasonally ice–covered seas–corrigendum to: Parameterization of vertical mixing in the Weddell Sea. *Ocean Modell.*, **6**, 83–100, doi:10.1016/S1463-5003(02)00061-6.

Toggweiler, J. R., J. l. Russell, and S. R. Carson, 2006: Midlatitude westerlies, atmospheric CO_2, and climate change during the ice ages. *Paleoceanography*, **21**, PA2005, doi:10.1029/2005PA001154.

Turner, J., T. J. Bracegirdle, T. Phillips, G. J. Marshall, and J. S. Hosking, 2013: An initial assessment of Antarctic sea ice extent in the CMIP5 models. *J. Climate*, **26**, 1473–1484.

Turner, J., J. C. Comiso, G. J. Marshall, T. A. Lachlan-Cope, T. Bracegirdle, T. Maksym, M. P. Meredith, Z. Wang, and A. Orr, 2009: Non-annular atmospheric circulation change induced by stratospheric ozone depletion and its role in the recent increase of Antarctic sea ice extent. *Geophys. Res. Lett.*, **36**, L08502, doi:10.1029/2009GL037524.

Turner, J., T. Phillips, G. J. Marshall, J. S. Hosking, J. O. Pope, and P. Bracegirdle, T J. Deb, 2017: Unprecendented springtime retreat of Antarctic sea ice in 2016. *Geophys. Res. Lett.*, **44**, 6868–6875,, doi:10.1002/2017GL073656.

Wählin, A. K., X. Yuan, G. Björk, and C. Nohr, 2010: Inflow of warm Circumpolar Deep Water in the Central Amundsen Shelf. *J. Phys. Ocean.*, **40**, 1427–1434, doi:10.1175/2010JPO4431.1.

Walker, D. P., M. A. Brandon, A. Jenkins, J. T. Allen, J. A. Dowdeswell, and J. Evans, 2008: Oceanic heat transport onto the Amundsen sea shelf through a submarine glacial trough. *J. Geophys. Res.*, **34**, L02602, doi:10.1029/2007JC004284.

Warren, B. A., 1990: Suppression of deep oxygen concentrations by Drake Passage. *Deep-Sea Research*, **37**, 1899–1907.

Whitworth, T., W. Nowlin, and S. Worley, 1982: The net transport of the Antarctic Circumpolar Current through Drake Passage. *J. Phys. Ocean.*, **12(9)**, 960–971, doi:10.1175/1520-0485(1982)012¡0960:TNTOTA¿2.0.CO;2.

Wilchinsky, A. V. and D. L. Feltham, 2009: Numerical simulation of the Filchner overflow. *J. Geophys. Res.*, **114**, C12012, doi:10.1029/2008JC005013.

Wilson, E. A., S. C. Riser, E. C. Campbell, and A. P. S. Wong, 2019: Winter upper–ocean stability and ice–ocean feedbacks in the sea ice–covered Southern Ocean. *J. Phys. Ocean.*, **49**, 1099–1117, doi:10.1175/JPO-D-18-0184.1.

Worby, A. P., C. A. Geiger, M. J. Paget, M. L. Van Woert, S. F. Ackley, and T. L. Deliberty, 2008: Thickness distribution of Antarctic sea ice. *J. Geophys. Res.*, **113**, C05S92, doi:10.1029/2007JC004254.

Wu, X., W. F. Budd, V. I. Lytle, and R. A. Massom, 1999: The effect of snow on Antarctic sea ice simulations in a coupled atmosphere–sea ice model. *Clim. Dyn.*, **15**, 251–268, doi:10.1007/s003820050.

Yuan, X., 2004: ENSO-related impacts on Antarctic sea ice: a synthesis of phenomenon and mechanisms. *Antarctic Science*, **16(4)**, 415–525, doi:10.1017/S0954102004002238.

Zhang, J. L., 2007: Increasing Antarctic sea ice under warming atmospheric and oceanic conditions. *J. Climate*, **20(11)**, 2515–2529, doi:10.1175/JCLI14136.1.

— 2014: Modeling the impact of wind intensification on Antarctic sea ice volume. *J. Climate*, **27**, 202–214, doi:10.1175/JCLI-D-12-00139.1.

Zunz, V., H. Goose, and F. Massonnet, 2013: How does internal variability influence the ability of CMIP5 models to reproduce the recent trend in Southern Ocean sea ice extent. *The Cryosphere*, **7**, 451–468, doi:10.5194/tc-7-451-2013.